2014-01-01

An Experimental Investigation Of The Cooling Channel Geometry Effects On The Internal Forced Convection Of Liquid Methane

Adrian Trejo
University of Texas at El Paso, atrejo2@miners.utep.edu

AN EXPRIMENTAL INVESTIGATION OF THE COOLING CHANNEL GEOMETRY EFFECTS ON THE INTERNAL FORCED CONVECTION OF LIQUID METHANE

ADRIAN TREJO

Environmental Science and Engineering

APPROVED:

Ahsan Choudhuri, Ph.D., Chair

Norman Love, Ph.D.

Shaolin Mao Ph.D.

Felicia Manciu, Ph.D.

Bess Sirmon-Taylor, Ph.D.
Interim Dean of the Graduate School

AN EXPRIMENTAL INVESTIGATION OF THE COOLING CHANNEL GEOMETRY EFFECTS ON THE INTERNAL FORCED CONVECTION OF LIQUID METHANE

by

ADRIAN TREJO, B.S., M.S. Mechanical Engineering

DISSERTATION

Presented to the Faculty of the Graduate School of

The University of Texas at El Paso

in Partial Fulfillment

of the Requirements

for the Degree of

DOCTOR OF PHILOSOPHY

Environmental Science and Engineering

THE UNIVERSITY OF TEXAS AT EL PASO

May 2014

Abstract

Rocket engine fuel alternatives have been an area of discussion for use in high performance engines and deep spaceflight missions. In particular, LCH_4 has showed promise as an alternative option in regeneratively cooled rocket engines due to its non-toxic nature, similar storage temperatures to liquid oxygen, and its potential as an in situ resource. However, data pertaining to the heat transfer characteristics of LCH_4 is limited. For this reason, a High Heat Transfer Test Facility (HHTTF) at the University of Texas at El Paso's (UTEP) Center for Space Exploration Technology and Research has been developed for the purpose of flowing LCH_4 through several heated tube geometry designs subjected to a constant heat flux. In addition, a Methane Condensing Unit (MCU) is integrated to the system setup to supply LCH_4 to the test facility. Through the use of temperature and pressure measurements, this experiment will serve not only to study the heat transfer characteristics of LCH_4; it serves as a method of simulating the cooling channels of a regeneratively cooled rocket engine at a subscale level. The cross sections for the cooling channels investigated are a 1.8 mm x 1.8 mm square channel, 1.8 mm x 4.1 mm rectangular channel, 3.2 mm and 6.34 mm inside diameter channel, and a 1.8 mm x 14.2 mm high aspect ratio cooling channel (HARCC). The test facility is currently designed for test pressures between 1.03 MPa to 2.06 MPa and heat fluxes up to 5 MW/m^2. Results show that at the given test pressures, the Reynolds number reaches up to 140,000 for smaller cooling channels (3.2 mm diameter tube and 1.8 mm x 4.1 mm rectangle) while larger cooling channel geometries (6.35 mm diameter and HARCC) reached Reynolds number around 70,000. Nusselt numbers reached as high as 320 and 265 for a 3.2 mm diameter tube and 1.8 mm x 4.1 mm rectangular channel respectively. For cooling channel geometries with 6.35 mm diameter and HARCC geometry, Nusselt numbers reached 136 (excluding an outlier) and 106 respectively. Heat transfer predictions applied to the data yielded theoretical correlations within 40% of the experimental data. However, typical theoretical values fall within 10%-15% of the experimental values showing agreeable correlations and supporting theories stated in the present study.

Table of Contents

List of Tables

List of Figures

Chapter 1: Introduction

1.1 Project Overview

Due to high temperatures associated with a rocket combustor chamber, cooling techniques are necessary to avoid failure due to heat fluxes which may exceed the working limits of the rocket combustor material. Regenerative cooling is a technique widely used in rocket engines as well as ablative cooling, dump cooling, and radiation cooling. In regeneratively cooled rocket engines (regen engines), a cooling jacket equipped with cooling channels are placed surrounding the contour of the engine. The design of these cooling channels is largely responsible for the overall efficiency and life of the engine. Though regen engines are common in current aerospace applications, the use of LCH_4 is limited. However, several advantages concerning deep space exploration and practical uses in rocket engine applications are assessed using LCH_4 [1]. For this reason, this experiment will investigate the heat transfer characteristics of LCH_4 flowing through several cooling channel geometries. A High Heat Flux Test Facility (HHFTH) is specifically designed to achieve heat fluxes comparable to those experienced in lander class rocket engine. The HHFTF will test these cooling channels by providing an asymmetric heating configuration at a constant heat flux currently absent in current test configurations when testing LCH_4. The geometries taken into consideration include rectangular channels representative of milled channel wall designs seen in the Space Shuttle Main Engine (SSME) rocket engine. In this case, qualities such as the rib effectiveness and the aspect ratio of the channel are all critical elements in analyzing the geometry. Circular channels will also be tested to represent brazed tubes or gun-drilled cooling channels as used in the RL-10 rocket engine.

1.2 Subcritical Methane Study

The investigation of LCH_4 heat transfer has primarily involved computational fluid dynamics (CFD) and has lacked the backing of empirical data. This will present a challenge in that verifying experimental data will be quite limited. This study aims to advance the knowledgebase of LCH_4 empirical data and details a practical method in capturing the heat transfer effects of liquid propellants.

A focal point in this experiment is the acquisition of quantitative LCH_4 data for applications in possible regen engine design configurations. Currently, an emerging demand for LCH_4 is in large part

due to its non-toxic nature and the increasing study in the in situ resource utilization (ISRU) research area. Liquid hydrogen (LH_2) is widely used as the fuel/coolant in regen engine technology due to its cooling capabilities, flame temperature, and energy density. However, LCH_4 temperatures are similar to that of liquid oxygen (LOX) eliminating the need for separate storage equipment and technology .In addition, LCH_4 is approximately five times less dense than hydrogen which can reduce the payload and the overall cost while increasing the performance for long duration space missions. This point is emphasized in Figure 1.1 showing a graph comparing LOX/LCH_4 energy density with currently used propellants. Non-liquid propellants, such as hypergolic propellants, are produced on earth offering no potential in ISRU applications. Furthermore, typical hypergolic propellants such as monomethylhydrazine and nitrogen tetroxide are toxic creating complications in storage and handling.

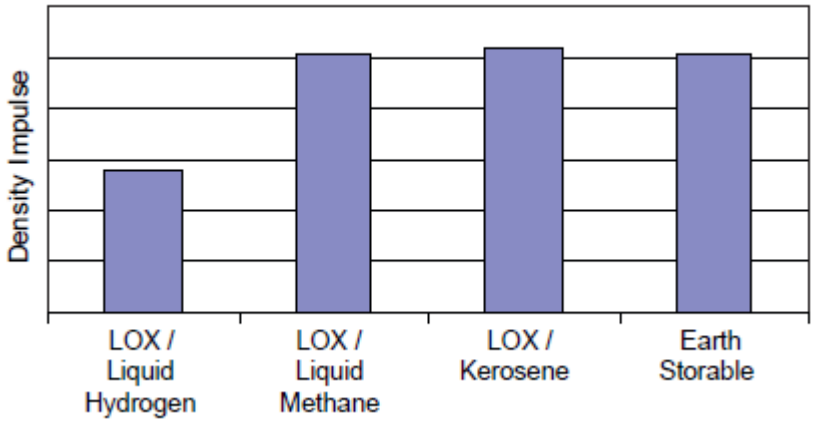

Figure 1.1: Density Impulse Comparisons Showing Methane Comparable with Traditional Propellants [1]

1.3 Experimental Approach

Several heat flux facilities have been designed for the purpose of fundamentally understanding the heat transfer characteristics of propellants and other fluids (i.e. water and R-134a). Several methods exist in attaining a constant heat flux on a cooling channel including arc heating, resistive heating, and conduction heating thermal concentrators. In this experiment, each cooling channel will be heated using a heat conduction technique that will provide heat fluxes driven by the temperature of a copper heating block in contact to the copper test section. Resistive heating is an approach used in several heated tube experiments by electrically driving the temperature by implementing a current onto the tube. However,

electrically driven phenomena as well as possible degradation from the tube material could not be ruled out as an influencing factor in the results as reported in Ref. [2]. In addition, heat fluxes attained have come at the expense of currents well over 1000 amps. Finally, asymmetric heating to represent hot-wall temperatures from rocket engine combustion is achievable with conduction heating more simply than in resistive heating. Figure 1.2 shows a model of a regen engine with milled cooling channel. This figure intends to express the configuration of a regen engine while also depicting the manner in which each cooling channel is heated by combustion gases.

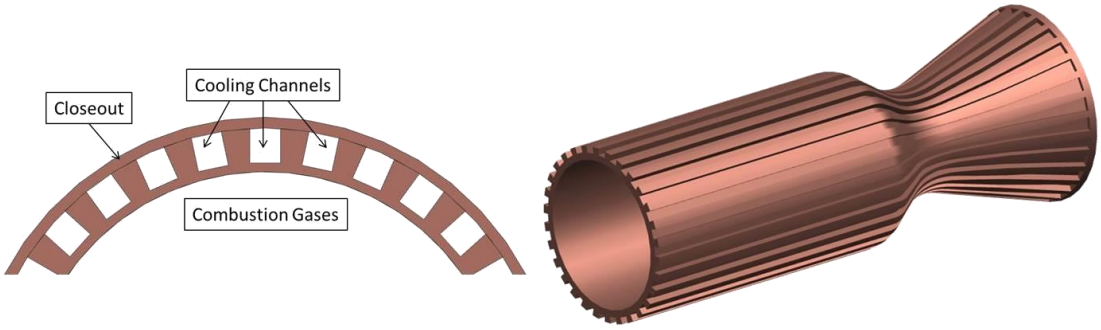

Figure 1.2: Regeneratively Cooled Engine Diagram

1.4 Project Objectives

The purpose of this research task is to experimentally understand the behavior of subcritical methane flowing through a cooling channel subjected to a constant heat flux. To accomplish this, the HHFTF will conductively heat a copper cooling channel asymmetrically and produce heat fluxes on the scale of lander class engines. Previous objectives included a system qualification to determine the system limitations. These limitations determined the test points while keeping the life of the system at a reasonable state. The planned testing temperatures and pressure ranges are from 200 °C – 450 °C and 1.0 MPa – 2.1 MPa respectively. All tests are conducted in vacuum conditions at a minimum of .5 torr.

In addition to testing with LCH_4, acquiring LCH_4 is a key issue when attaining quantitative results and performing the assigned experimental conditions. Currently, a 13 L LCH_4 capacity tank is capable of attaining steady state data and the heat transfer behavior associated. To further understand the behavior, four cooling channels with different cross sectional geometries will be applied to compare and characterize the heat transfer effects. These cooling channels were designed to replicate cooling

channels directly applicable in current regen engine technology such as milled channels and brazed tubes.

1.5 Relevance

The results from this experiment will attempt to verify and give a better understanding of the fluid characteristics of LCH_4. This data is relevant to designers attempting to either verify or build around a design case using the parameters met in this study. This will lead into using the Nusselt (Nu) number correlations presented in this work to calculate associated heat transfer coefficients and possible wall temperatures avoiding failure. This study will also provide a means of verification for CFD simulations performed by researchers in test cases pertaining to this study. In conjunction, the heat transfer characterization of the cooling effects of different cooling channel geometries will be studied. This experimental analysis will develop a design base when designing cooling channels in heat exchangers pertaining to regen engines with LCH_4 as the coolant. All of the above statements are important contributing factors in the analysis for a final product especially in the aerospace industry.

In terms of experimentation, the test setup of the HHFTF provides a robust method in testing liquid propellants. Along with the HHFTF, a 13 L methane condensing unit with cryogenic handling capabilities was designed to provide steady state wall temperatures and intended specifically for subscale testing while avoiding hazards due to large amounts of fuel. The design of both test stands demonstrates a method of design and testing for future sub-scale test facilities. The design of the HHFTF and MCU are detailed in the work herein.

Chapter 2: Literature Review

2.1 High Heat Flux Facilities

The experimental heat transfer characterization of liquid propellants applicable to regen engines is simplified by developing subscale test facilities utilizing turbulent forced convection through a heated tube. Subscale test facilities offer the advantage of investigating and ultimately predicting the thermal performance of coolant at various temperature, heat flux, and pressure conditions. In addition, material compatibility, cooling channel design, and coking limits have also been studied through the use of subscale test facilities simulating the combustion phenomena experienced in a rocket engine chamber yielding a constant heat flux to the combustion chamber wall/cooling channel. Several methods are developed in order to achieve this constant heat flux. The following two methods (resistively and conductively heated tubes) were investigated in the present study as liquid propellants such as RP-1, liquid natural gas (LNG), and LCH_4 were the main focus at each respective test facility.

2.1.1 Resistively Heated Tubes

Resistively heated tube facilities (also known as ohmic heated tube facilities) use a method of passing a current through a tube releasing heat from the tube material. This method has been used by NASA/Rocketdyne to investigate the heat transfer characteristics of LCH_4 and the two phase heat transfer of liquid propellants. Above needs citation

Rocketdyne

In 1984, R. T. Cook presented experimental data produced by Rocketdyne's heat flux facility for the purpose of evaluating the heat transfer characteristics and coking thresholds of hydrocarbons flowing through a resistively heated tube [3]. This test setup was designed to replicate high pressure and heat flux operating conditions of the Main Combustion Chamber (MCC) designed for LOX//CH_4 propellants with a design based off of the Space Shuttle Main Engine (SSME). Using 3 arc reactors each producing up to 2000 AMPS, wall temperatures between 316 °C to 482 °C (600 °F to 900 °F) and constant heat fluxes up to 139.0 MW/m^2 (85 Btu/in^2-sec) were achieved. Working pressures in the cooling channel were tested at 34.5 MPa (5000 psia) which is typical of a 20.7 MPa (3000 psia) pressure chamber engine design. Coking investigations for a copper coil and stainless steel tube showed to have no factor in the

results when subjected to the heat fluxes mentiones. The cooling channel geometries were 76.2 mm and 178 mm (3 in. and 7 in.) in length. The inside diameter was recorded to be 2.1 mm (.083 in.) while the outer diameter was recorded to be .083 inches. The tube was reinforced by encasing the tube with Monel K-800 similar to the channel material developed for the space shuttle main engine. Electrical preheaters were used to vary the inlet temperature and turbine flow meters were used to measure the fluid flow rates [3].

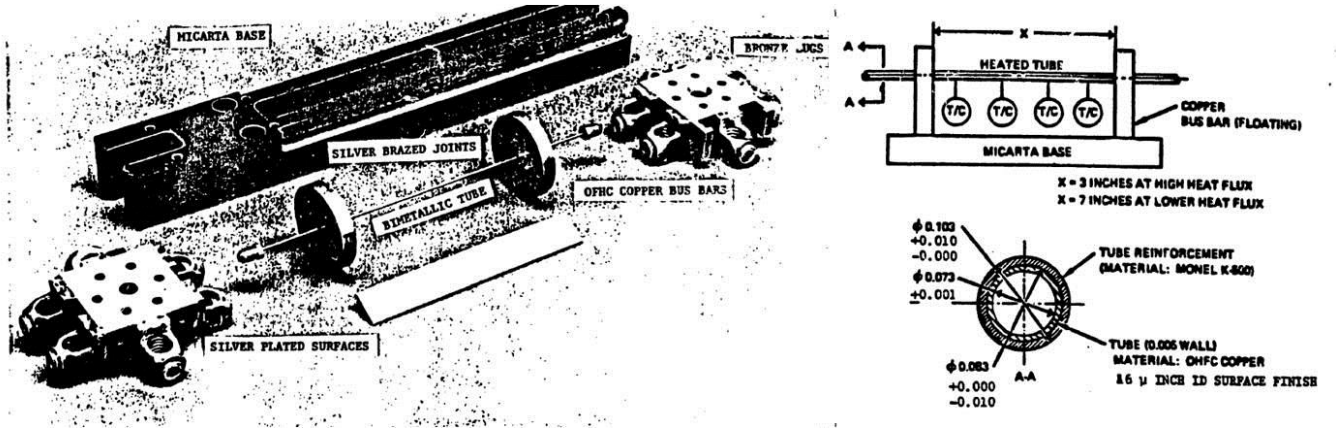

Figure 2.1: Rocketdyne-MSFC Components for the Resistively Heated Heat Flux Facility [3]

NASA Glenn Research Center

In 1991 NASA Glenn Research Center (GRC) published a paper on the renovation of a Heated Tube Test Facility built in the 1960s [4]. This heated tube facility generated a total of 6000 A to heat the tube to the desired heat fluxes. In 2010, NASA GRC used the same HTF to investigate the heat transfer effects of liquid and two phase methane. The resistively heated tube shown in Figure 2.2 produced a maximum average heat flux of about 10.1 MW/m^2 and reached temperatures up to 726 °C. To reach the maximum heat flux and temperatures, a current of 1500 A was drawn using a 100 Vdc power supply. The mass flow rates used varied between 2.27 g/s – 31.7 g/s with inlet pressures up to 3.9 MPa. The properties of methane were taken in the subcooling regime with temperatures between 188 to 255 R. For temperature measurements, a total of 15 thermocouples were spot welded along the test section. These temperatures determined the state at which methane went from transition boiling to film boiling. The critical heat flux was determined for velocities up to 45.4 m/s. In addition, fluid quality was calculated

based on the outlet temperatures and the calculated enthalpy. Channel inside diameters ranging from 1.4 mm to 2.1 mm and an outside diameter range of 2.4 mm - 3.2 mm were tested in the experiment [5].

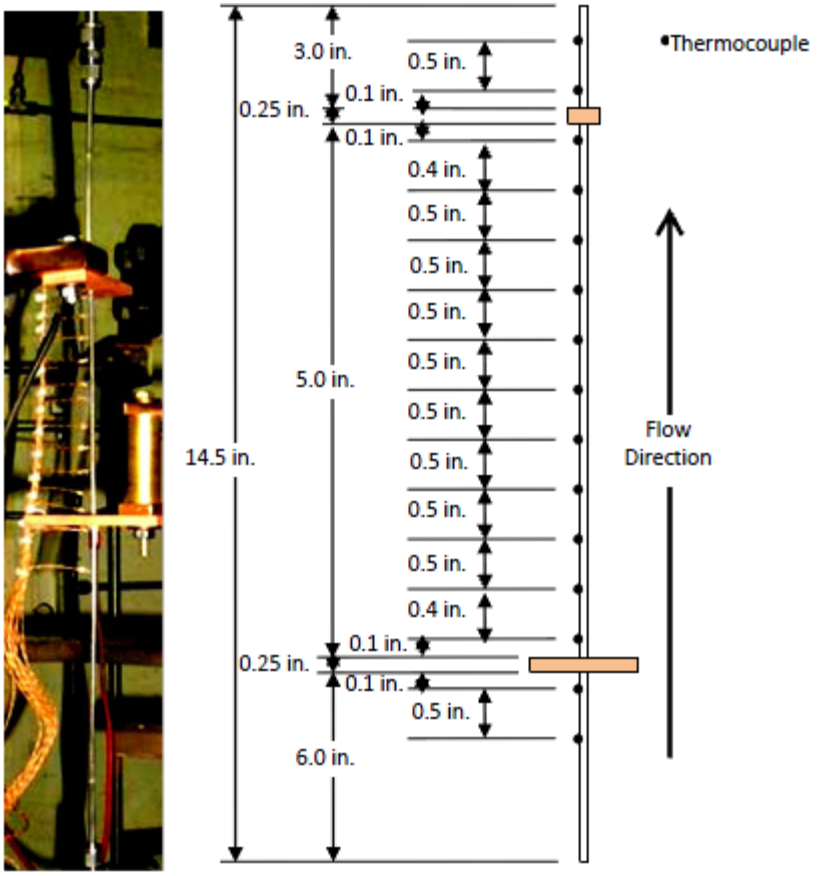

Figure 2.2: NASA-GRC Heated Tube Test Facilities Restively Heated Tube Configuration [5]

2.1.2 Conductively Heated Tubes

Heat fluxes generated using conductive heating techniques utilize a heat source such as a heater block coming into direct contact to the test section cooling channel to supply a constant heat flux. Although thermal losses exist from the heater block, it is believed that conductively heated facilities offer the closest simulation to a rocket engines combustion chamber heating a cooling channel asymmetrically without compromising results by introducing electrically driven phenomena to the thermocouples.

Air Force Research Laboratory High Heat Flux Facility (AFRL)

An interest was taken by the AFRL in reusable hydrocarbon-fueled engine technologies and analyzed several heated tube designs. From 2004-2007 a High Heat Flux Facility (HHFF) was designed for the purpose of experimentally investigating copper cooling channel geometries focusing on RP-2 fuel [2, 6, 7, and 8]. Initially in 2004, the AFRL investigated several heating block configurations to maximize the thermal performance with regard to the contact with the test section cooling channel to provide the heating from a copper heater block. A first generation design was constructed by conductively and asymmetrically heating a copper tube by internally heating a copper heating block with cartridge heaters. The block is then used to geometrically focus the thermal energy onto a small section of the heating block. The system was also placed into an altitude chamber to create an environment close to the altitude conditions and prevent oxidation to the heated copper sections. Three separate configurations of the test rig were first simulated before the final design was constructed shown in Figure 2.3 [2, 6]. The final test configuration chosen was selected due to the ability for the test section to reach uniform temperature. A key feature of this design was the capability to change the geometry of the cooling channel by simply replacing the test section. Pressures of up to 31.0 MPa (4500 psi) and maximum wall temperatures of 650 °C (1200 °F) were tested.

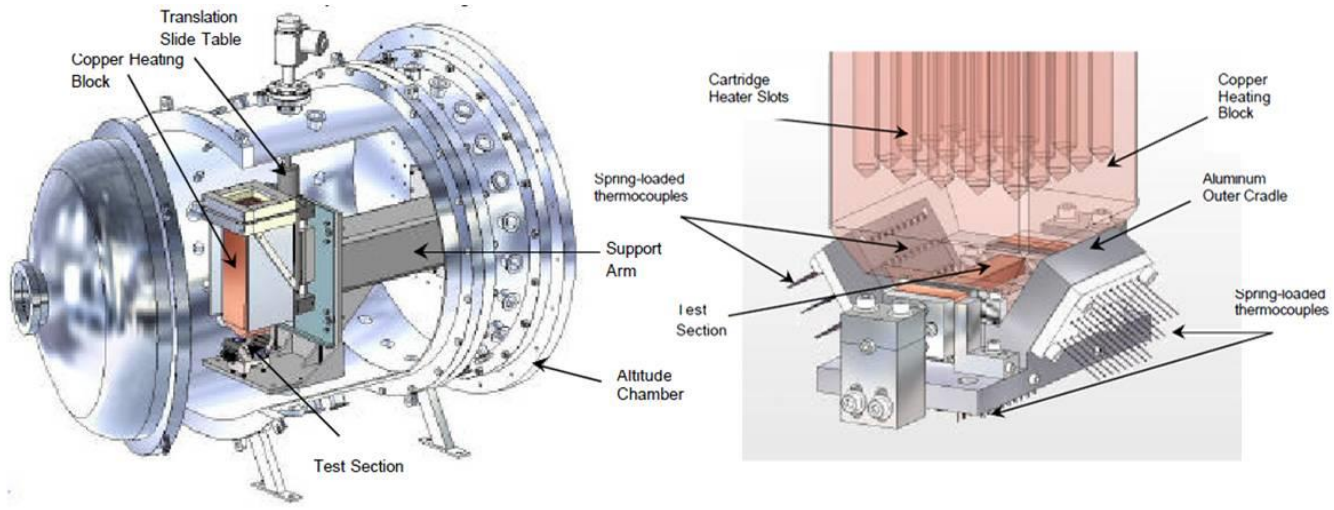

Figure 2.3: AFRL High Heat Flux Facility [2, 6]

A second design was constructed for the purpose of maximizing the heat transfer between the test section and heating block and thus improving upon the previous design. An improved configuration to the previous HHFF's heating block was designed to improve the conduction, alignment, and contact. As opposed to having the test section and cooling channel separate from the heating block, the cooling channel is integrated into the heating block by machining the channel geometry into the block itself. This causes for the construction of a new heating block each time a new channel is investigated. Figure 2.4 a) shows the configuration of the heating block presented in 2004, and a modified configuration is shown in Figure 2.4 b) [7]. The improved design was to find the heat transfer characteristics of RP-2. Experimental results displayed a Nusselt and Reynolds number plot and correlated several a Nusselt number in terms of Reynolds and Prandtl number correlations. The Dittus-Boelter correlation was determined to be the closest correlation to the empirical data gathered by the AFRL for RP-2.

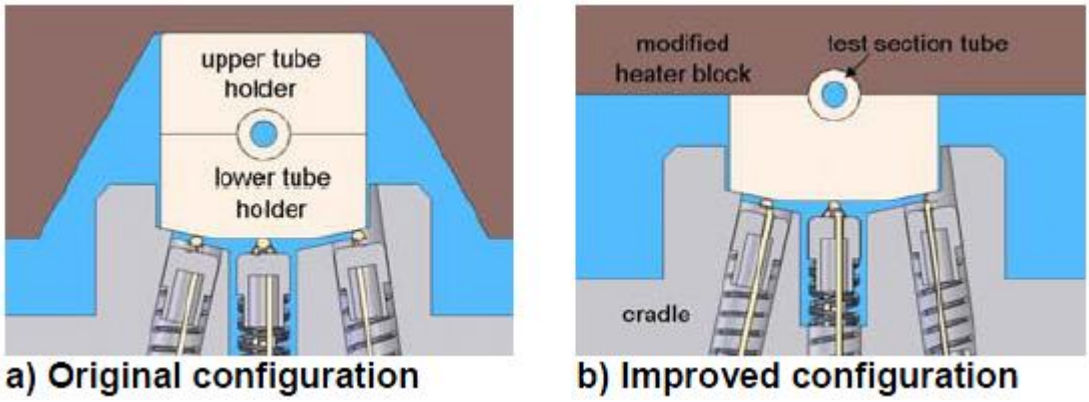

Figure 2.4: AFRL Original Configuration to Improved Configuration Comparison [8]

2.2 Cooling Channel Geometries

Cooling channel designs in literature were investigated based upon the feasibility and use in rocket engine development. Two channel designs widely used in regen engine technology deal with circular tubes and High Aspect Ratio Cooling Channels (HARCC). Several driving factors come into consideration when designing and manufacturing the proper cooling channel. The following cooling channels represent the most investigated and applied cooling channels to date.

2.2.1 Circular Cooling Channels

Tubular or circular channels are representative of brazed tubes used in regen engines such as the RL-10 and F-1. Brazed tubes offer the advantage in fabrication, cost, and as opposed to square channels the tube inner walls act as the combustion chamber leaving no gaps along the jacket of the engine. This gives the advantage in offering a larger wetted surface as opposed to square channels. Figure 2.7 shows a sketch representative of an engine with brazed tube cooling channels and the outer jacket of the RL-10 rocket engine.

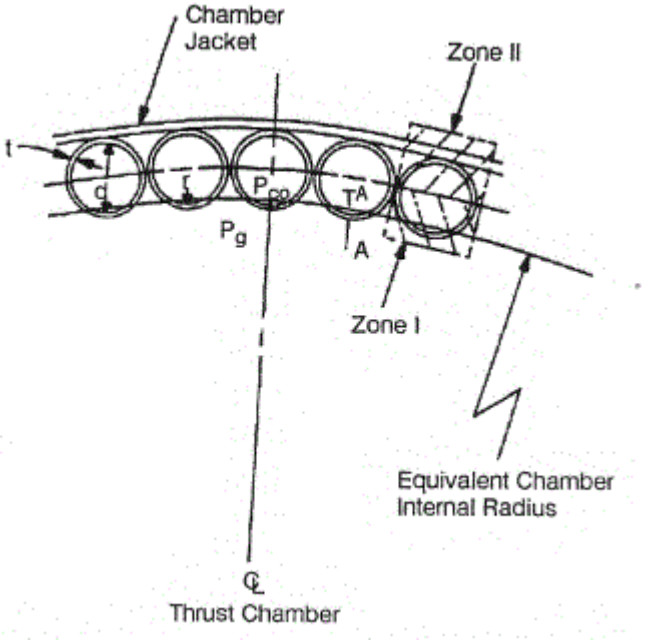

Figure 2.5: Configuration of Circular Tubes used in a Regen Engine [9]

2.2.2 Rectangular/Milled Channels

The rectangular channels in this experiment represent milled channel wall designs and will investigate the effects of the aspect ratios. Figure 2.8 shows rectangular channels implemented in typical regen engine. The heat transfer benefits of using milled or square channel geometries is due to an additional benefit in the fin effects scene in many electronic applications. The fins developed when machining the cooling jacket act as a heat sink and absorb the heat from the combustion process. The fin effectiveness described by [10]:

$$\varepsilon_{fin} = \frac{\dot{Q_{fin}}}{\dot{Q}_{no\ fin}} \qquad [2.1]$$

is defined by the ratio between the fin heat transfer rate and the heat transfer rate of the object without fins. Recent studies have placed emphasis in HARCCs due to the fin effectiveness concept. The aspect ratio, defined as the height divided by the width, is considered "normal" when kept in the range of 2 – 2.5. Currently, the term "high aspect ratio" is defined as a ratio of approximately 8. One of the most notable regen engines to use rectangular channels is the Space Shuttle Main Engine (SSME). Its 2,279 kN thruster applied 430 cooling channels around the chamber with aspect ratios up to 5.

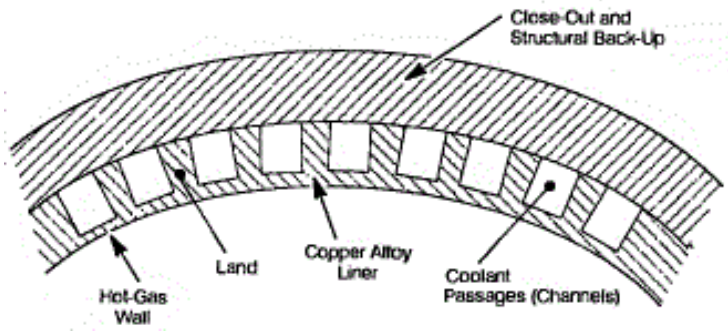

Figure 2.6: Configuration of Rectangular Channels used in a Regen Engine [9]

Computational efforts have been performed to study the heat transfer effects of HARCCs on the engine combustion chamber. NASA performed an analysis through the use of Two Dimensional Kinetics (TDK) and Rocket Thermal Equilibrium (RTE) on a LOX/LH_2 engine. A baseline condition of an 89 kN thrust chamber developed at NASA with a maximum aspect ratio of 2.5 was used to compare the effect of HARCCs. This effort was to investigate the heat transfer effects and pressure loss without compromising the heat transfer. The aspect ratios simulated were as low as 5 and as high as 40. Results showed that an aspect ratio of 8.9 produced the lowest hot-gas-wall temperatures of about 22% from the baseline case and pressure drop increases as low as 7.5% [11].

2.3 Subcritical Methane

Although experimental heat transfer data of LCH_4 is limited, transport properties of LCH_4 such as the densities, conductivities, etc. are commonly known by databases such as NIST REFPROP. Also known are the thermodynamic conditions in which each of the three phases of CH_4 exists. Figure 2.6 shows a methane phase diagram developed "in house" by exporting methane property data from a table found in a journal article published in 1987 by the National Engineering Laboratory [12]. The transport

and thermophysical properties of several hydrocarbons were presented in this paper including methane. The CH_4 phase diagram provided the necessary criteria (pressure and temperature points) particularly in the design process of several CH_4 condensing units designed to supply LCH_4 to the test section explained in further detail in this report.

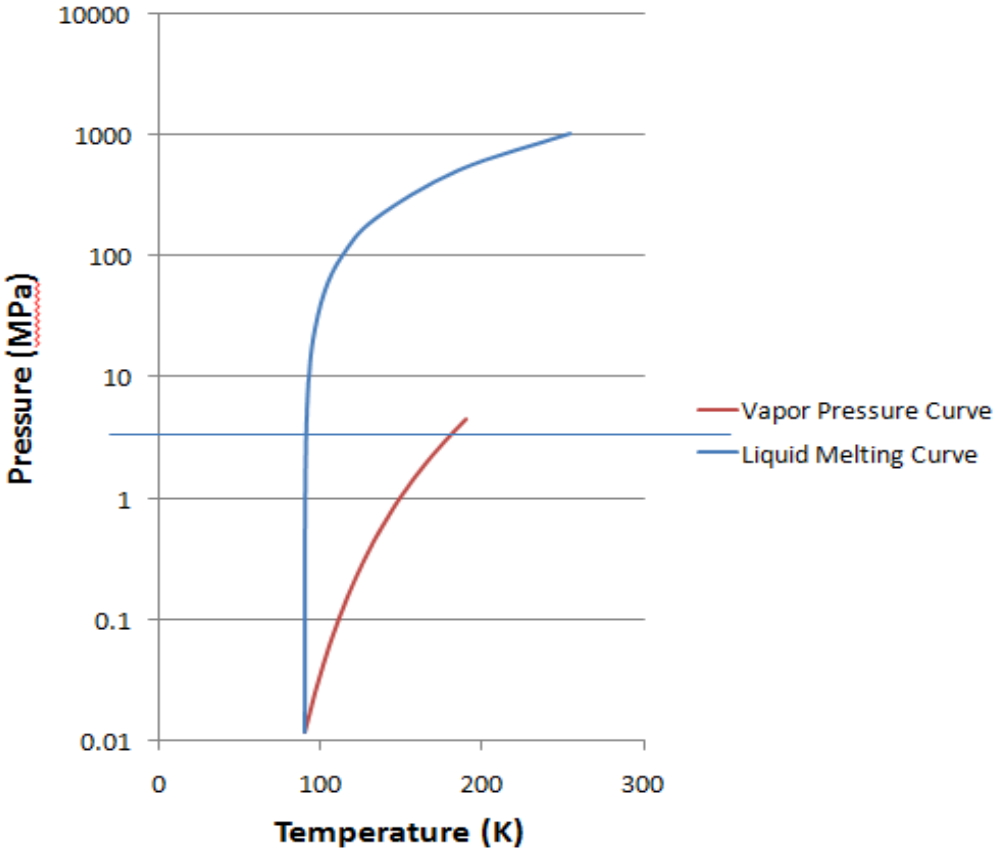

Figure 2.7: Methane Phase Diagram

The previously mentioned Rocketdyne and NASA MSFS collaboration effort designed a heated tube test for the purpose of finding the heat transfer characteristics of LCH_4. The final results in characterizing the heat transfer were reached by finding the relation between the Nusselt number in terms of Reynolds and Prandtl number. Several relations were used for this characterization and are listed in the equations below. Figure 2.5 shows the results attained from the Rocketdyne experiment through smooth tubes. During final analysis from the UTEP High Heat Flux Test Facility, this data correlation will be attempted [3].

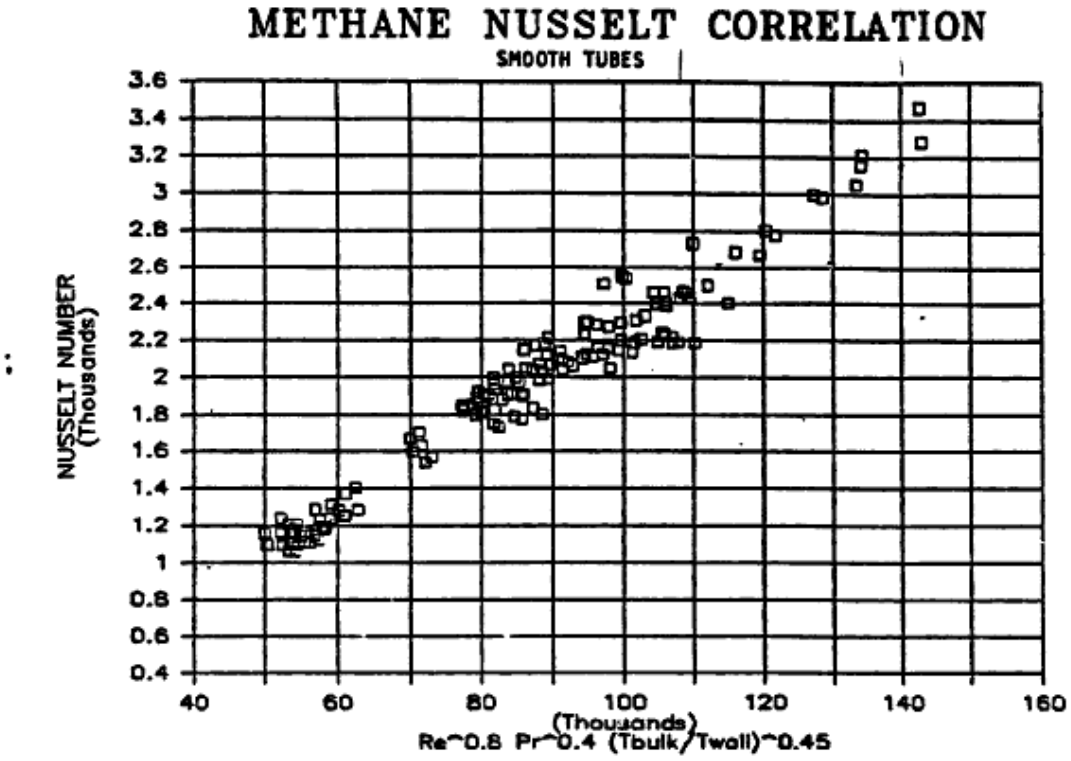

Figure 2.8: Nusselt Number Correlation developed by Rocketdyne-NASA MSFC [3]

The most recent study of LCH_4 heat transfer exists in reference [13]. This data was taken using the same HHFTF described in this study. The cooling channel geometry tested was a 1.73 x 173 mm square cross manufactured at White Sands Test Facility (WSTF) for the testing subscale regen engine cooling channel. Figure 2.9 highlights the overall Nusselt number vs. bulk Reynolds number range for the test conditions for the particular study. Nusselt number ranged from 30 to 260 and Reynolds numbers ranged from 190,000 to 140,000.

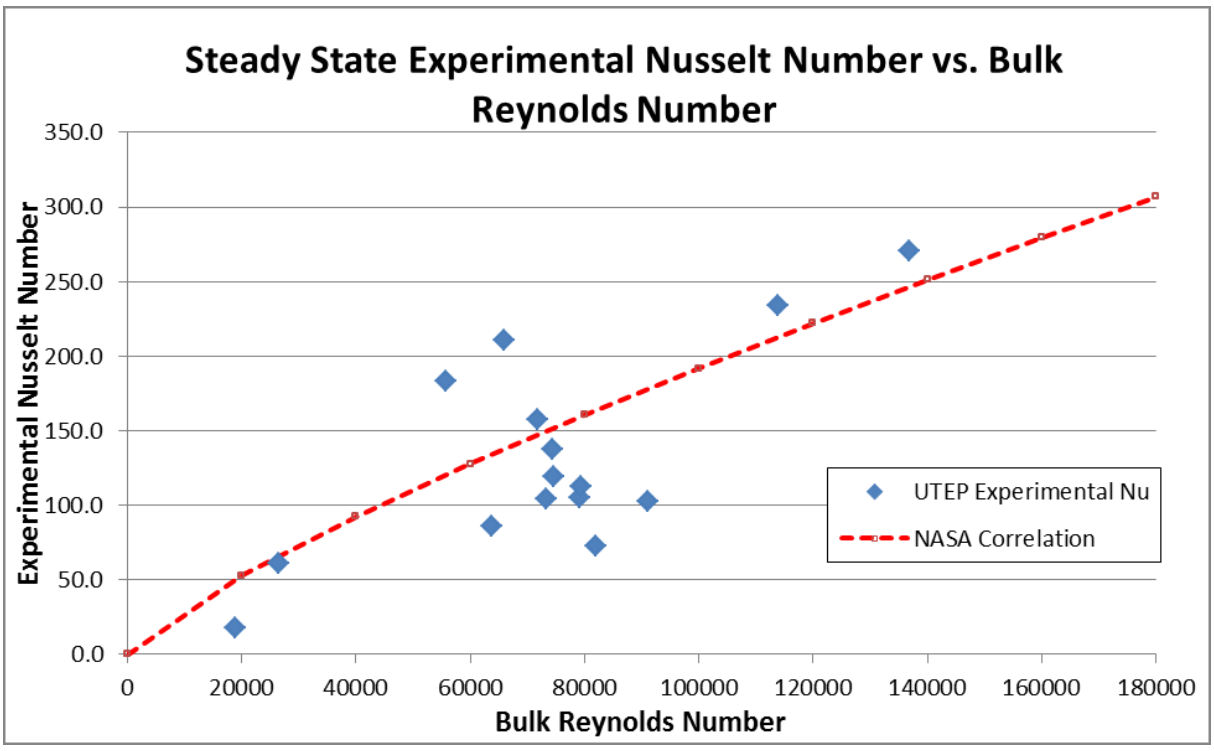

Figure 2.9: Experimental Nusselt Number vs. Bulk Reynolds Number [13]

When subjecting cryogenic fluids to high heat fluxes, possible boiling effects must be considered. Studies have shown regions in which certain boiling regimes exist and relate the heat flux to the wall temperature. Figure 2.10 shows a boiling curve for water using a resistively heated tube. The physical behavior however, should be consistent for all fluids. Once the fluid reaches the critical heat flux, the wall temperature continues to increase, alternatively, the heat flux decreases. The next governing phenomenon is known as film boiling. The wall temperature continues to increase with an increasing heat flux as the sub-cooled fluid converts to superheated fluid.

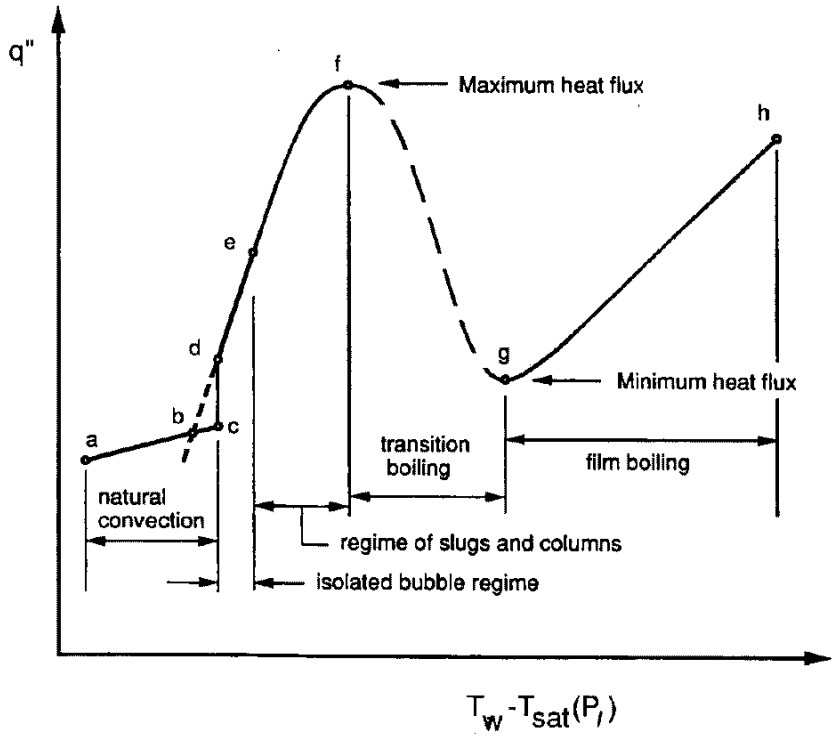

Figure 2.10: Boiling Curve Diagram for Saturated Water Flowing through a Heated Tube [14]

2.4 Nusselt Number Correlations

The Nu number in eqn 1 is defined as the ratio of the convective to conductive heat transfer across a defined boundary layer. In this experimental study the heat transfer coefficient h_x is the main driver in the definition of Nu numbers as the characteristic length $\boldsymbol{L}$ is constant throughout the test and the thermal conductivity $\boldsymbol{k}$ of LCH_4 is relatively constant at the tested conditions assuming single phase CH_4 flowing through the test section.

Several Nu number historical formulations have been empirically developed in literature for the purpose of predicting the heat transfer behavior at certain conditions. The most relevant Nu correlations for the experimental data generated in this work involve Seider-Tate, Dittus Boelter, and the Modified Colburn Equation number correlations. Each of these correlations is particular to turbulent flow for internal forced convection.

In 1930, Dittus Boelter developed a Nu correlation considering liquids and gases with Pr numbers greater than 0.7 and Re_D numbers between 20,000 and 300,000. Two versions of the equation

were generated depending on the cooling or heating environment of the fluid (Pr number of 0.4 if heating and 0.3 if cooling). Eqn 2.3 shows the Dittus Boelter correlation for a heated fluid [15].

$$Nu = 0.23{Re_D}^{0.8}Pr^{0.4} \quad [2.3]$$

The worked provided by Seider-Tate in 1936 resulted in a correlation integrating a viscosity correction factor by testing three oils with widely different viscosities [16]. The purpose of this test was to develop a heat transfer prediction for single phase liquids and develop an identical correlation for both heated and cooled fluids. The data presented showed a strong correlation shown in Eqn 2.4 where μ_b is the viscosity evaluated at the bulk temperature and μ_w is the viscosity evaluated at the wall temperature [15].

$$Nu = C_1{Re_D}^{0.8}Pr^{1/3}\left(\frac{\mu_b}{\mu_w}\right)^{0.14} \quad [2.4]$$

A Nusselt number correlation highlighted in this work is a modified version of the previously mentioned Taylor Nusselt presented in Ref. [2] and also used in Ref. [13]. Though this correlation is mainly used for gaseous fluids, using CH_4 as the main test fluid was significant for this study to apply this correlation to the test data. This correlation applies a temperature correction factor as seen in Eqn 2.5 where the T_b is the bulk temperature and T_w is the average wall temperature.

$$Nu = C_1{Re_D}^{0.8}Pr^{0.4}\left(\frac{T_b}{T_w}\right)^{0.14} \quad [2.5]$$

Additional Nusselt number correlations are investigated in this study and are mentioned in a table in the Appendix. This includes two additional correlations to the previously mentioned Nusselt number with a short summary for each correlation.

Chapter 3: Design of a Methane Condensing Unit

3.1 First Generation Proof of Concept

The MCMU is a product of a progressive study in the condensation of methane. A first generation condensing unit was developed as a proof of concept system that produced up to 1 L of LCH_4 in a vacuum insulated flask. Figure 3.1 shows the initial setup of the 1st generation condensing unit. This concept utilized a shell and coiled tube heat exchanger in which LN_2 was passed through the coil inside the condenser flask as gaseous methane was pressurized to 34.4 kPa (5 psi). The flask is placed on a weigh scale in order to estimate the amount of LCH_4 produced and is verified by an E-type thermocouple placed at a defined height to indicate the presence of 1 L of LCH_4 when the temperature reads 108 K. The purpose of this test was to demonstrate the ability to handle cryogenics and develop safety habits when dealing with liquid propellants.

Figure 3.1: 1st Generation LCH_4 Proof-of-Concept Production Setup

3.2 Second Generation Transient Methane Testing

Successful trials in condensing LCH_4 led to an upgraded 2nd generation design of 2 L LCH_4 capacity condensing/run tank. The MCMU is designed for mobility by allowing the transportation of the

pressurant, fuel, and condensing tanks to supply LCH_4 to several experiments throughout the cSETR Goddard Laboratory. The MCMU applies a transfer process in which two separate tanks are linked together composing of the condensing and run tank subsystems as shown in Figure 3.2 and Figure 3.3 (a) and (b). Due to machining done to customize the condensing tank, safety issues prohibit pressurizing the tank over 34.4 kPa (5 psi). For this reason, a separate run tank is placed for pressurizing and flowing LCH_4 to the test section. All components and gas tanks are placed on a stainless steel cart. The purpose of the MCMU design was to further prove the ability to condense methane at increased volumes. In addition, the design of this system allowed the possibility to attain the transient heat transfer characteristics when integrated to the HHFTF providing useful data not presently studied.

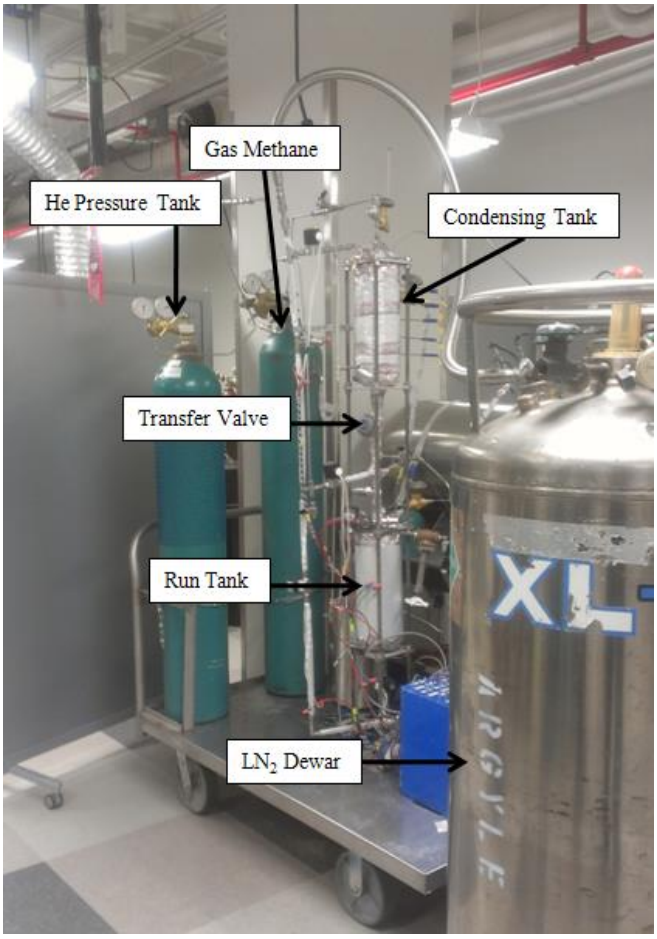

Figure 3.2: System Setup of the MCMU

Figure 3.3: (a) 2.2 L condensation Tank Wrapped with Cryogel Insulation and Fitted with Five Thermocouples. (b) Run Tank Wrapped with Copper Coil.

3.3 Third Generation 13 L Methane Condensing Unit (MCU)

A 3rd generation 13 L condensing unit was constructed to simplify the LCH_4 production process by eliminating the transfer process altogether. This was achieved by rating a stainless steel double ended cylinder to approximately 2.76 MPa (400 psi). Similar to the previous condensation unit, coils are placed around the tank to chill the thermal mass of the outer wall. Another similar characteristic to the previous system, the 13 L MCU is placed on a mobile cart for transportation purposes. However, the main purpose of the tank size was to fulfill the requirements of the HHFTF experiments. As steady state wall temperatures were required to reach final conclusions of the cooling of LCH_4 a higher capacity tank of 13 L was determined. Figure 3.4 shows the setup of the 13 L condensing tank with copper coiled wrapped around. Figure 3.6 shows a CAD model depicting the 13 L MCU system.

Figure 3.4: 13 L MCU CAD Model

Chapter 4: High Heat Flux Facility

4.1 High Heat Flux Test Facility Design Approach

The HHFTF system is developed primarily to test the heat transfer characteristics of fluids, particularly LCH_4. Materials selection for the construction of test stand was based on the compatibility with LCH4, the ability to withstand temperatures of at least 650 °C, and operability under temperatures as low as -175 °C. The full assembly of the HHFTYF in the vacuum chamber can be seen in Figure 4.1 and illustrates a close view of the test section and the idea of how the thermal energy is geometrically focused. The function of each component is explained in detail. The components that encompass the HHFTF are:

1. Stand
2. Cradle
3. Heating block
4. Test Section

The purpose of the vacuum chamber is to simulate altitude conditions, reduce the heat losses due to convection, and reduce the oxidation during heating.

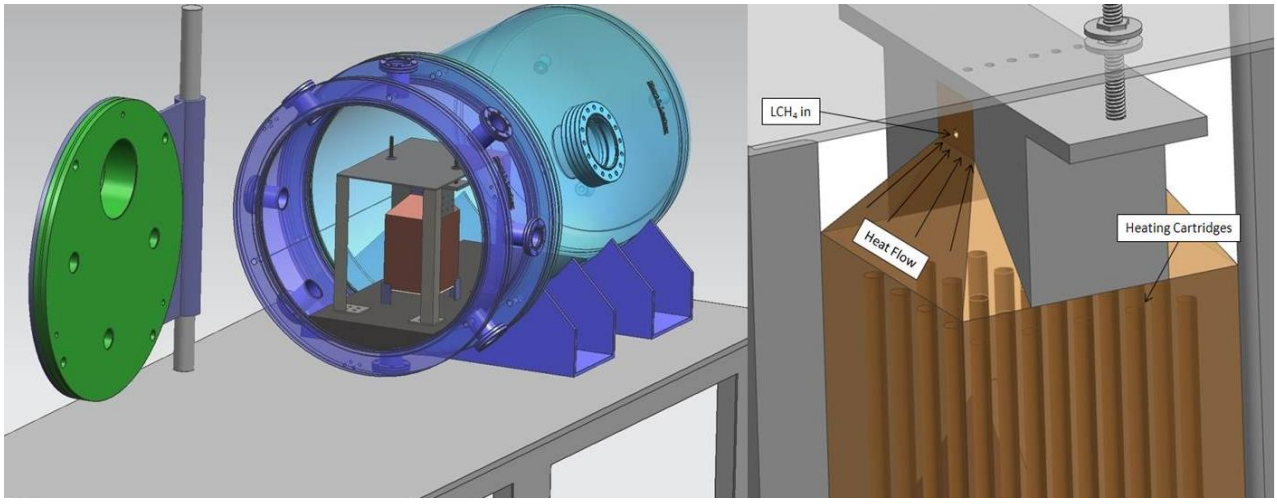

Figure 4.1: CAD Assembly of the High Heat Transfer Test Facility

4.2 Components

4.2.1 Stand

The HHFTF is supported by the stainless steel stand shown in Figure 4.2. The total weight of the HHFTF system is approximately 17.2 kg and sets the load that the supporting structure must withstand. The stand supports the heating block using small plates welded onto L-shaped brackets. The plates support the four corners of the block and leave the middle to support wiring from the heating cartridges. Atop the stand are two steel bolts which connect to the cradle. The stainless steel base plate extends past the heating block, offering placement of extra equipment such as a camera or an IR temperature camera.

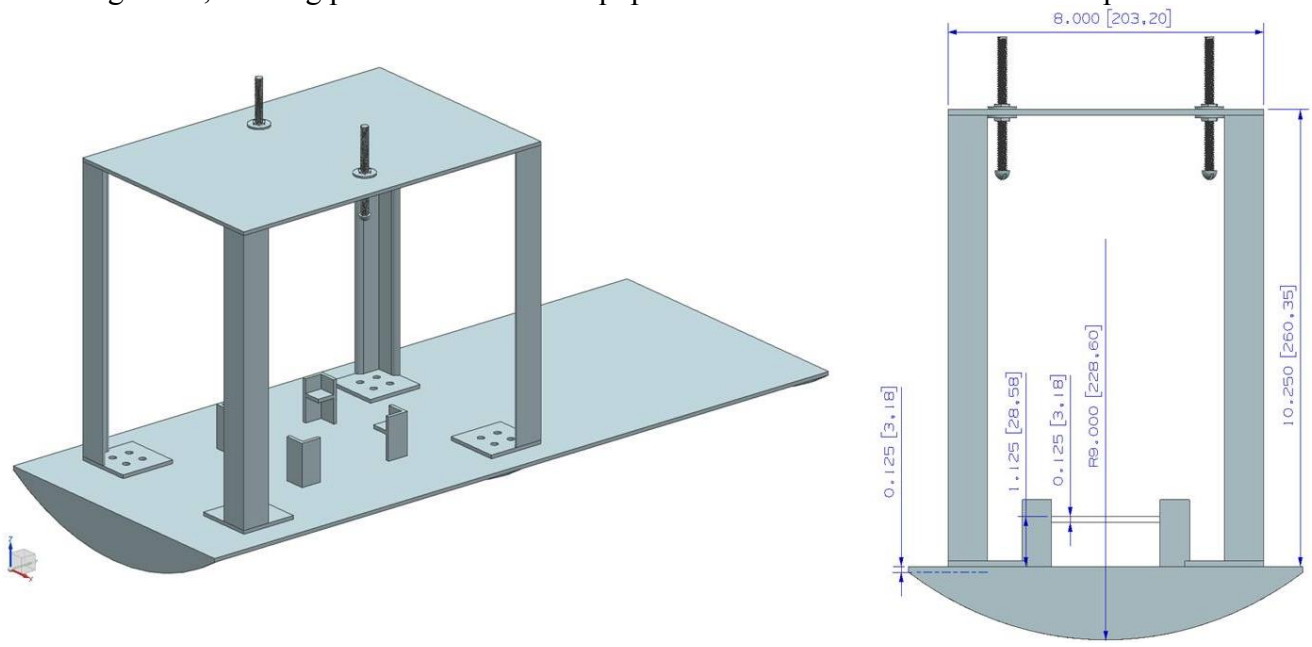

Figure 4.2: CAD Model of the Stainless Steel Stand

4.2.2 Cradle

The function of the cradle shown in the Figure 4.3 is to allow for firm contact between the test section and heating block. Aluminum T-6061 was chosen as the cradle for cost and machinability as compared to stainless steel. Figure 4.4 shows the two-bolt connection between the cradle and the stand for added pressure between the test section and heating block, ensuring a limited heat transfer loss due to a loose connection. A 3.175 mm slit is machined along the top of the cradle to allow for thermocouple placement.

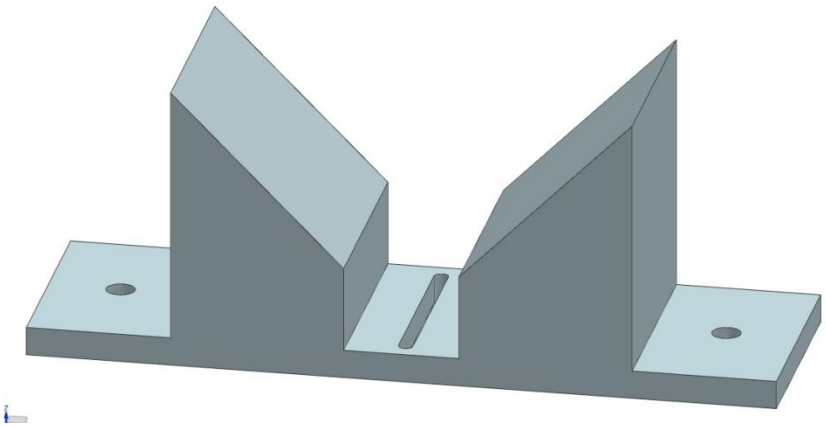

Figure 4.3: Aluminum Cradle

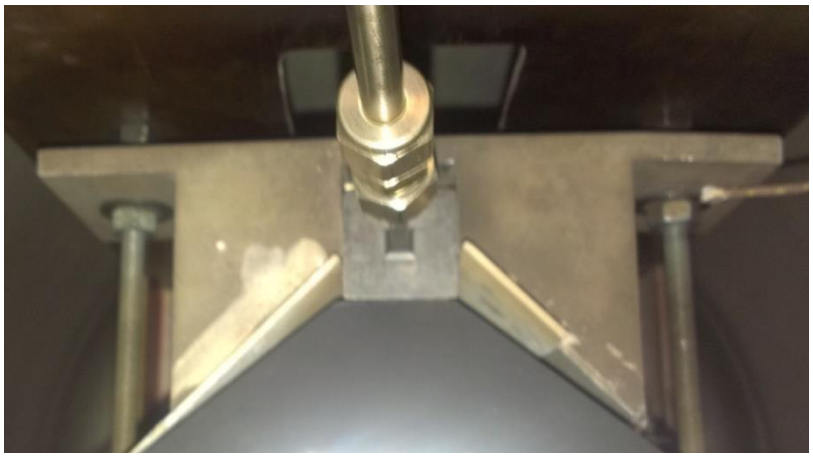

Figure 4.4: Assembly of the Cradle-to-Stand Connection

4.2.3 Heating Block

The heat source is generated by fitting up to 25 heating cartridges into a c122 copper block. The 10.2 cm x 10.2 cm x 17.78 cm heating block shown in Figure 4.5 is designed to geometrically focus thermal energy onto a 2.5 cm x 5.0 cm surface. Copper was chosen due to the material characteristics concerning the working temperature of 760 °C and thermal conductivity of approximately 365 W/(m °C). The temperature of the heating block is monitored by a set of K-type thermocouples placed along the tapered surface in between the cradle and heating block. This temperature is monitored partly due to safety concerns as well as the interest in retrieving the temperature test point corresponding to a given heat flux. Another consideration is that, due to oxidation, heat transfer from the heating block to the test

section may be compromised. For this reason, the surfaces of the heating block are cleaned every three to four tests.

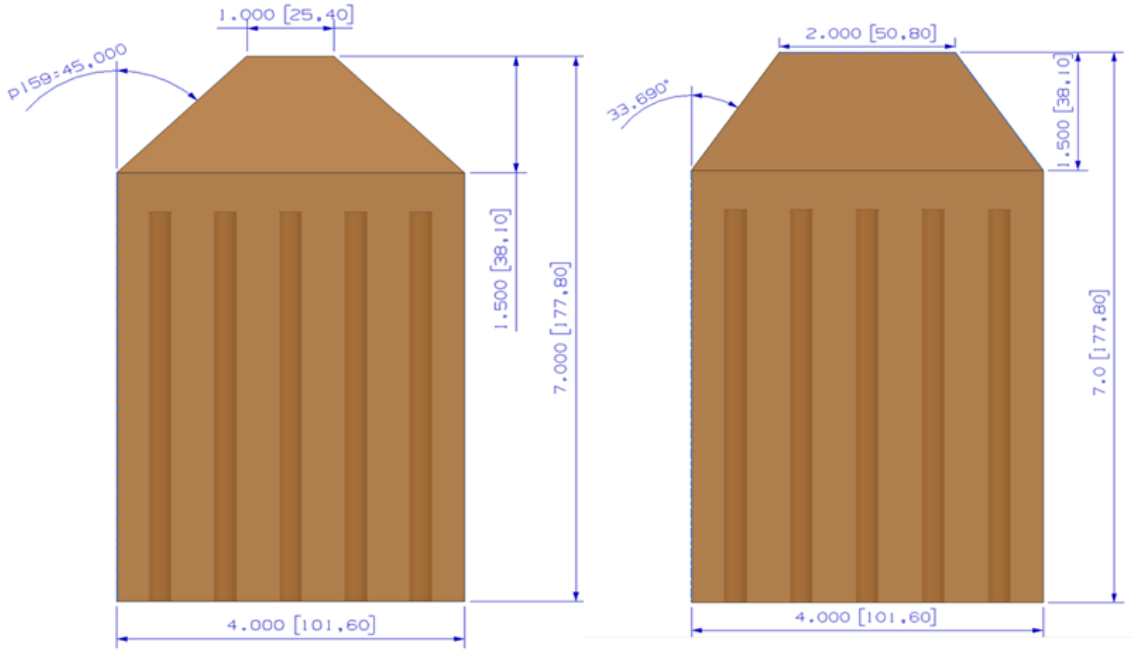

Figure 4.5: Copper Heating Block

Another area of concern in the performance of the heat transfer is the heat radiation loss. A preliminary experiment was conducted to investigate the heat transfer losses due to radiation by taking radiometry data as the block is heated. At the maximum test temperature of 400 °C, a 2.5% radiation loss was measured. Nonetheless the heating block is insulated with ceramic insulation fitted in between the cradle and heating block. Cloth fiber insulation is wrapped around the four sides of the heating block to reduce the heat radiation from the larger surface areas. Figure 4.6 shows an actual image of the heating block assembled with the insulation, thermocouples, and piping.

Figure 4.6: Heating Block and Test Section Assembly with Insulation

4.2.4 Test Sections (Cooling Channels)

The test section for the experimental setup is described as the section characterizing the heat transfer of LCH_4. The test section comprises of a single copper cooling channel (C18150) capable of flowing cryogens and handling temperatures of up to 800 °C. This cooling channel is equipped with six E-type thermocouples to measure the wall temperature of the channel and inlet and outlet wetted temperature measurements to measure the temperature of the fluid. When discussing the lack of LCH_4 heat transfer data, this absence also includes the investigation of cooling channel geometries most applicable in regen engines. Five cooling channels were machined each with a different hydraulic diameter (i.e. shape and size) representing milled and circular cooling channels. For this reason, the HHFTF features the ability to substitute test sections in a modular approach without the need to alter the heating block. A test section diagram is shown in Figure 4.7 specifying the exit length, the main heated segement, and the exit length locations. Cooling channels representing milled channels contain an extra

transition entry to smooth the flow of as LCH_4 enters the entry region. The following sections describe each test section cooling channel in detail.

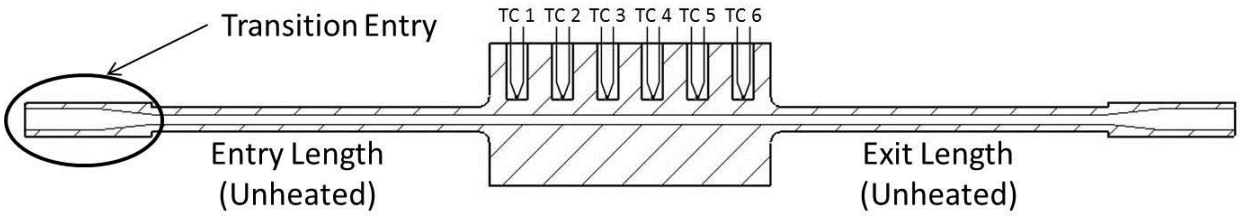

Figure 4.7: Drafting Model of a Test Section

Milled Cooling Channels

Three test sections representing milled cooling channels are tested based off of availability and importance in the scientific community. An initial effort to characterize milled cooling channel configurations commenced with testing a cooling channel with a 1.8 mm x 1.8 mm square cross section (Figure 4.8). The initial purpose of this test section was to test the transient heat transfer characteristics of LCH_4 employing the 2 L MCMU. This channel was developed during a collaboration effort by UTEP/NASA and manufactured at NASA White Sands Test Facility (WSTF). This channel represents a subscale representation of a milled channel located around the nozzle area suitable for the HD3 engine used for Project Morpheus' vertical test bed vehicle. The characterization of this location is key due to higher temperatures occurring at this location due to the decrease in area and increase in the velocity of the combustion gases.

Figure 4.8: Test Section with a Square Cross Section (1.8 mm x 1.8 mm)

The second test section contains a cooling channel with the same width (1.8 mm) but with a slight increase in height (4.1 mm height). This test section was also developed by NASA WSTF for the

purpose of representing a cross section located just after the combustion chamber upon entering the nozzle. Moreover, the increase in hydraulic diameter (D_h) has been a point of interest in determining the difference in heat transfer effects as increasing the height will cause an additional heat transfer enhancement by serving as a heat sink.

Figure 4.9: Rectangular cross section cooling channel (1.8 mm x 4.1 mm) installed into the HHFTF

The final milled cooling channel tested was a 1.8 mm x 14.4 mm HARCC. This cooling channel features an aspect ratio of 8 (height to width ratio) shown in Figure 4.10. As previously stated, an aspect ratio of eight is still considered to be beneficiary in terms of cooling. Though the fin effectiveness associated with the aspect ratio is beneficial in regen engines, this advantage does not necessarily apply due to the single channel design of the test section. However, advantages are still considered since the increase in height will give way to dissipating heat as the channel height increases. The heat transfer will be compared to the previously mentioned channels and verify this hypothesis. A note must be made concerning a minor flaw in the machining process of this test section. As can be observed in Figure 3.15, a cut not included in the final design was suffered during the machining process. Hence, an extra copper piece was welded to the heated segment. Although the weld itself is still copper, it must be noted in the case of uncharacteristic temperature deviations at this location or in the overall temperature behavior.

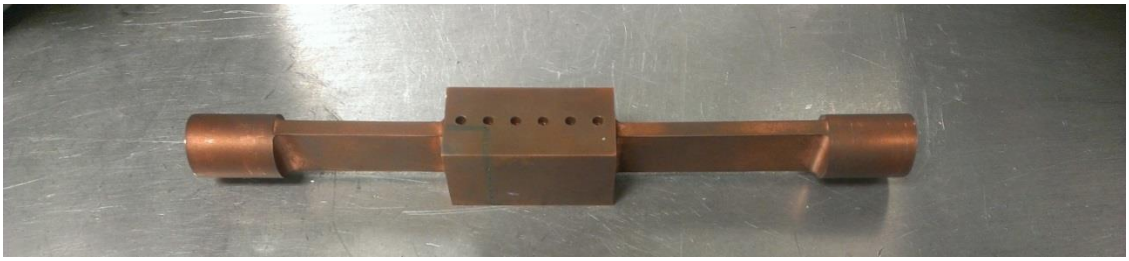

Figure 4.10: High Aspect Ratio Cooling Channel

Circular Cooling Channels

Circular cooling channels were designed to compare similar hydraulic diameters with different shapes and observe any benefit in thermal performance. Two circular test sections were implemented into the HHFTF. The first test section included a cooling channel configuration of an inside diameter (I.D.) of 3.2 mm. The design was chosen as a baseline to simplify the installation process. The outside diameter (O.D.) is designed to be 6.35 mm taking advantage of the Swagelok fittings and keeping the thermal mass relatively low. Figure 4.11 shows a picture of this test section.

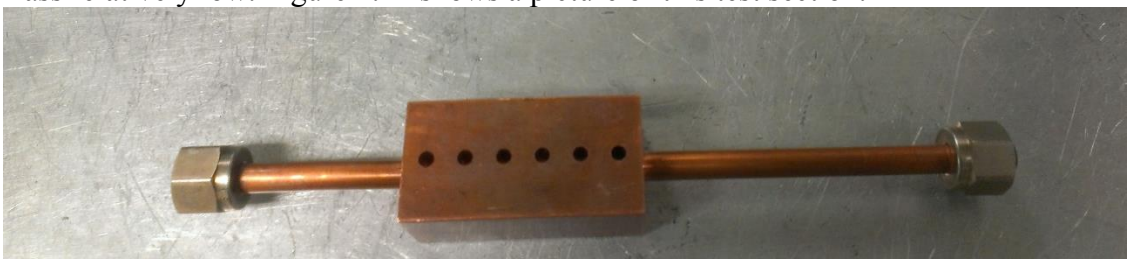

Figure 4.11: Circular 3.2 mm I.D. Test Section Cooling Channel

The final circular channel chosen for testing was designed to have a 6.35 mm I.D. and a 9.5 mm O.D. This design investigates the heat transfer behavior when increasing the diameter while keeping the thermal mass relatively low as possible. Figure 4.12 shows an image of the cooling channel.

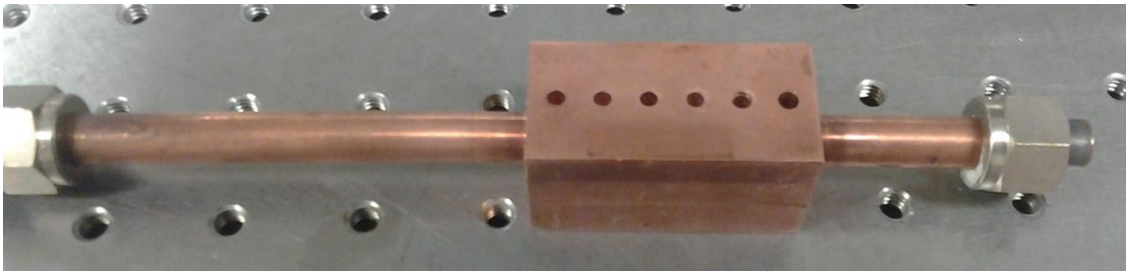

Figure 4.12: Circular 6.35 mm I.D. and 9.5 mm O.D. Test Section Cooling Channel

Chapter 5: System Integration and Components

5.1 System integration

The full experimental setup shown in Figure 5.1 shows the HHFTF integrated with the MCU. An experimental procedure is generated for simultaneous operation between the MCU and HHFTF arranged to meet the set conditions concurrently for the flow of LCH_4. The complete system setup consists of various components that must handle cryogenic temperatures, set testing temperatures, and electrical components that must endure vacuum conditions. A mass equipment and measurement list is tabulated in the Appendix for reference.

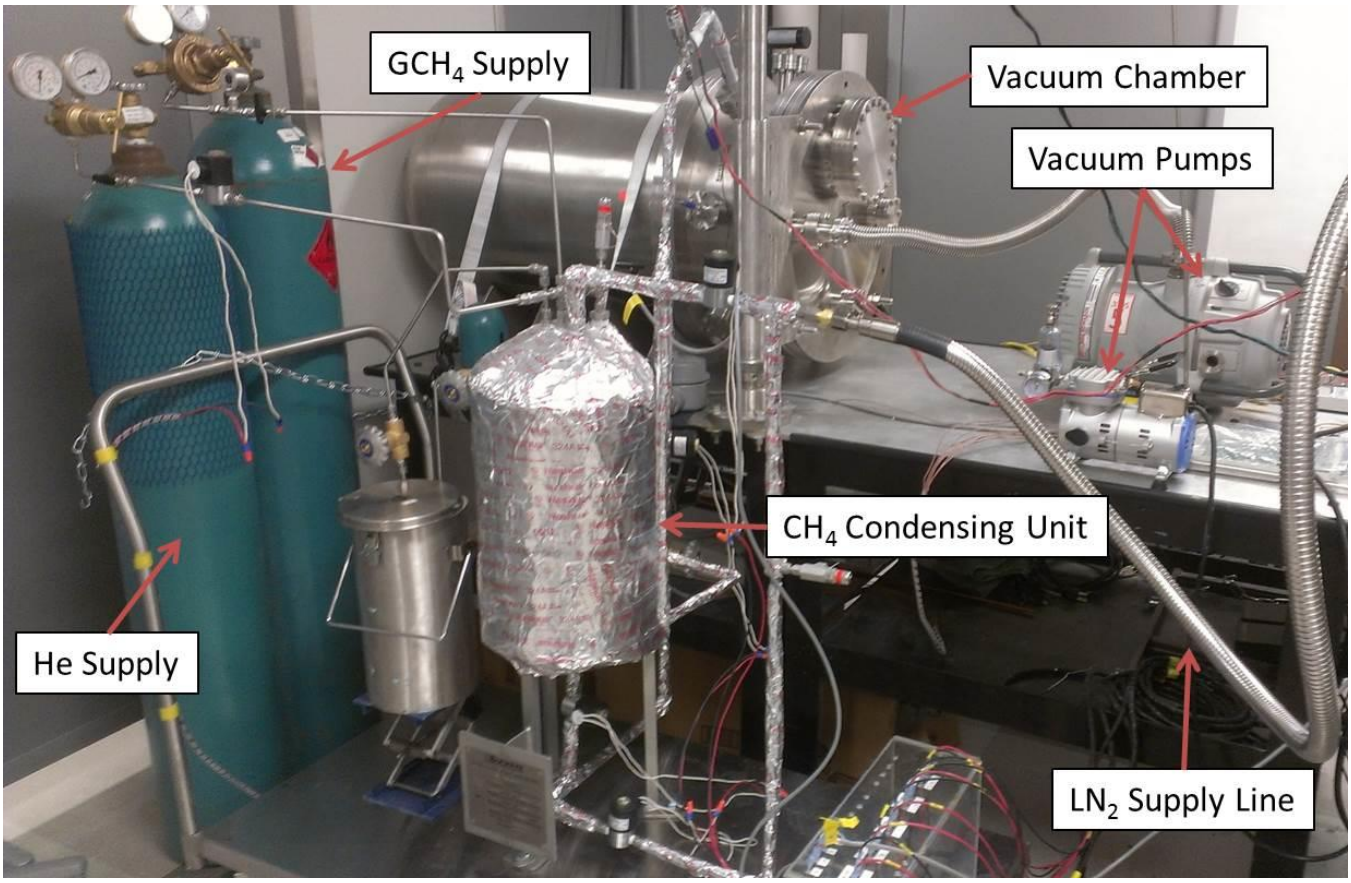

Figure 5.1: Experimental Setup with all Components

5.2 System Measurements

The measurement system is classified into three component categories including mass flow, temperature, and pressure measurements. These components comprise of a large part of the data analysis

and redlines incorporated into the test procedure. During a test, each member of the research team is responsible for carefully observing each measurement displayed in the DAQ system.

5.2.1 Temperature Measurements

As stated before, E-type thermocouples monitor the fluid level and the wall temperatures of both the condensing and run tank as well as the block temperature and surface temperature of the cooling channel. To measure any fluid and surface temperatures including the heating block and wall run tank temperature, sheathed thermocouples are used due to their resilience and life as compared to wired thermocouples. Wired thermocouples are used to measure the block temperature as they offer the advantage of measuring temperatures in small areas in a confined space. Figure 5.2 shows the variety of thermocouples used for this experiment.

Figure 5.2: Wired and E-Type Thermocouples used in the Experiment

5.2.2 Pressure Measurements

In addition to the thermocouples, thin film cryogenic pressure transducers (PT) shown in Figure 5.3 are installed into a line connected to the run tank. This pressure transducer acts as a set point when running experiments at the desired tank pressure. Additional PT's are installed upstream and downstream of the test section measuring the pressure drop across the channel. This also aids in the correlation of the mass flow rate of the fluid further discussed in the results section. These PTs are rated to 0 – 6.9 MPa and claim an accuracy of +/- .25% of the measured reading.

Figure 5.3: Omega Thin Film Cryogenic Pressure Transducer

5.2.3 Mass Flow Meter

The flow meter is secured into the propellant line just upstream of the test section. The flow meter utilizes a turbine to spin at a certain rpm depending on the density and velocity of the fluid. The flow meter used in this case is specially calibrated for use of LCH_4. Figure 5.5 shows an image of a Hoffer tied into the system propellant line. The flow meter contains a maximum flow rate of 17 LPM and is accurate to +/- .1% of the measured reading.

Figure 5.4: Hoffer Turbine Flow Meter Installed into the HHFTF Propellant Line

5.2.4 Data Acquisition System

A data acquisition (DAQ) system was put in place to inspect the system as the heating and condensing take place and to record data as the testing commences. Two NI 9213 16-Channel

thermocouple input modules are connected via USB to record all temperature measurements associated with the HHFTF. Data is recorded by an analog signal produced by the DAQ at a rate of 10 samples per second. Other measuring devices such as the pressure transducers are connected to a SCC-68 set at 10 Hz which is in turn connected to a NI PCI-6533. Each pressure transducer is connected to a 1/8 DIN process meter and controller sold by OMEGA. This process meter is used for signal conditioning and offers added convenience as the display can be seen by the personnel monitoring the pressure in the lines.

Figure 5.5: From Right to Left: NI PCI-6533, NI SCC-68, NI 9213 and Omega 1/8 DIN Process Meter (Bottom)

The setup of the panel display to view the real time output signals from the DAQ system is shown in Figure 5.6. The block diagram associated with the panel is shown in Figure 5.7. The front panel shows the measurements recorded from the test section, in-line pressures, heating block, condensing temperatures, and run tank wall temperatures. When the system is prepared and the test is ready to commence, a switch labeled “record on” is activated to begin recording data.

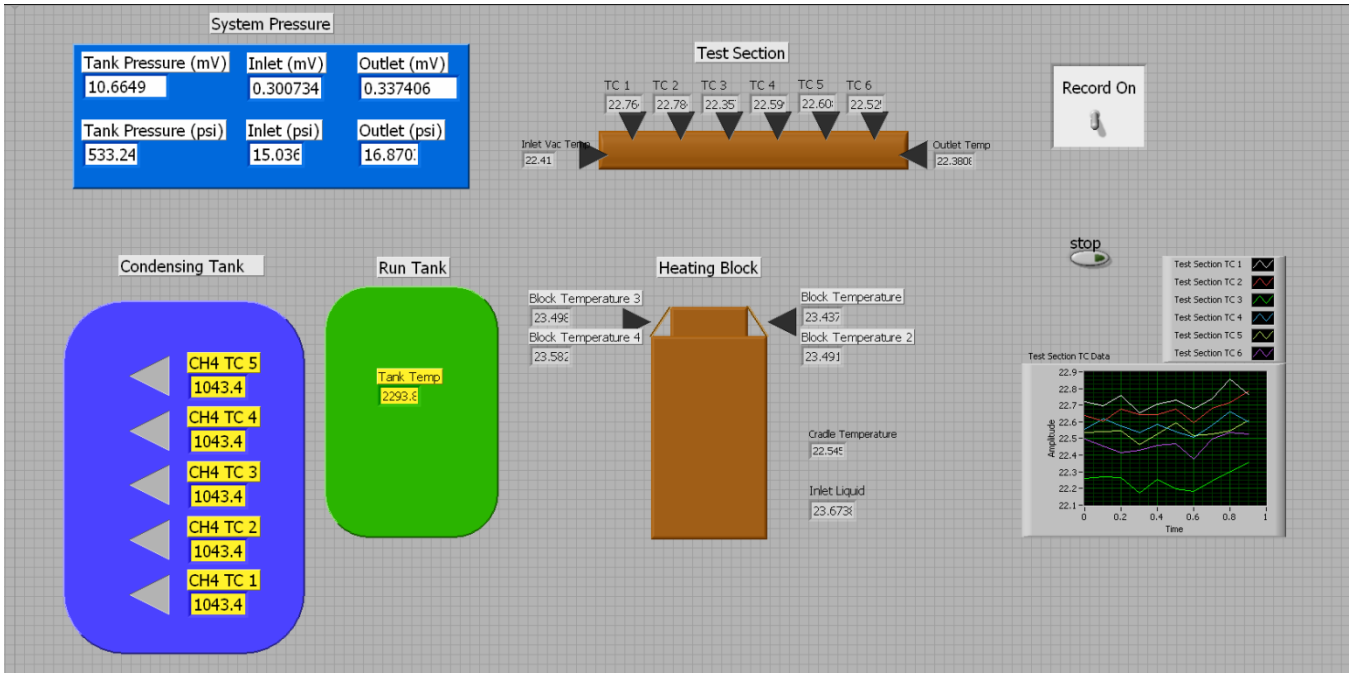

Figure 5.6: NI LabVIEW 9.0 Front Panel Interface

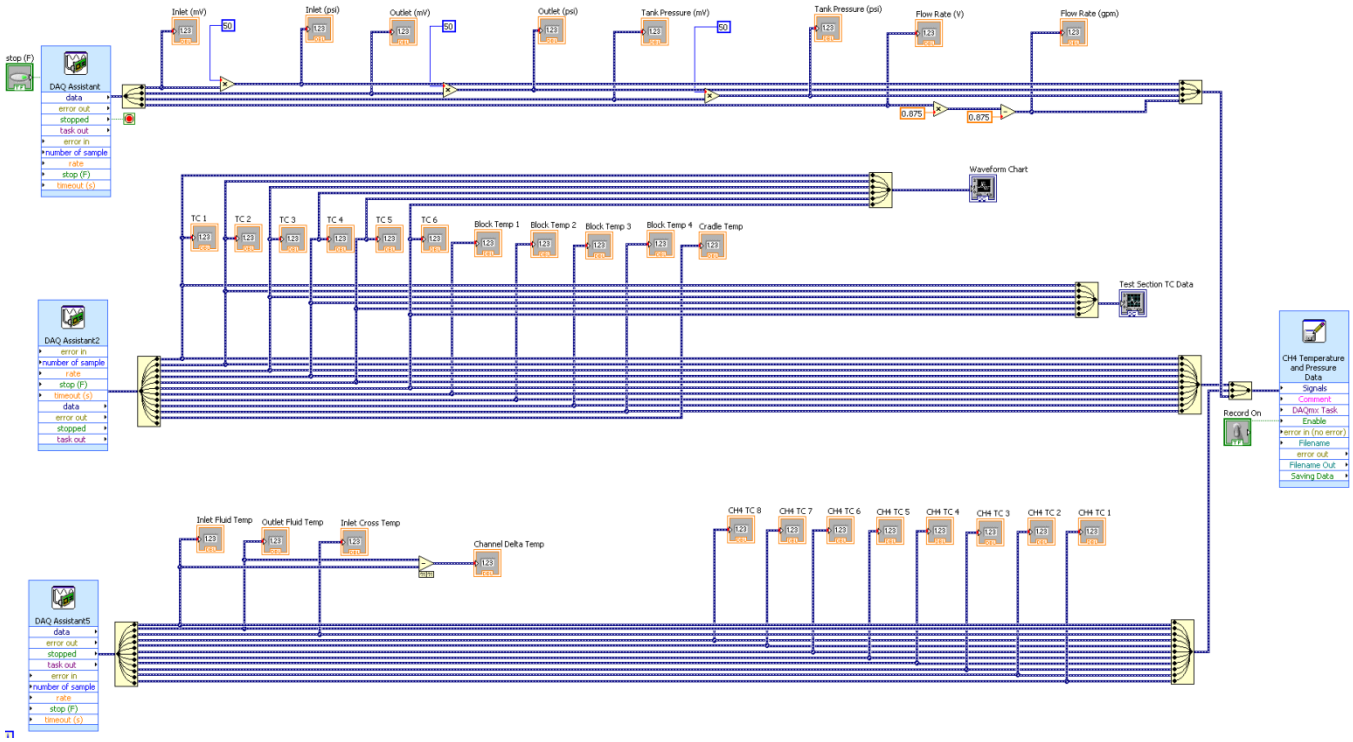

Figure 5.7: NI LabVIEW 9.0 Block Diagram

5.3 Valves

Five normally closed Gems sensor solenoid (Figure 5.8a) valves are installed for increased handling typically during a test sequence. These actuated valves are rated for cryogenic temperatures making them suitable for placement at any location where cryogenic fluid will pass through the system specified in the flow schematic (Figure5.14). An actuated valve is also placed after the run tank to open the flow for LCH_4 into the test section. The actuated valves are connected to an external power supply providing 5 Vdc.

Cryo-rated manual valves are primarily used to generate back pressure for the flow of cryogens. This gives a handle on the amount of LN_2 either preventing over-chill of the system or decreasing the temperature of LCH_4. Similarly, a back pressure valve shown in Figure 5.8b is placed downstream of the test section to provide adequate control of the flow rate of LCH_4 passing through the test section.

Simple quarter turn valves not rated for cryogenic conditions are used to protect vacuum pumps, allow CH_4 into the condenser tank, and allow supply of helium for pressurizing the condenser tank. Figures of each valve can be seen in Figure 5.9 a-c. Each valve is checked before a testing session for proper function.

Figure 5.8: a. Gem Sensor Solenoid Valve b. Manual Valve (Back Pressure Valve) c. Swagelok Quarter Turn

5.4 Gases and Propellant Line

The gaseous methane supplied to the condensing tank is C.P. (chemically Pure) grade 99.0% methane pressurized by C.P. grade gaseous helium to force LCH_4 through the test section at a given

pressure. Helium is chosen due to its inert characteristics and liquefies at a significantly lower temperature (1.2 K) than CH_4 eliminating the risk of condensing the pressurant.

Risk mitigations include the evacuation of air in all propellant lines and condensing tank. This ensures that CH_4 does mix with any surrounding air creating a flammable environment. In addition, the copper test section is heated to temperatures such that an oxidation layer will from along the inner walls of the channel creating dissimilar surfaces for each test if vacuum is not pulled. Vacuum is pulled through the propellant lines using a Rocker 300 vacuum pump.

Figure 5.9: Rocker 300 Vacuum Pump

Similar to the previous vacuum pump, the XDS 5 (Figure 3.20) vacuum pump pulls vacuum in the altitude chamber to prevent oxidation forming on the heating block and possibly the contact surface between the test section and heating block hindering the heat transfer between the two surfaces. In addition, pulling vacuum down to 8×10^{-2} torr (.002 psi) will minimize convection losses thus providing higher heat fluxes and simplifying data analysis.

Figure 5.10: XDS 5 Vacuum Pump used for the Vacuum Chamber

5.4 Electrical Components

System heating is driven by an electrical system to support up to 25 3.33 amp, 120 V, 400 W cartridge heaters shown in Figure 5.11. The cartridge heaters are controlled by a series of 6 solid state relays (SSR) each with a threshold of 50 amps (Figure 5.12). The SSR's are triggered manually by a switch connected to a DC power supplying 5 V. When the circuit is completed by turning on the switch, all relays activate allowing power to the heating cartridges. A complete electrical schematic pertaining to the cartridge to relay connection is shown in the Appendix.

Figure 5.11: Gordo Sales Inc. 400 Watt Heating Cartridges

Figure 5.12: 6 Omega Solid Sate Relays Connecting the Heating Cartridges

The power system is combined with the use of two Extech Quad Output DC power supplies (Figure 5.13) and standard 120 V power outlets. The power supply grants the ability to allow multiple components to be integrated into the system while limiting the amount of power outlets and thus, limiting the capacity of wires in the setup. Components connected to this power supply are the actuated valves and pressure transducers mentioned previously. The actuated valves are also activated manually by supplying a voltage of 5 V. The cryogenic pressure transducers are activated by producing an excitation voltage of 10 Vdc.

Figure 5.13: Extech Quad Output Power Supply

5.5 Test Procedure

The test procedure focuses on two simultaneously occurring processes: the heating of the block and the condensation of LCH_4. A step by step procedure is included in the Appendix, however, a brief

overview of the procedure is covered in the following sections. The schematic in Figure 5.15 is used as a reference when monitoring components and following the test procedure.

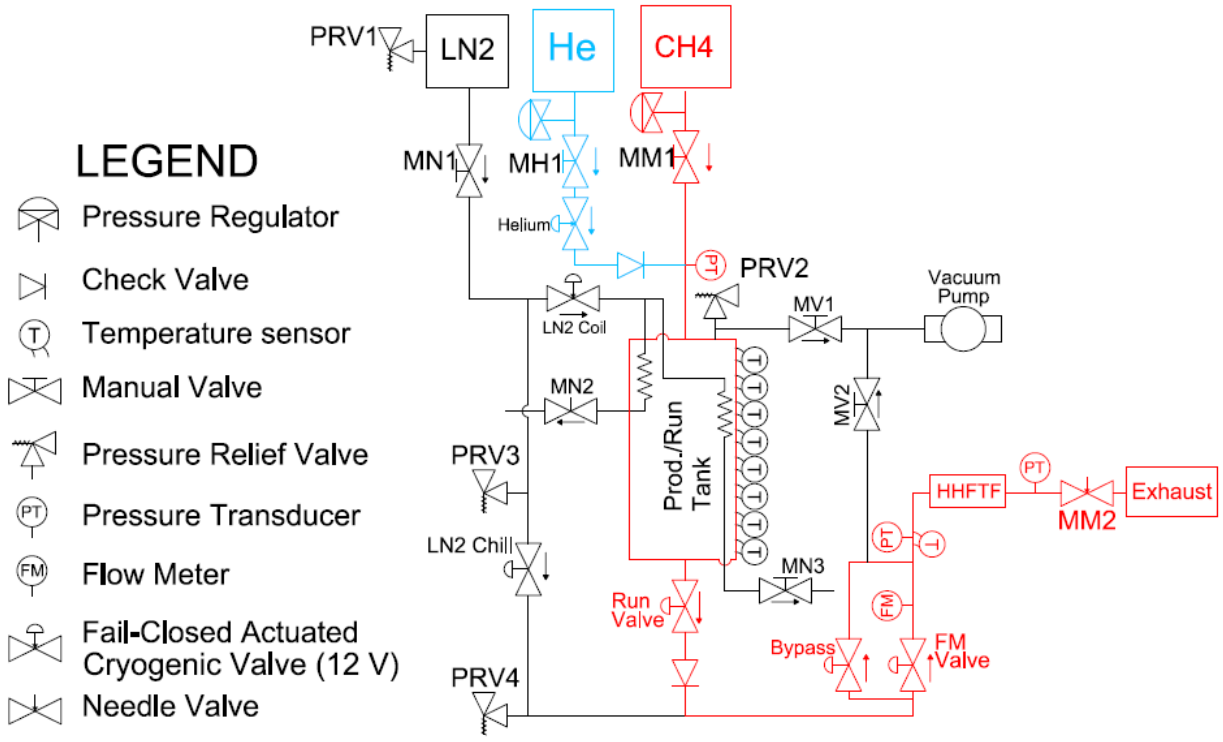

Figure 5.14: Flow Schematic of the MCMU Integrated with the HHFTF

5.5.1 Condensation and Transfer Procedure

The condensation process begins by evacuating the condensing tank and propellant lines of air. Then the outer and inner coil of the condenser are chilled with LN_2 until the tank temperatures measure approximately 170 K (312 R). The tank is then pressurized to approximately 1.4 MPa (200 psi) where typical condensing times take roughly one hour to condense nearly 13 L of CH_4. Tank temperatures are closely monitored to avoid any freezing that may occur either in the condensing tank or propellant lines. Temperatures approaching 95 K run a risk of freezing, thus, LN_2 is either shut off or the flow rate is decreased through the use of a back pressure valve until operable temperatures are reached.

5.5.2 Block Heating

The heating process is conducted in parallel to the condensation process. Before the block is heated, vacuum is pulled in the vacuum chamber using a XDS 5 vacuum pump shown in Figure 5.11. Typical vacuum conditions exist at approximately .5 torr. The heating cartridges are controlled via

manual switch installed onto a control box shown in Figure 5.16. The heating of the block is gradual. To aid in preventing failure of the heating cartridges, the block is heated at a ramp rate of about .5 °C per second.

5.5.3 LCH_4 Flow Test

Once the testing temperature is set, the lines are prepped to flow LCH_4 by chilling the test section until the inlet temperature reaches approximately 108 K. The same control box housing the heating switch (Figure 5.16) also accommodates for switches to control the actuated valves connected to the MCU. The data recording system is initiated once the pressure and block temperature/heat flux conditions are set. The DAQ system block diagram and system recording shown in Figure 5.7 allows the operator to examine the measurement readings as the experiment progresses.

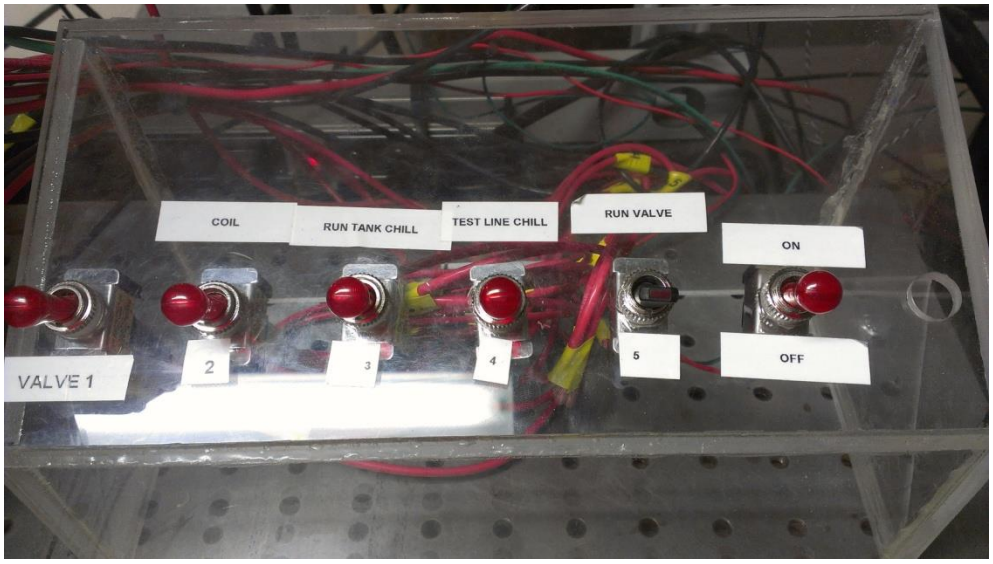

Figure 5.15: Control Paneling Controlling the Solenoid Valves and Temperature of the Block

As LCH_4 passes through the test section, the inlet and outlet temperatures and test section surface temperature profiles decrease as the fluid absorbs the heat. Once the LCH_4 has passed, the test section temperatures increase signifying the flow of helium. The condensing tank temperature levels are also closely monitored to verify the depletion of LCH_4.

5.5.4 Post Test Procedure

The LCH_4 captured is disposed of in a non-flammable environment by venting the remaining methane through a vent system. This process is combined with introducing an inert gas into the catch tank and vent system reducing the flammability levels of CH_4 to nearly zero. The piping system is purged with helium for several minutes to evacuate the tanks and exhaust the system of methane. All manual valves are opened to prevent trapping cryogenics into the system and over pressurizing the lines. In case of possible over pressure, relief valves set at 2.4 MPa are placed throughout the system. Cleaning of surfaces is done on the heating block and test section every 3-4 tests to limit the heat transfer losses due to oxidation build up. The resistance of each heating cartridge is measured to inspect the working condition of the cartridge. The maximum resistance of a unit is calculated to be 36 ohms. However, if the resistance is measured lower than 30 ohms, the cartridge is replaced. Thermocouples are tested before each experiment by measuring the temperature of known substances such as ice at 0 °C. Thermocouples reading temperature disparities of about +/- 5 °C in ice are replaced. During tests, thermocouple measurements may vary from other temperature measurements enough to give reason to replace the thermocouple.

Chapter 6: Results and Discussion

6.1 Test Matrix Development

The test conditions incorporated into each test matrix are focused primarily on the heat flux and test pressure (flow rate). The resultant heat fluxes are predicated by a water calorimeter test performed by correlating the block temperature to the heat flux applied to the test section. The test pressures are directly related to flow rates and subsequent Reynolds numbers. The flow rates are determined by performing a calibration test relating the pressure difference and the flow rate from a turbine flow meter. With both of these parameters, a test matrix is generated for each cooling channel tested.

6.1.1 Water Calorimeter test

The purpose for performing a water calorimeter test is to find the heat flux at a given block temperature. This is done by flowing water at a known flow rate while the tube is heated and measuring the inlet and outlet fluid temperatures. Knowing the properties of water with the addition of the mass flow rate and heat capacity, a heat flux can be calculated by using the conservation of energy equation for the steady flow of a fluid in a tube expressed as [17]:

$$Q = \dot{m}_{water} C_{p_{water}} \Delta T_{water} \tag{6.1}$$

This heat flux takes into account the resistance between the copper heating block and the test section. This heat flux is then used as a test point in the subsequent methane tests based on the temperature of the heating block. Due to the change in thermal mass from each test section, a specific heat flux will be extracted particular to the block temperature. Due to the size increase from some test sections, it is be impossible to reach the same maximum heat fluxes for each cooling channel considering a maximum block temperature of 400 °C. For this reason, each cooling channel will have a different set of test heat fluxes particular to the maximum heat flux attainable. Figure 4.1 shows the heat flux vs. block temperature relation from test section 1.8 mm x 1.8 mm cooling channel cross section. Ideally, the heat flux to block temperature relationship should yield a straight line. However, due to losses from the heat block to test section contact surface and additional losses, a curve fit yields a nonlinear behavior.

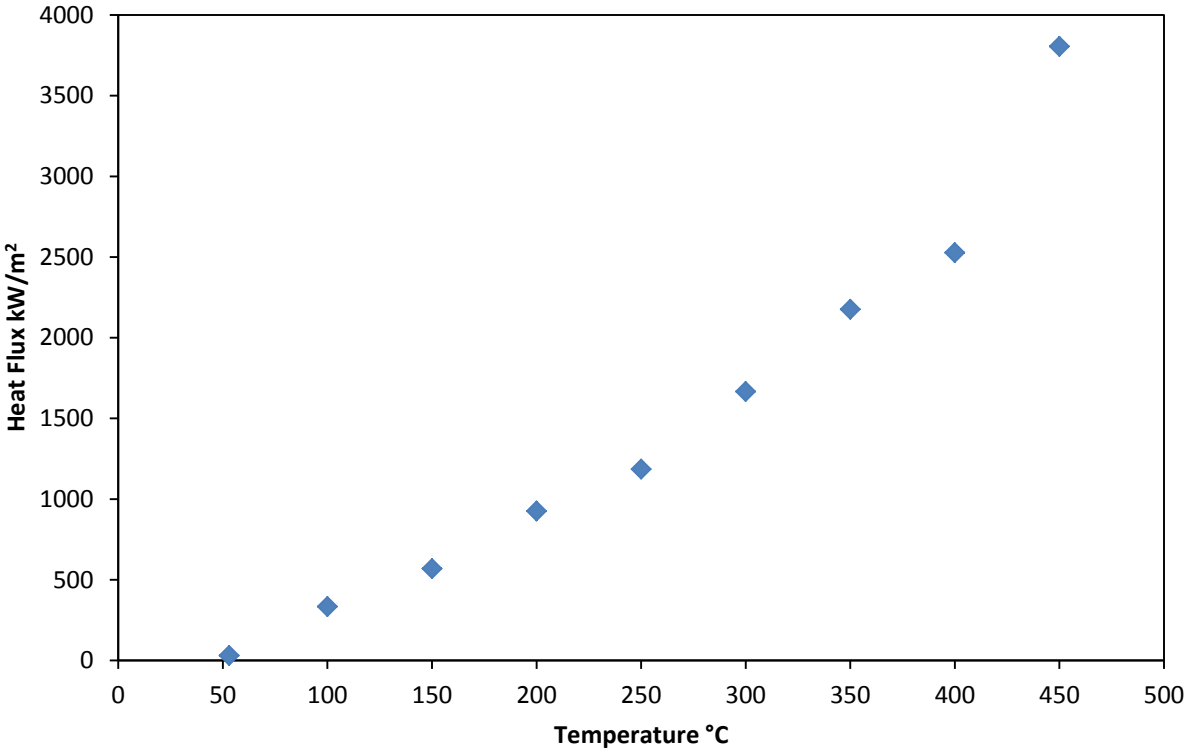

Figure 6.1: Water Calorimeter Tests used to find the Heat Flux at Set Block Temperatures for a 1.8 x 1.8 mm Cooling Channel.

6.1.2 Flow Rate Calibration Test

Similar to the water calorimeter test, a flow rate calibration test is performed to relate the flow rate to a pressure difference (ΔP) between the tank pressure and inlet pressure of the test section. The ΔP is induced by the back pressure valve shown in Figure 5.2 placed downstream of the test section. During a flow calibration test, the valve is opened gradually until the valve is fully opened while flowing LCH_4. The tank pressure during this run is set at 2.04 psi (300 psi). Though the calibration test is not dependent on the test section geometry, it is still performed after installation of each test section to ensure consistent results. The calibration provides a ΔP vs. mass flow rate curve as seen in Figure 6.2 (1.8 x 1.8 mm test section). The purpose of the test is not only to generate this relationship, but to relieve the turbine flow meter from failure. Cryogenic turbine flow meters are especially susceptible to malfunctions when exposed to flowing gases for short durations. This causes an over-spin of the turbine due to the high velocity of the gas.

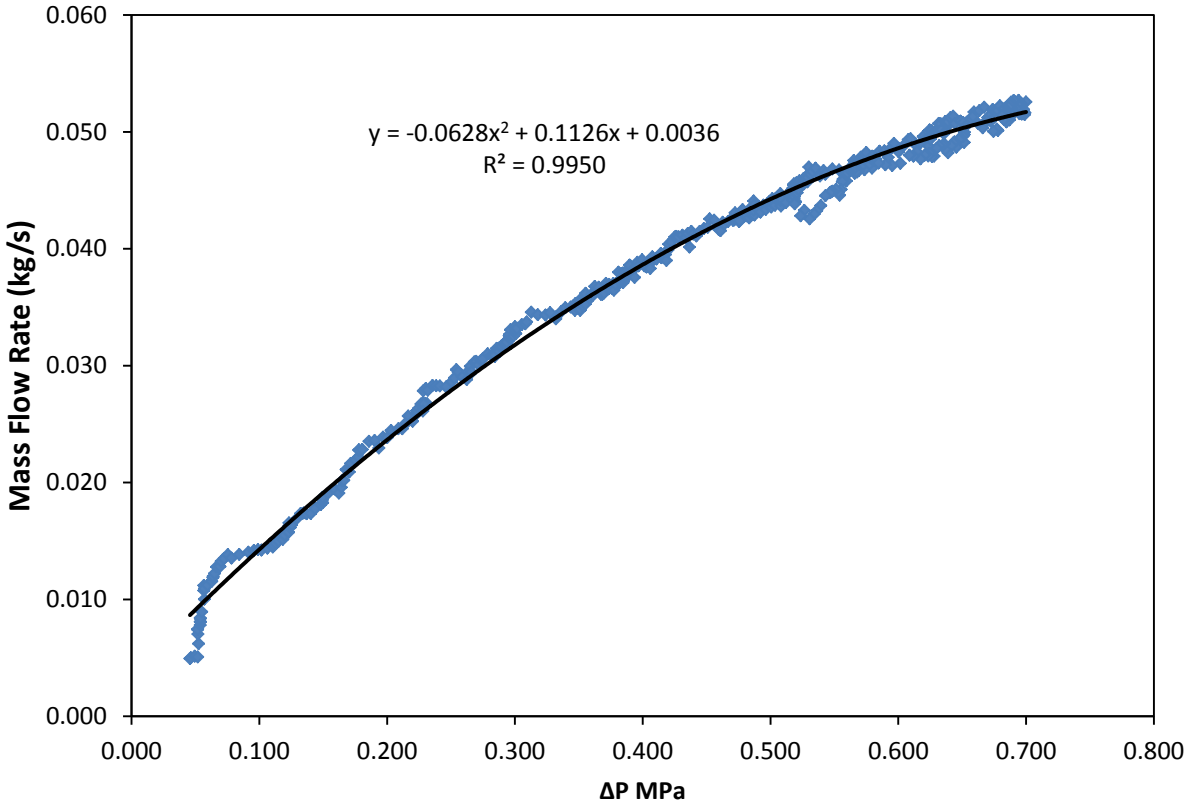

Figure 6.2: Methane Flow Calibration Test Relating the Flow Rate vs. ΔP

6.1.3 Test Matrices

The parameters kept constant for each test is the inlet temperature and tank pressures. The inlet temperature is kept approximately at -165 °C (-265 °F) or 108 K (195 R). The tank pressures range from 1.03 MPa to 2.07 MPa (150 psi to 300 psi). Table 4.1 shows the test matrix for the 1.8 x 1.8 mm cooling channel to investigate the transient heat transfer effects of LCH_4. Tables 6.1 to 6.5 show the test matrices of the channels explained previously. Each test section tested for steady state wall temperatures comprise of twenty tests each. As expected, the increase in thermal mass results in lower overall heat flux.

Table 6.1: Test Matrix for a 1.8 mm x 1.8 mm Square Channel

1.8 x 1.8 mm Cooling Channel					
Pressure (MPa)	Flow Rate (kg/s)	Heat Flux (MW/m^2)			
1.03	0.023	1.2	1.5	2.1	2.8
1.38	0.025	1.2	1.5	2.1	2.8
1.73	0.035	1.2	1.5	2.1	2.8
2.07	0.041	1.2	1.5	2.1	2.8

Table 6.2: Test Matrix for a 1.8 mm x 4.1 mm Cooling Channel

1.8 x 4.1 mm Cooling Channel						
Pressure (MPa)	Flow Rate (kg/s)	Heat Flux (MW/m^2)				
1.03	0.022	0.75	1.1	1.7	2.4	3.3
1.38	0.031	0.75	1.1	1.7	2.4	3.3
1.73	0.034	0.75	1.1	1.7	2.4	3.3
2.07	0.039	0.75	1.1	1.7	2.4	3.3

Table 6.3: Test Matrix for a 1.8 mm x 14.1 mm Cooling Channel

1.8 x 14.4 mm Cooling Channel						
Presssue (MPa)	Flow Rate (kg/s)	Heat Flux (MW/m^2)				
1.03	0.024	0.25	0.4	0.59	0.8	1.0
1.38	0.032	0.25	0.4	0.59	0.8	1.0
1.73	0.036	0.25	0.4	0.59	0.8	1.0
2.07	0.042	0.25	0.4	0.59	0.8	1.0

Table 6.4: Test Matrix for a 3.175 mm I.D. Cooling Channel

3.175 mm Cooling Channel						
Pressure (MPa)	Flow Rate (kg/s)	Heat Flux (MW/m^2)				
1.03	0.021	1.5	2.1	2.6	3.6	4.9
1.38	0.029	1.5	2.1	2.6	3.6	4.9
1.73	0.035	1.5	2.1	2.6	3.6	4.9
2.07	0.037	1.5	2.1	2.6	3.6	4.9

Table 6.5: Test Matrix for a 6.35 mm I.D. Cooling Channel

6.35 mm Cooling Channel						
Pressure (MPa)	Flow Rate (kg/s)	Heat Flux (MW/m^2)				
1.03	0.020	0.54	0.72	1.0	1.2	1.7
1.38	0.026	0.54	0.72	1.0	1.2	1.7
1.73	0.028	0.54	0.72	1.0	1.2	1.7
2.07	0.032	0.54	0.72	1.0	1.2	1.7

6.2 Test Section Measurements

When analyzing the results, two primary measurements taken from the test section are the temperatures and pressures. A more descriptive image showing the wall temperature measurements can be seen in Figure 6.2. The surface or skin temperature is measured by placing six E-type thermocouples along the channel 8.3 mm apart. Before the vacuum chamber is sealed, the thermocouple-to-channel surface contact is ensured by checking continuity between the thermocouple and the channel surface using a volt meter.

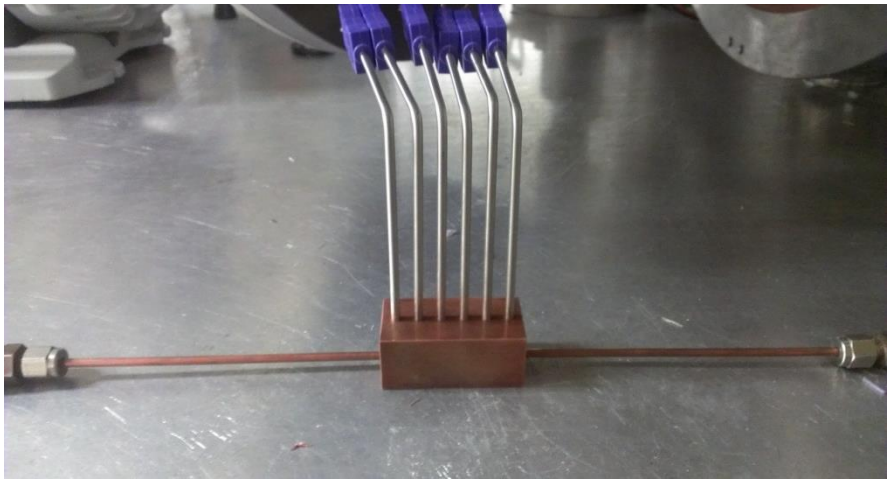

Figure 6.3: Test Section with Thermocouples placed on the Channel Surface

The fluid temperature measurements act as a method for determining the start of LCH_4 entering the channel and the moment when the LCH_4 supply has finished. In addition, in measuring the inlet and outlet wetted temperatures, the heat flux from the fluid can be calculated using the energy equation for the steady flow of a fluid in a tube stated previously but LCH_4 in this case. This calculation will then be

used to find the heat transfer coefficient. Figure 6.4 shows as representative illustration where the thermocouples are placed in the cooling channel and on the surface of the cooling channel. The first thermocouple was placed just before the entry length to prevent any obstruction from influencing the flow of LCH_4 from fully developing.

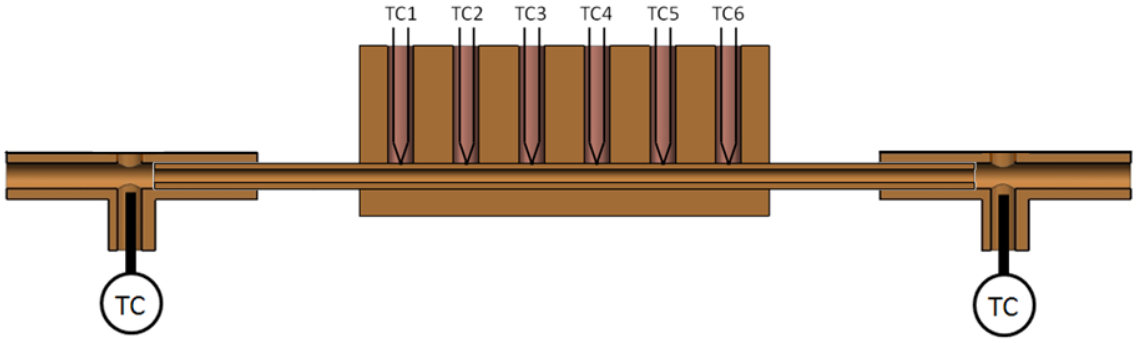

Figure 6.4: CAD Model of the Thermocouples Placed to Measure the Fluid Temperatures

In addition to the tank pressure, pressure transducers are placed at the inlet and outlet of the vacuum chamber. Figure 6.4 shows an image of the locations of the PT's. The locations can also be seen in the schematic (Figure 5.15). The fluid properties are evaluated at the bulk temperature and pressure due to the relatively large difference in wall temperature and bulk temperature [14].

6.3 Transient Methane Testing

Figure 6.5 and 6.6 show the fluid temperatures and surface temperature of the channel. The experiment is assumed to have begun when the temperature begins to decrease due to the flowing LCH_4. Even though the inlet temperature decreases as low as -150 °C in each experiment, the analysis is performed at points that yield subcooled LCH_4 according to NIST REFPROP based of the fluid properties when using the bulk temperature and pressure. The two temperature figures represent the highest heat fluxes of 2527 kW/m^2 with the highest and lowest pressures tested. This shows the effect that the increase in flow rate has on the wall temperature profile and the inlet/outlet wetted fluid temperatures. The temperature plots show that an increase in flow rate decreases the wall temperatures at a faster rate as expected. Due to the longer run time, the 1.03 MPa case shows an overall lower wall temperature at the end of the test. Run times are longer in lower pressure cases due to the capacity of LCH_4 for this test configuration (2 L capacity).

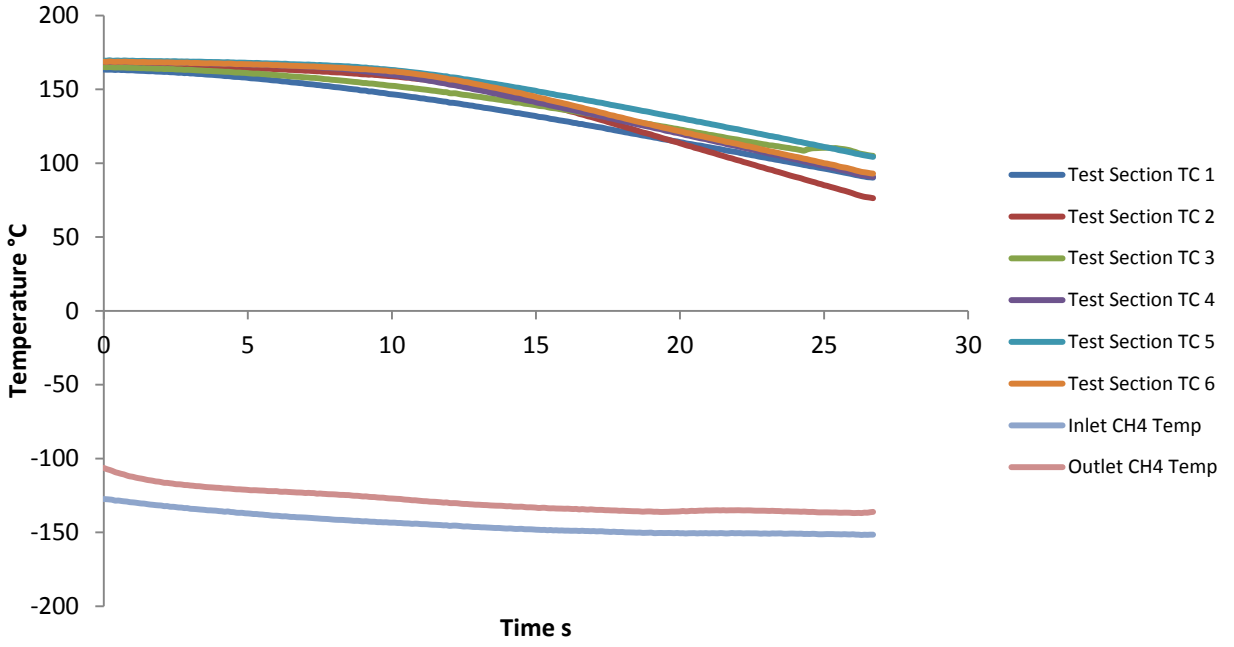

Figure 6.5: Fluid Inlet and Outlet Temperatures Along with the Surface Temperature Dispersion for Pressure 1.03 MPa and a Heat Flux of 2527 kW/m^2

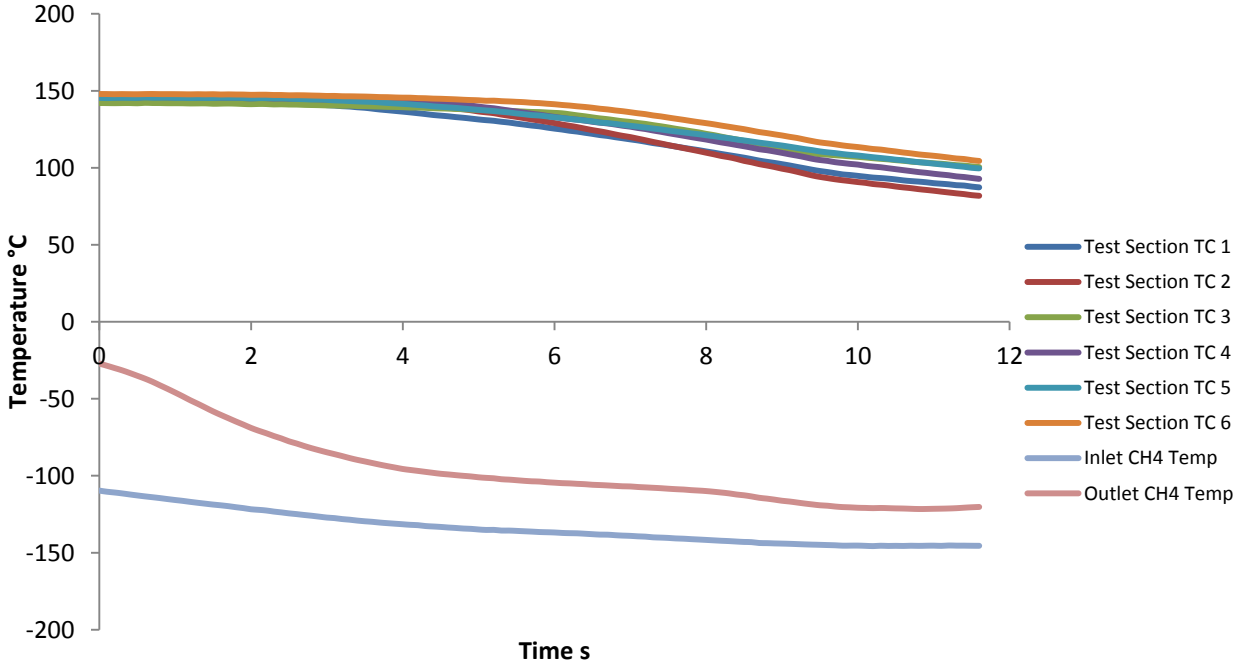

Figure 6.6: Fluid Inlet and Outlet Temperatures Along with the Surface Temperature Dispersion for Pressure 1.03 MPa and a Heat Flux of 2527 kW/m^2

The data is analyzed in a similar manner in Figure 6.7 where specific time steps are evaluated to calculate subsequent properties. The first time step is at time "0" when methane is considered to be subcritical. The number of time steps varies for each test due to the difference in run times between the test conditions. The Figure also illustrates the specific time steps for this particular test with the conditions in Figure 6.5. This particular plot shows that at "time step 15" (45 seconds on x-axis), the data is no longer evaluated. In the case for this test as well as the remainder of the tests, the presence of helium influences the wall temperatures even before an increase in wall and fluid temperatures which can be seen when calculating the heat transfer coefficient.

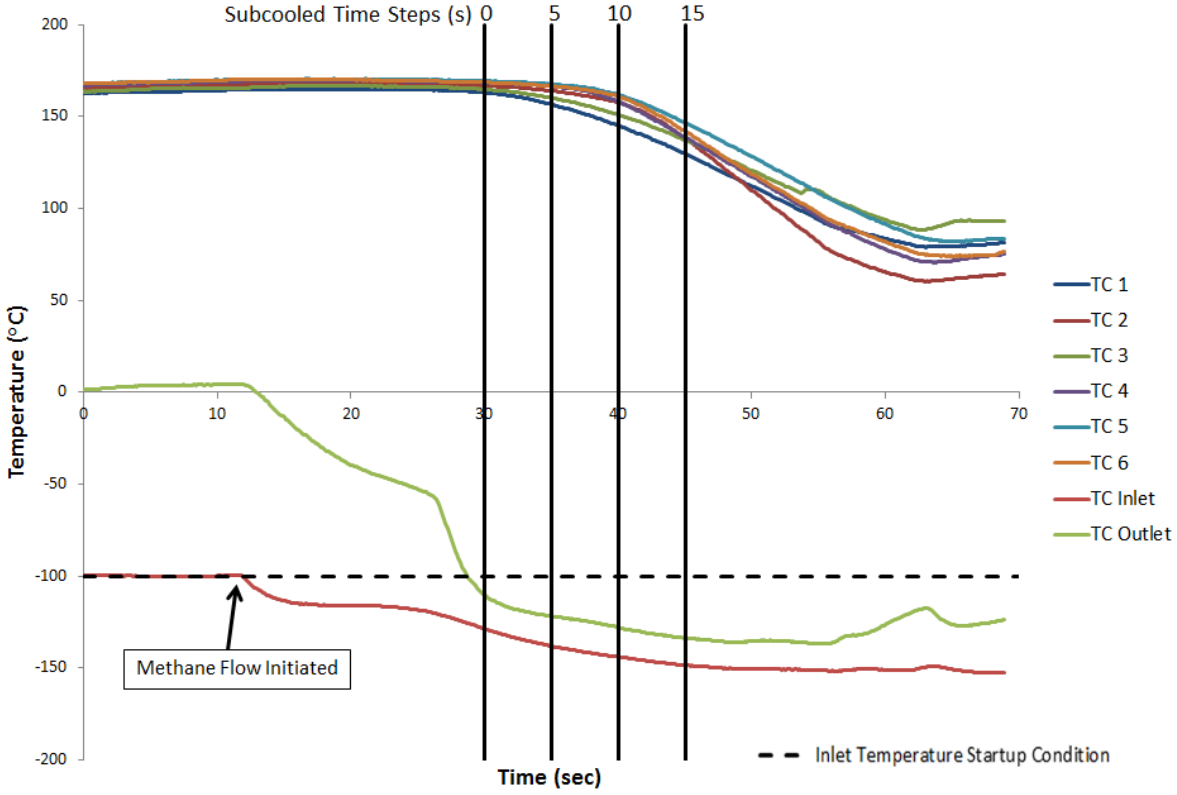

Figure 6.7: Temperature Plot Showing the Transient Wall and Inlet/Outlet Fluid Temperatures

Figure 6.8 and 6.9 show the inlet fluid and wall temperature relationship at the defined axial location. The ratio of T_s/T_i (surface temperature divided by the inlet temperature) in Figure 6.8 shows an increase as the time step increases. This is caused by the inlet temperature decreasing at a faster rate than the average surface temperature of the cooling channel. This is seen for every test due to the transient nature of the data. In addition observation is made in the same plots are the temperatures with respect to

the axial distance. The axial distance (x/L) presented in the Figures corresponds to the thermocouples (TC 1 to TC 6) shown in Figure 6.4. Where x is the location at a designated point along the channel and L is the total heated length of the cooling channel. For the test case presented in Figure 6.8, at TC2 (x/L = .26) the overall temperature spikes slightly and then proceeds to drop for the next two subsequent locations (TC3 to TC5). The pressure then increases slightly at the final axial location. These temperatures variations are attributed to film boiling occurring at these locations.

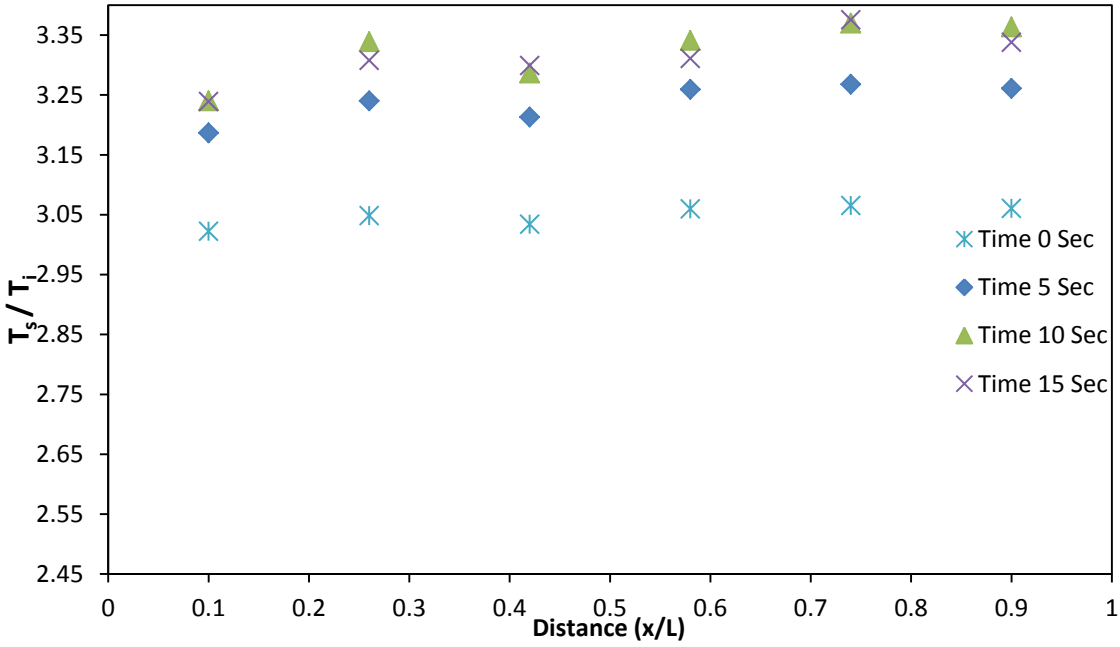

Figure 6.8: 3D Plot of the Normalized Temperature, Normalized Channel Distance, and Time for Test Point 1.03 MPa and a Heat Flux of 2527 kW/m^2.

Figure 6.9 shows a test case with the same heat flux but with a higher test pressure resulting in a higher flow Reynolds number. What is markedly noticeable in this figure occurs at TC 3 where a sharp temperature spike occurs. Then the temperature drops and stays constant for locations TC 3 and TC 4. The next two locations show a temperature increase through the end of the heated segment of the channel. This plot also agrees that film boiling is occurring in the channel before the flowing fluid has a chance to reach steady state. The temperature plots for each test show similar behavior with boiling occurring and also changing locations through the channel.

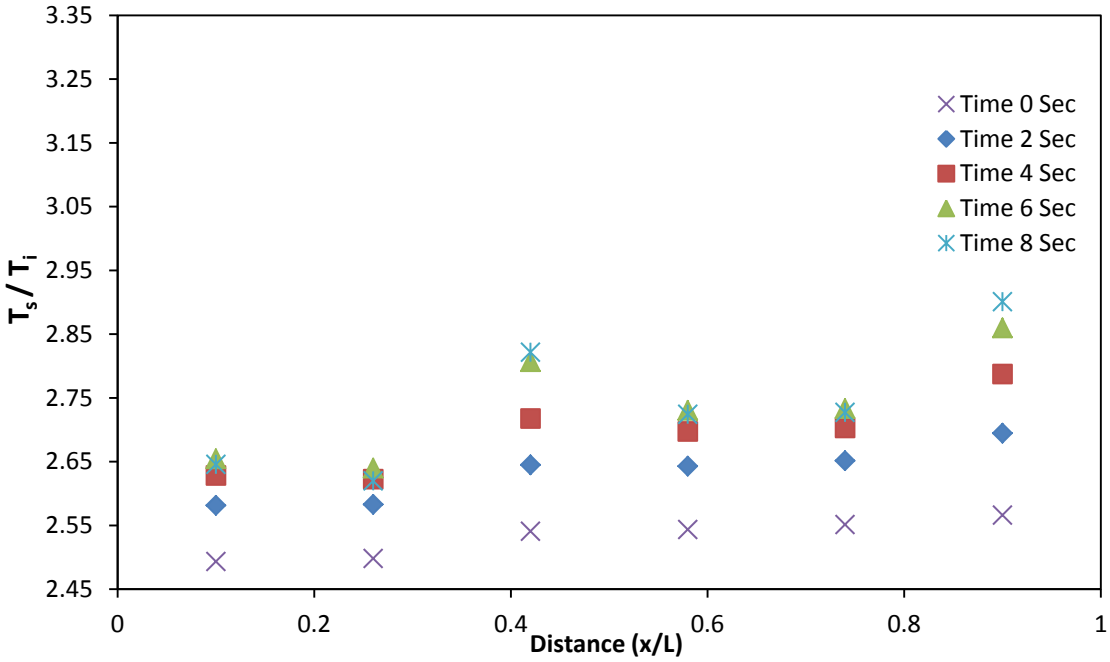

Figure 6.9: 3D Plot of the Normalized Temperature, Normalized Channel Distance, and Time for Test Point 2.06 MPa and a Heat Flux of 2527 kW/m^2.

With the fluid temperatures used to calculate the heat flux, the surface temperatures are averaged at each thermocouple for each time step to calculate the log mean temperature difference. A heat transfer coefficient can then be calculated using Newton's Law of Cooling equation. The heat transfer coefficient is then plotted as seen in Figure 6.10 and Figure 6.11 with respect to a normalized distance at the allotted time steps. For Nusselt number calculations, an average heat transfer coefficient is calculated by integrating h_x over the distance.

Figure 6.10 and 6.11 agree with the previously shown temperature plots. Certain fluctuations in the heat transfer coefficient indicate boiling in certain axial locations. The heat transfer coefficient also increases as time passes and further increases with an increase in flow Reynolds number.

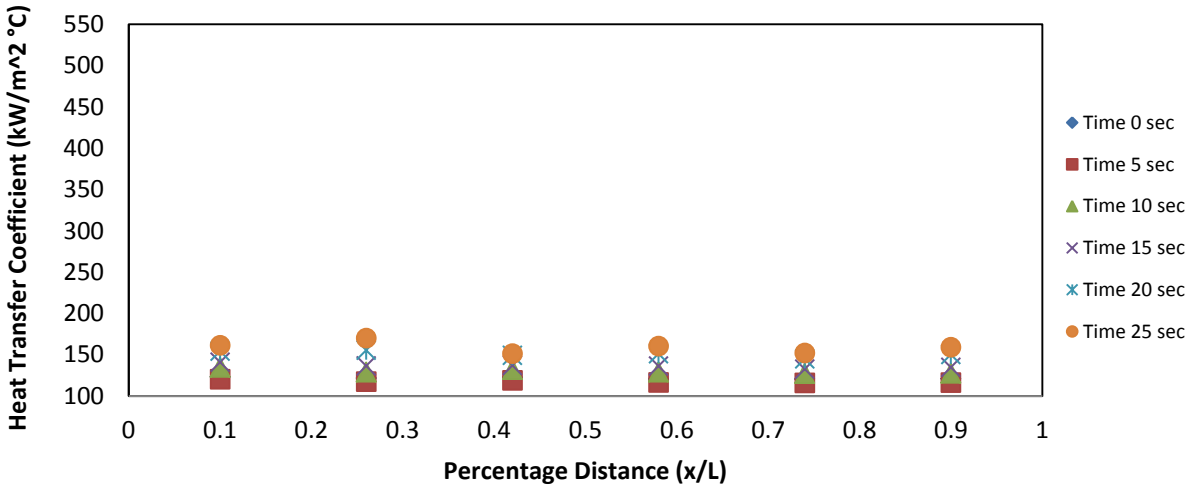

Figure 6.10: Heat Transfer Coefficient at a Determined Time Step at a pressure of 1.03 MPa and a Heat Flux of 2527 kW/m^2

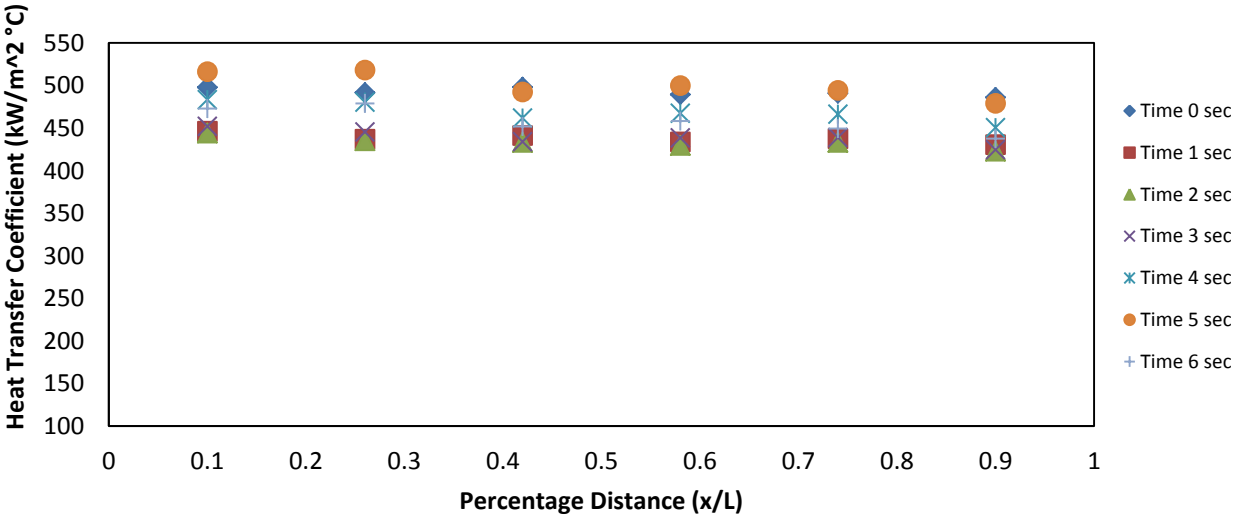

Figure 6.11: Heat Transfer Coefficient at a Determined Time Step at a pressure of 2.06 MPa and a Heat Flux of 2527 kW/m^2

Once the results were attained from quantities measured, a plot of the measured Nusselt number (Nu_L) in relation to the bulk Reynolds number (Re_b) was generated. NIST REFPROP version 8.0 is used to find the thermodynamic properties and to calculate the Nusselt and Reynolds numbers. The purpose of a Nusselt and Reynolds numbers is to examine the relationship between the fluid heat transfer

characteristics and the respective forces of the fluid flowing through the channel. The next step from this data is to develop an empirical correlation involving the Nusselt number in terms of Reynolds and Prandtl numbers incorporating fluid diffusivities in addition to the Re number.

Nu_L vs Re_b plot shown in Figure 6.12 is calculated with respect to each local heat transfer coefficient time step shown previously. A total of 84 Nusselt and Re_b numbers are calculated and plotted with a range between 120,000 and 370,000 demonstrating fully turbulent flow for each test. The trend of the data was fitted with three steady state forced convection empirical correlations including the Dittus Boelter, Seider-Tate, and the NASA Rocketdyne correlations. Of the three, the Seider-Tate (eqn 6.1) agrees the most considering the transient characteristics of the data. The viscosity correction term improves the agreement taking into account the variation of fluid properties due to the change in wall and fluid temperatures.

$$Nu_O = 0.012\, Re^{0.8} Pr^{1/3} \left(\frac{\mu_b}{\mu_w}\right)^{0.14} \tag{6.1}$$

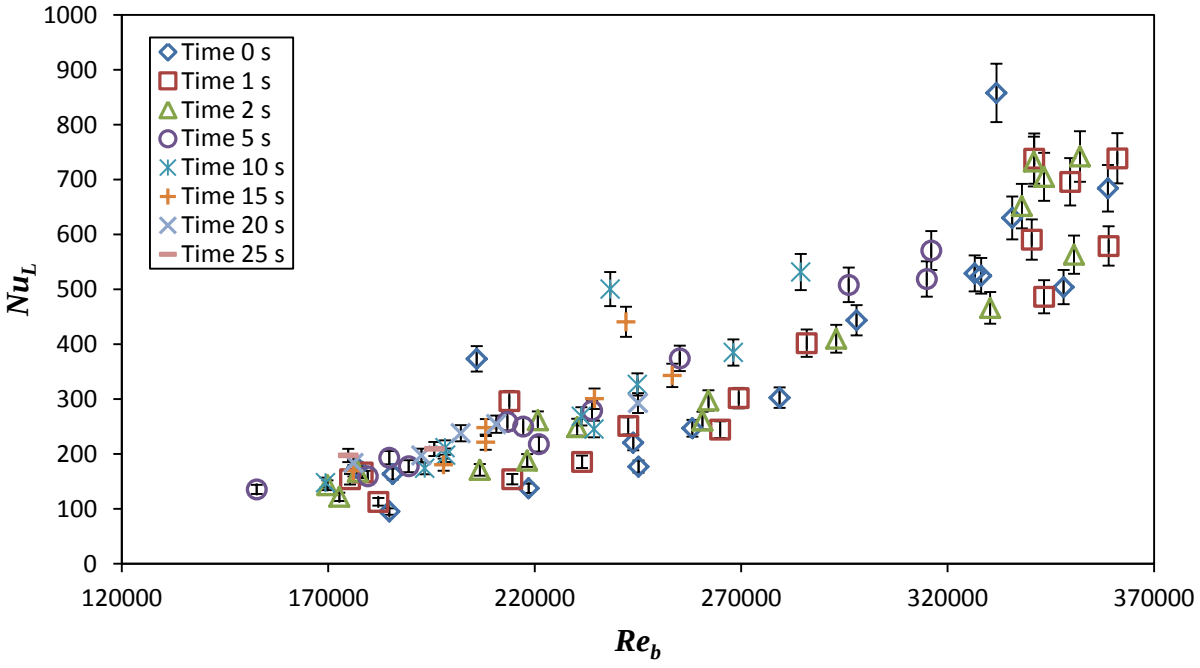

Figure 6.12: Measured Nusselt Number vs. Bulk Reynolds Number for Transient Forced Convection of LCH_4

6.4 Steady State Methane Data

The steady state heat transfer data is presented for the remaining four channels each with twenty test points. Analysis of the steady state data only considers the portion of data indicating steady state wall temperatures, relieving the necessity to observe the time steps for the allotted run times. Figure 6.13 shows a test run for a 1.8 x 4.1 mm rectangular channel with a heat flux of 1.7 MW/m^2 and pressure of 1.03 MPa (150 psi). The test is initiated when methane flows into the test section. The initial inlet and outlet temperature increases is the remaining LN_2 exiting the test section. Each test case includes similar temperature plots analyzed in this manner.

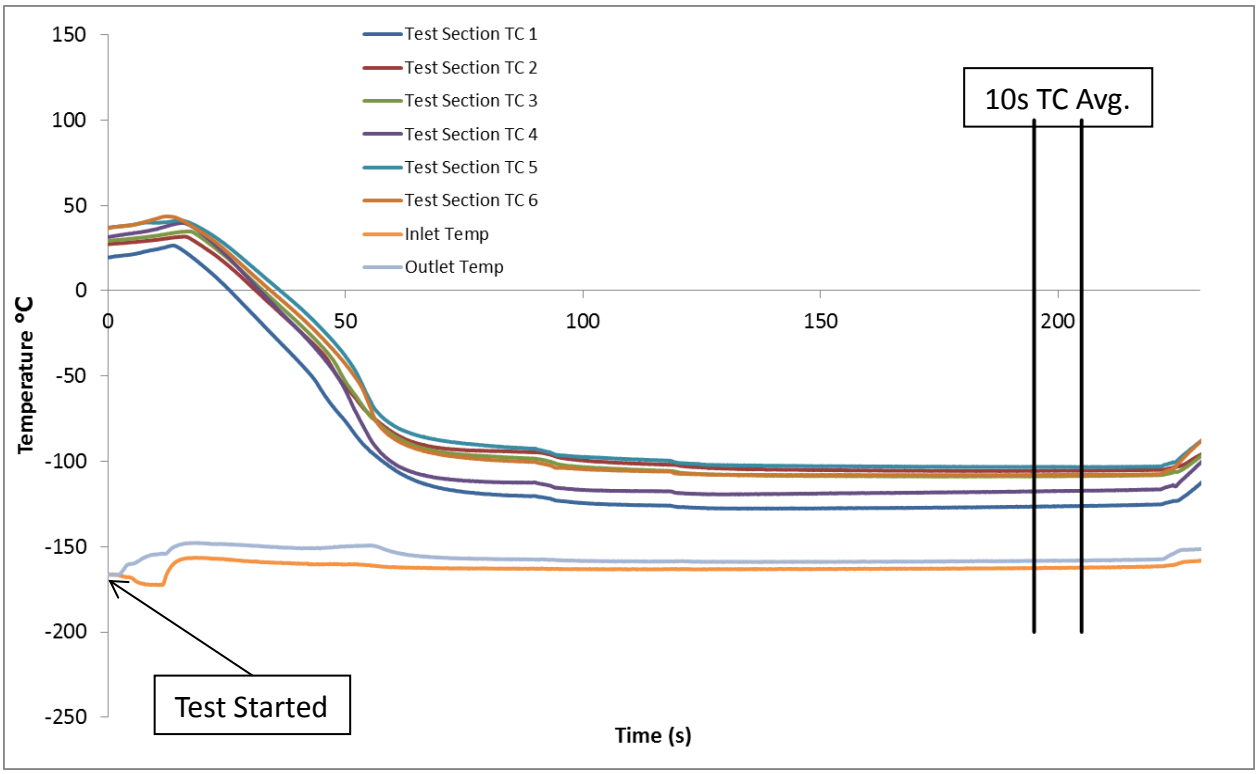

Figure 6.13: Wall Temperature vs. Time Plot Illustrating Steady State and the Point at which Data is Analyzed

6.4.1 1.8 x 4.1 mm Rectangular Channel

Initial steady state tests using a 1.8 x 1.8 mm square channel were performed by previous researchers to attain similar data in the present study. This data is presented in reference [13] and shown in Figure 2.9. The 1.8 x 4.1 mm channel and the latter geometries are a continuation to observe the heat

transfer effects when increasing the shape and aspect ratio. Figure 6.14 shows Nu_L vs. Re_b ranging between 65,000 and 132,000, achieving slightly lower Re numbers to the 1.8 mm square channel as expected due to the increase in D_h. Figure 6.14 also shows the data classified into two sets of data; "hot wall" and "cold wall". "Hot wall" is defined as temperature exceeding well over 0 °C and "cold wall" temperatures are below the said temperature. This separation was made to present the speculation of boiling transpiring in the channel at lower Nu number conditions. Though not indicated in the ensuing Nu_L vs. Re_b plots, the possibility for boiling is noted for each test section cooling channel by generating a plot similar to Figure 6.15.

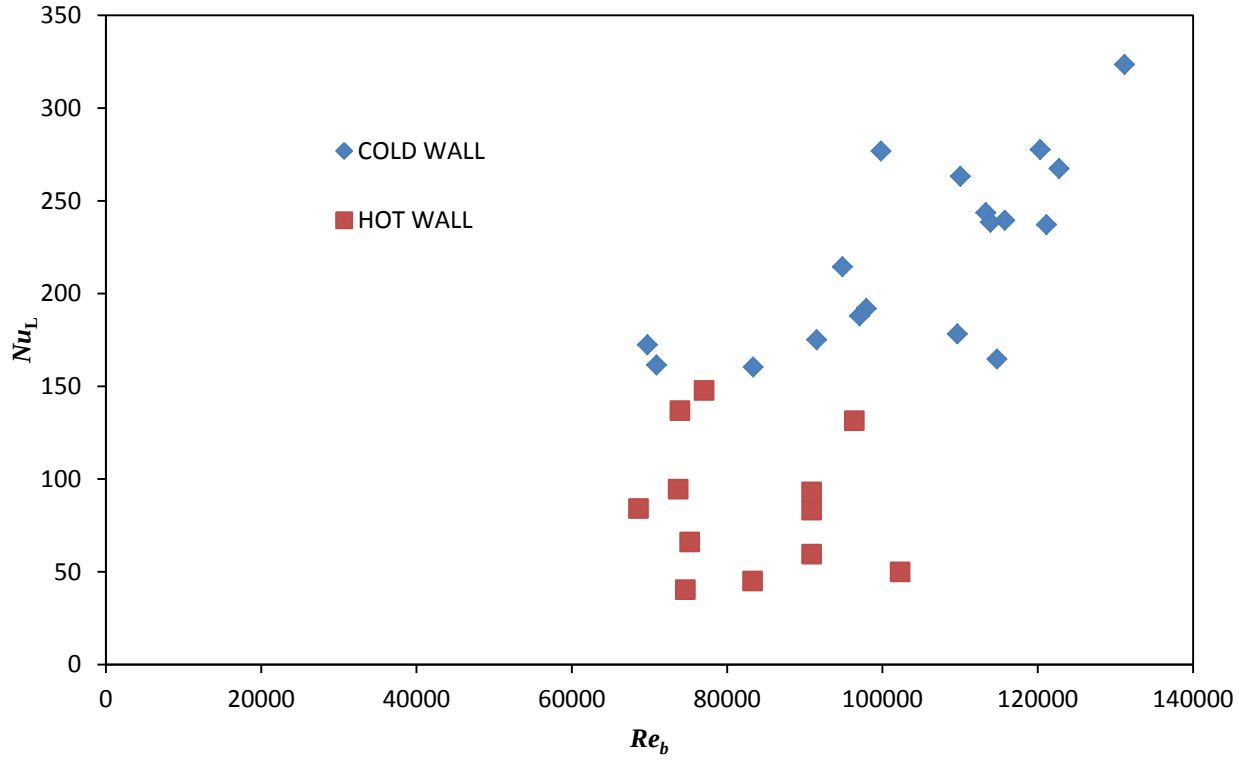

Figure 6.14: Nu_L vs. Re_b Plot for a 1.8 x 4.1 mm Channel

Transition boiling is speculated when observing Figure 2.10 and comparing this plot to Figure 6.15 (heat flux vs.ΔT_{sat}), where ΔT_{sat} is the difference between the average wall temperature and saturation temperature of the fluid at the average pressure. The velocities in m/s are also indicated showing the critical heat flux is largely dependent on the fluid velocity. The onset of transition boiling is speculated at approximately 100 K for velocities around 13-14 m/s with a critical heat flux of 2.5 MW/m^2 (1.5 BTU/(s-in^2)), similar to the critical heat flux reported by NASA Glenn. The speculation is

raised due to a decrease in heat flux with an increasing ΔT_{sat}. Critical heat fluxes are also observed for lower fluid velocities.

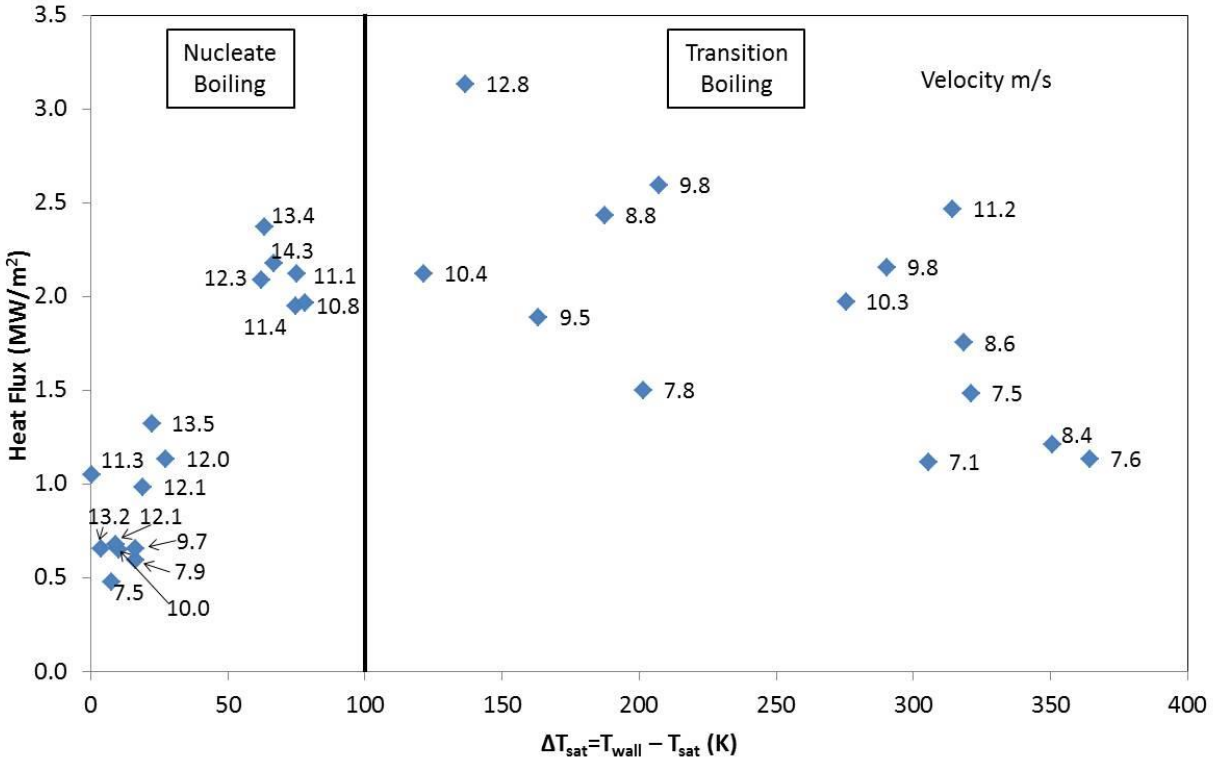

Figure 6.15: Heat Flux vs. ΔT_{sat} Plot Illustrating the Temperature and Heat Flux where Possible Transition Boiling Exists

Nusselt number correlations used to characterize the channel data were correlations investigated in literature concerning historical data, methane data, and data pertaining to boiling fluid effects. The correlation most representative of the dataset provided is the Jackson *Nu* number used for variations in thermal properties between the bulk and wall fluid properties. This correlation includes a density (ρ) and heat capacity (C_p) wall-to-bulk correction factor to take into account the variation in thermal properties in the radial direction [16]. Applying this correlation shows a coefficient of determination (R^2) of 0.77 linearizing the dataset for a relatively agreeable heat transfer prediction. The Jackson correlation was reported in [18] to work well with supercritical CH_4 in addition and additional supercritical fluids.

$$Nu_O = 0.026\, Re^{0.8} Pr^{0.4} \left(\frac{\rho_b}{\rho_w}\right)^{0.3} \left(\frac{C_{p,w}}{C_{p,b}}\right)^{0.4} \tag{6.2}$$

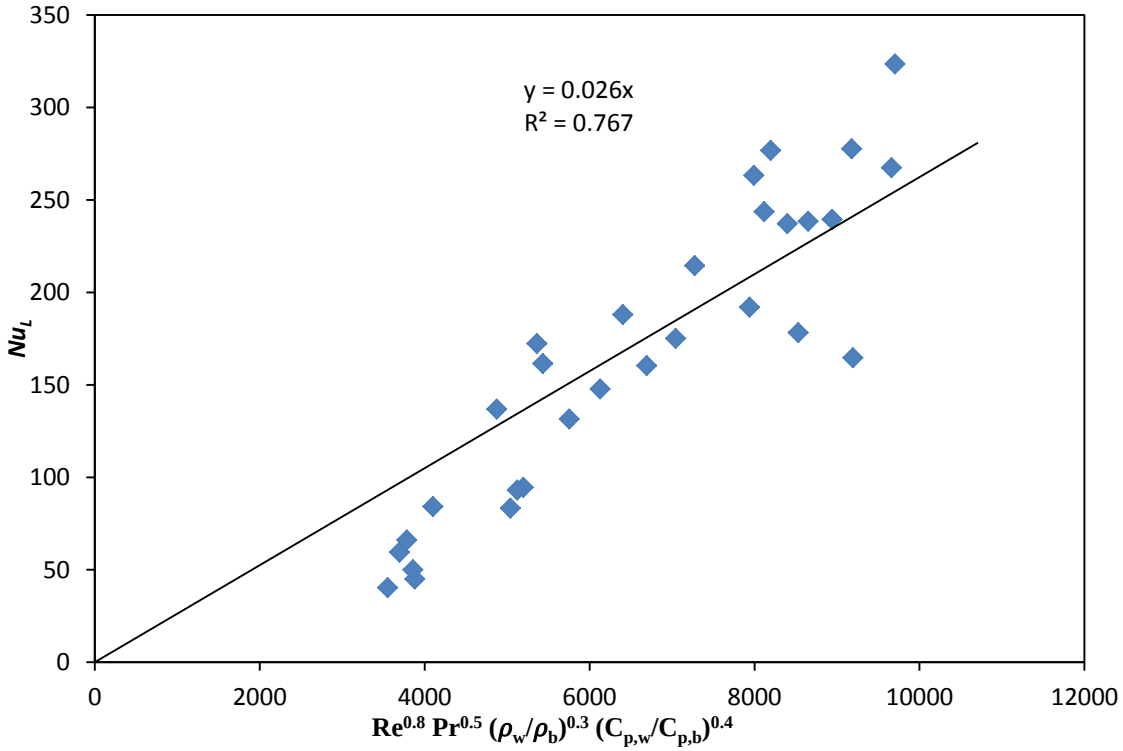

Figure 6.16: Measured Nusselt Number (Nu_L) vs. Theoretical Nusselt Number (Nu_O) Plot for a 1.8 x 4.1 mm Channel

Figure 6.17 shows a comparison between the measured (Nu_L/Nu_O) and theoretical *Nu* number (Nu_O). This serves to visually demonstrate the test points at which Nu_O agrees, over predicts, or under predicts Nu_L. At lower Re_b, Nu_O seems to over predict the empirical data with Nu_L/Nu_O ratios below one. As the Re_b number increases, Nu_O agrees slightly better with ratios closer to one. However, with the increase of Re_b, Nu_O under predicts the behavior seen in the measured data. The overall average ratios for each test point is approximately 0.9 showing the effectiveness of the prediction.

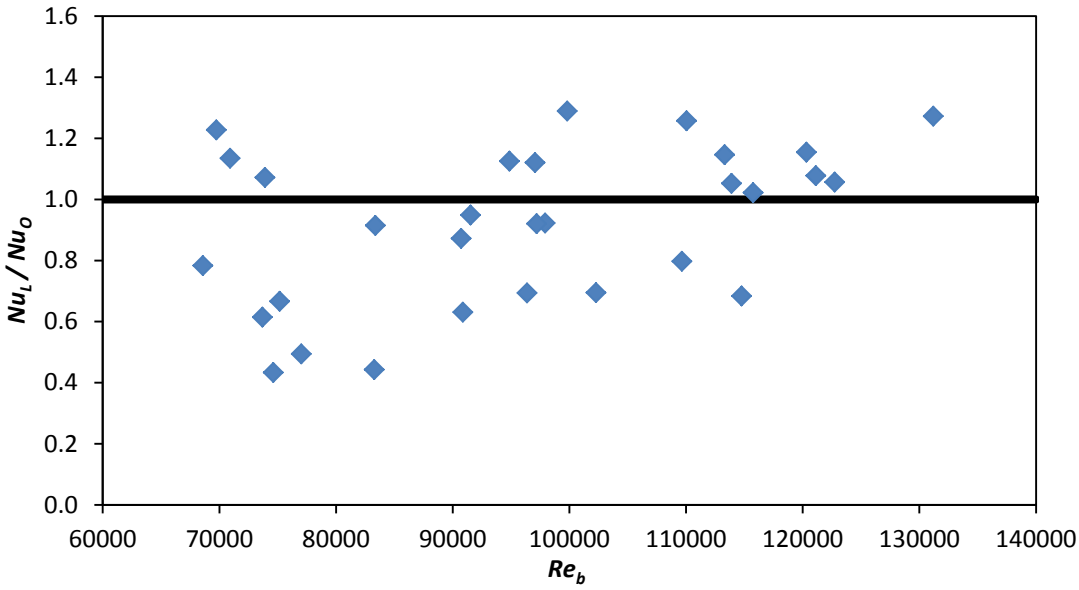

Figure 6.17: Nu_L/Nu_O vs. Re_b Plot for a 1.8 x 4.1 mm Channel

6.4.2 1.8 x 14.4 mm High Aspect Ratio Cooling Channel

The HARCC was influenced by ongoing research proving that aspect ratios up to 8 attain a thermal performance improvement especially when applied in regen engines due to the incorporation of the fin effectiveness as outlined previously. In this study, a single channel is used possibly nullifying this effect. In addition, the significant increase in thermal mass has shown lower heat fluxes resulting in the inability in possibly comparing the heat transfer performance between the two channels.

Figure 6.18 shows Nu_L vs. Re_b for twenty test points of the HARCC. Re_b ranges from 25,000 to 53,000, lower Re_b numbers than the previous two test sections. This is caused by the increase in D_h resulting in lower velocities directly affecting Re_b. The increase in area also decreases the heat transfer coefficient ultimately lowering Nu_L.

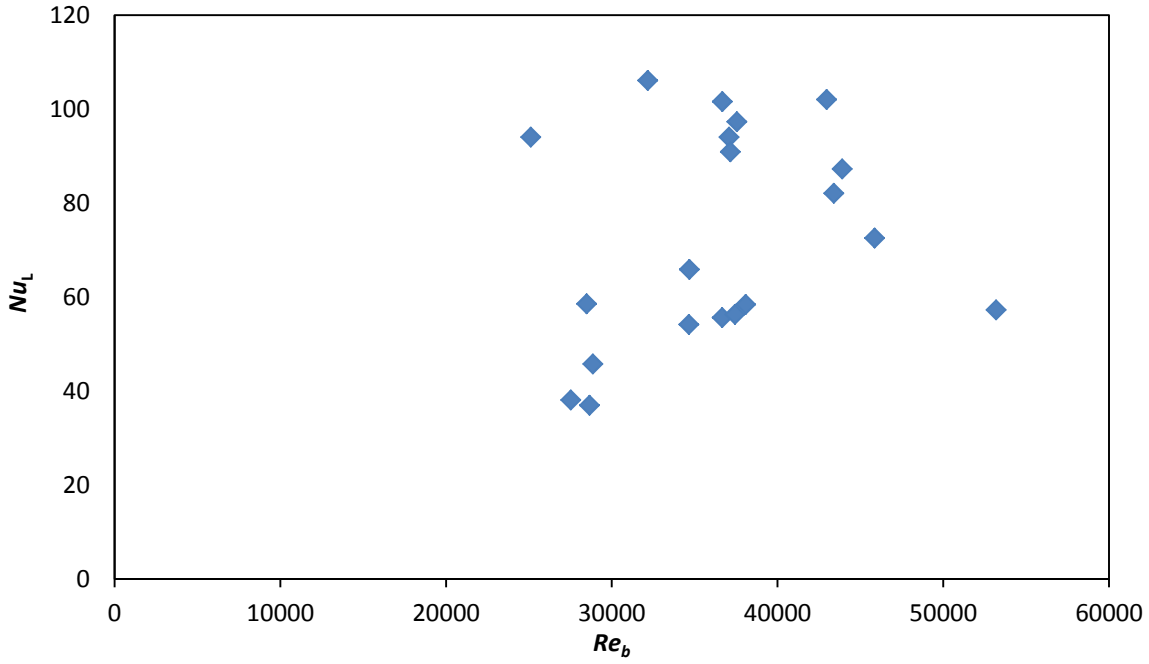

Figure 6.18: Nu_L vs. Re_b Plot for a 1.8 x 14.4 mm Channel

The presence of boiling is investigated in Figure 6.19 depicting the heat flux vs. ΔT_{sat} relationship. The graph shows insufficient evidence to prove the presence of boiling in the channel. However, in grouping similar velocities, the critical heat flux is nearly achieved particularly around 400 K for many of the velocity ranges attained.

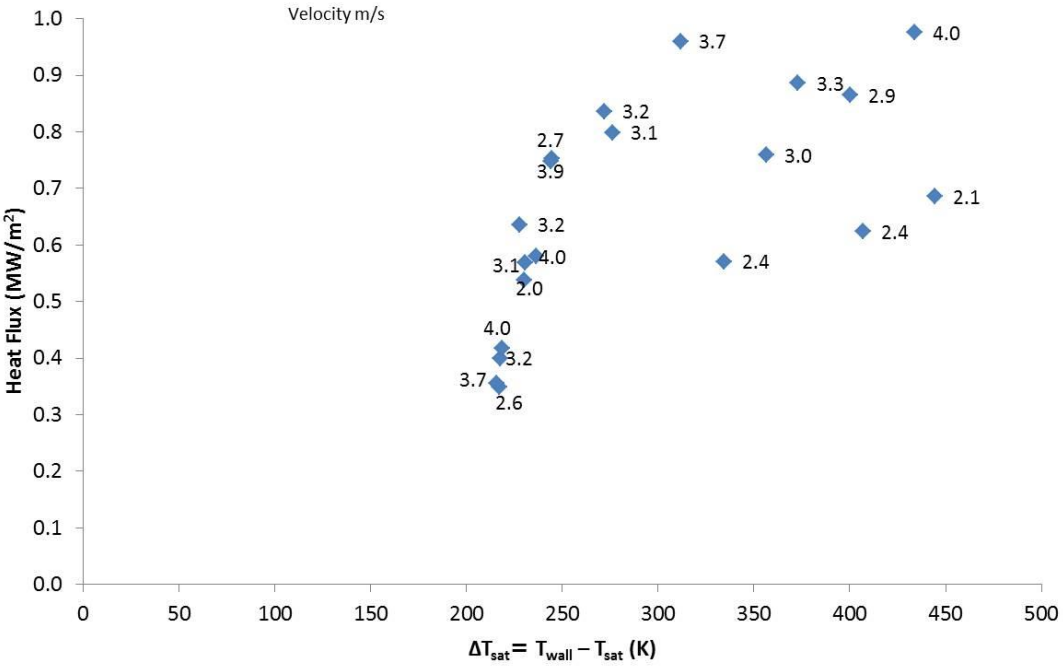

Figure 6.19: Heat Flux Curve Showing the Lack of Evidence for Boiling in the Channel

The correlation most representative of the HARCC heat transfer data was found to be a variation of the NASA/Rocketdyne *Nu* number correlation shown in Eqn 6.3 and presented in Figure 6.20. The R^2 factor is approximately 0.44, lower than the previous and ensuing test sections. This is caused by a greater deviation in Nu_O as Nu_L increases. Nu_O values larger than 150 show greater fluctuations (up to 38 % of Nu_L) of Nu_L compared to values lower than 150 which show a linear trend and correlate well to the heat transfer correlation. Additional tests must be employed in order to further investigate the behavior occurring at these values.

$$Nu_O = 0.443\, Re^{0.8} Pr^{0.4} \left(\frac{T_b}{T_w}\right)^{0.45} \tag{6.3}$$

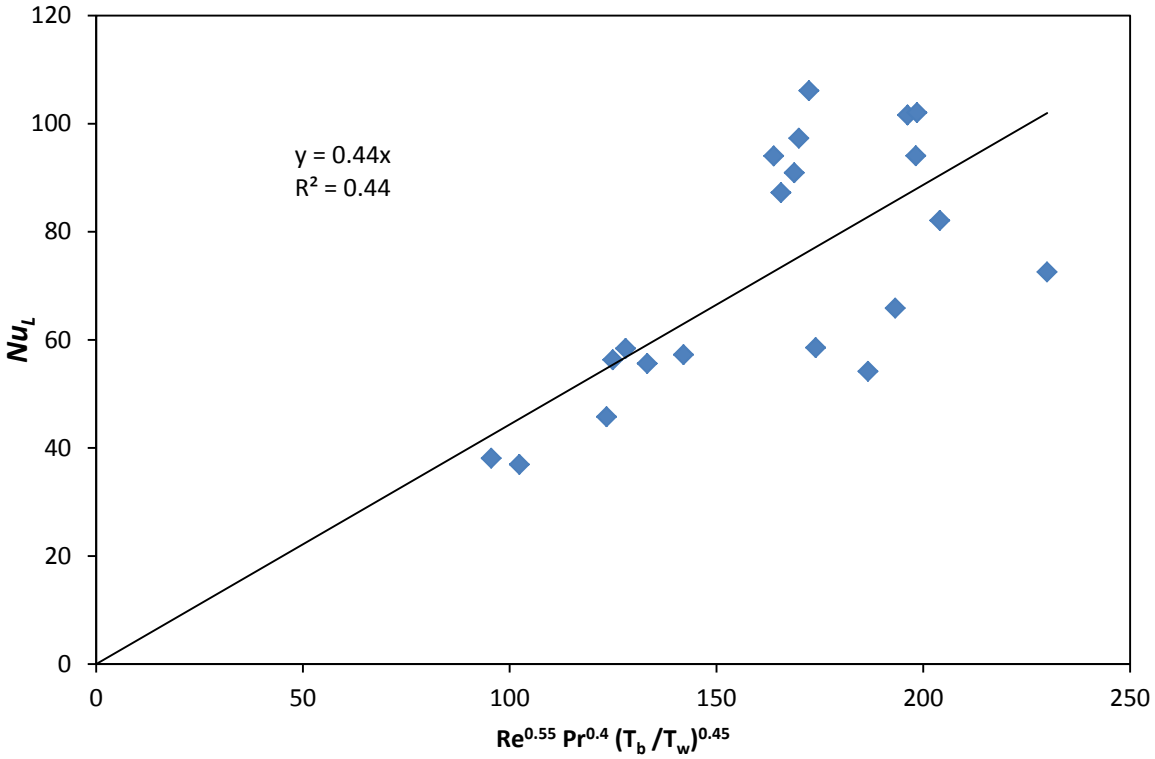

Figure 6.20: Nu_L vs. Nu_O for a 1.8 x 14.4 mm Channel

The comparison between Nu_L and Nu_O can be observed in Figure 6.21. The most over predicted values are above a Nu_L/Nu_O ratio of 0.8 expressing a close agreement to the theoretical values when the measured Nu_L is above 80. Under predicted Nu_O numbers (Nu_L number over 80) show ratio values just under 1.4. The variation in data shows that more tests need to be conducted to verify that the behavior is not due to measurement error and/or attributed to the error in the machining of the test section. However, when comparing the R^2 value seen in Figure 6.20 to the values in 6.21, the theoretical prediction does not necessarily deviate in such a manner where the R^2 is representative of the entire dataset.

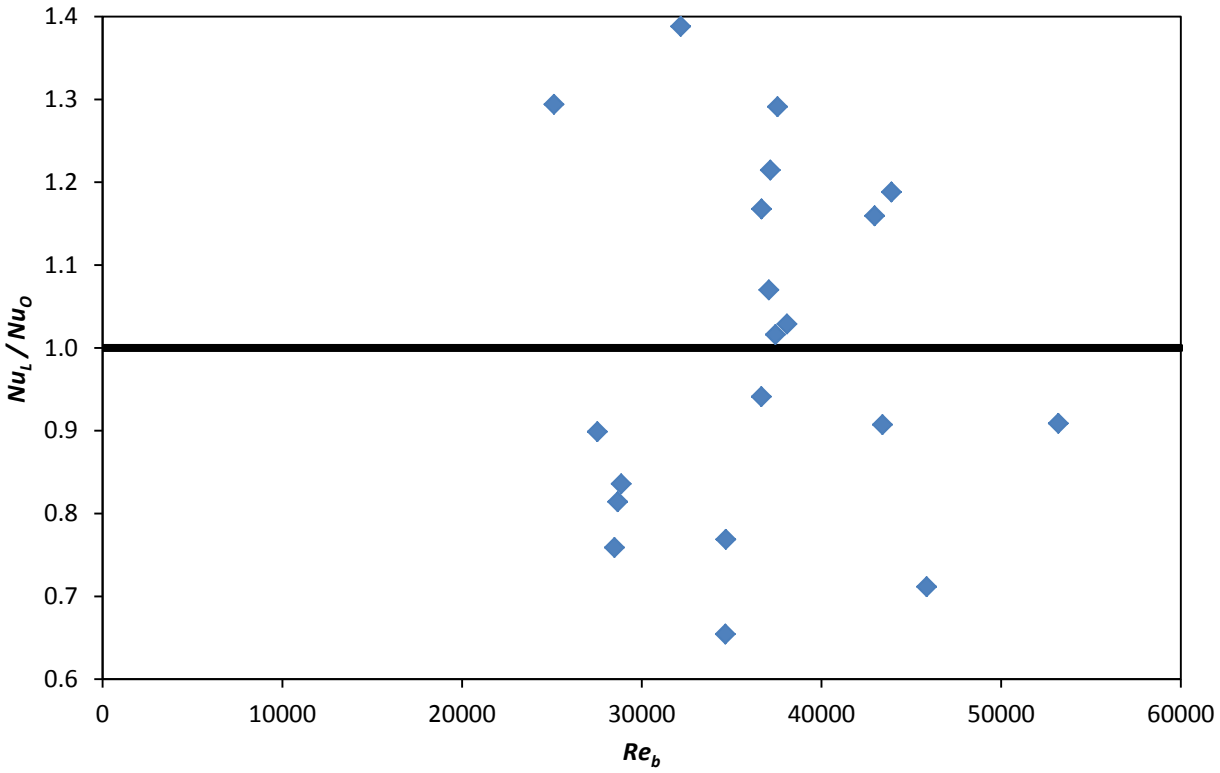

Figure 6.21: Nu_L/Nu_O vs. Re_b Plot for a 1.8 x 14.4 mm Channel

6.4.2 3.18 mm Inside Diameter Circular Cooling Channel

Circular cooling channels were chosen as part of a progressive study to investigate brazed cooling channels at a sub-scale level. A 3.18 mm I.D. channel was chosen as the simplest design to incorporate into the HHFTF. Figure 6.22 shows Nu_L vs. Re_b relationship displaying Re_b numbers up to 140,000 and Nu_L numbers up to 265 reaching higher Nu_L numbers than the HARCC but lower Nu_L numbers than the 1.8 x 4.1 mm channel.

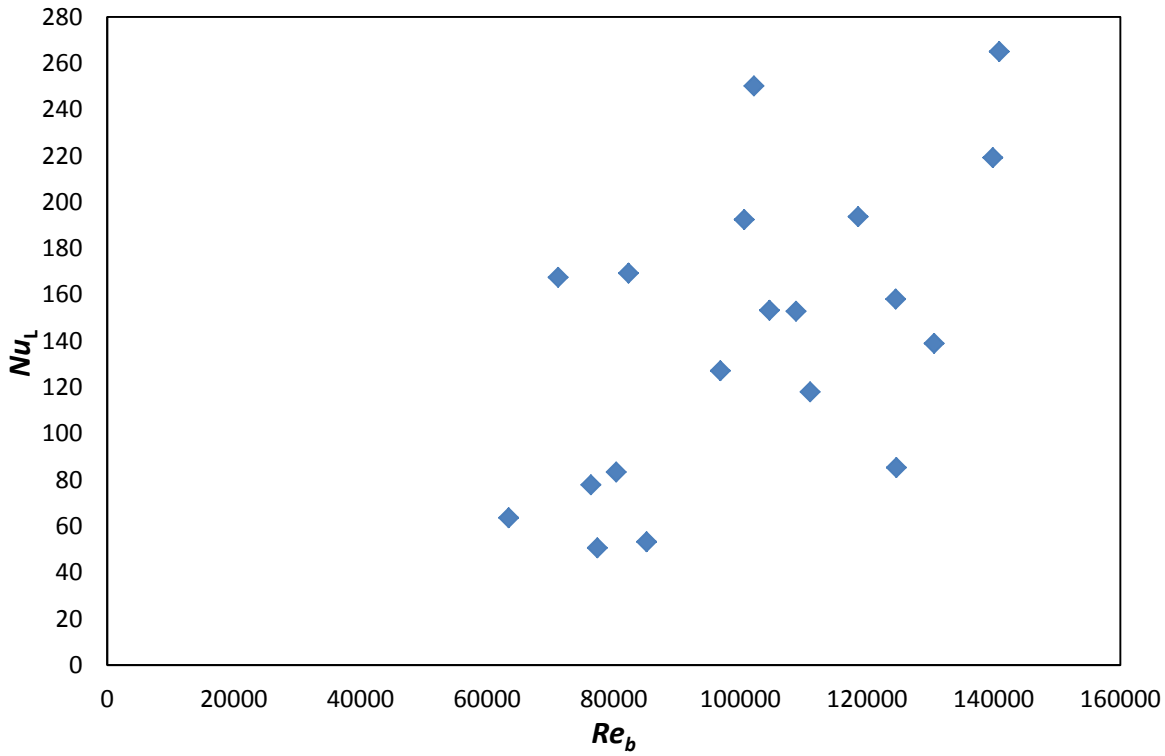

Figure 6.22: Nu_L vs. Re_b Number Plot for a 3.18 mm I.D. Tube

Comparing the heat flux to the wall temperature (Figure 6.23), a downward slope can be seen for the majority of the points and velocities. This possibility of the transition boiling for the entirety of the test points is speculated. An indication also aiming toward transition boiling exists in the critical heat flux of 2.5 MW/m^2 (1.5 BTU/(s-in^2)) experienced in the 1.8 mm x 4.1 mm channel. However, due to the lack of test conditions at lower heat fluxes, definitive proof indicating the onset of purely transition boiling is lacking and subsequent analysis will incorporate Nu_L predictions considering boiling effects.

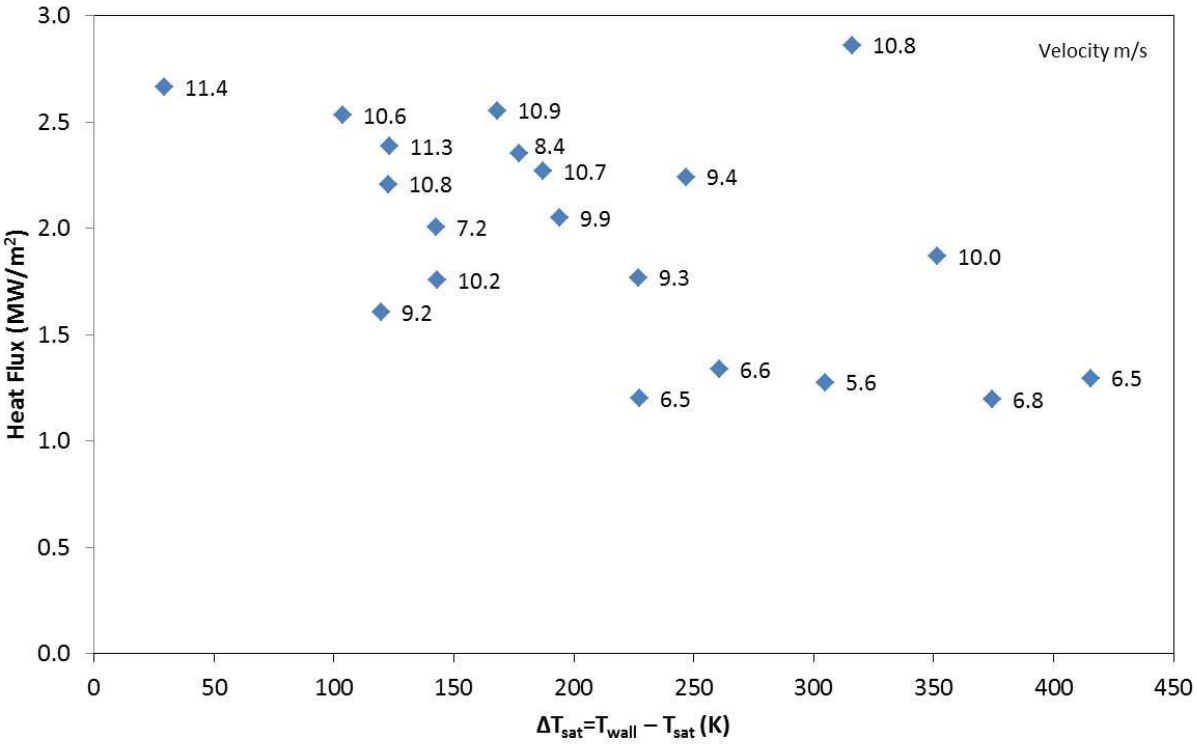

Figure 6.23: Heat Flux Curve Showing Possible Negative Slope Trend in the Channel for the Majority of Test Points.

Considering the possible onset of transition boiling occurring in the channel for each test point, a *Nu* correlation considering two-phase sub-critical fluids is applied to the current data. Eqn. 6.4 shows a correlation reported by Klimenko developed specifically to characterize two-phase fluid characteristics [19]. Figure 6.24 shows the agreement between the theoretical *Nu* number and $Nu_{L.}$ The R^2 value shows a strong correlation and supports the theory of transition boiling in the channel.

$$Nu_O = 0.026\, Re^{0.8} Pr^{0.5} \left(\frac{\rho_b}{\rho_w}\right)^{0.5} \left(\frac{k_b}{k_w}\right)^{0.6} \tag{6.4}$$

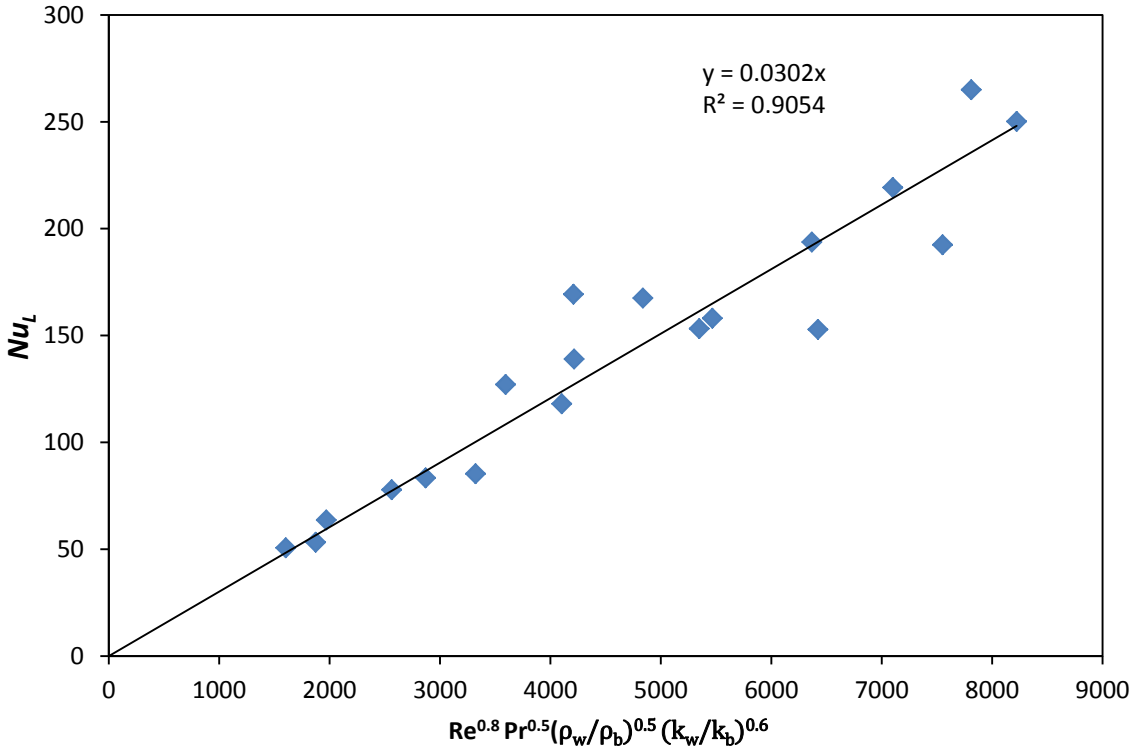

Figure: 6.24: Nu_L vs. Nu_O Plot for a 3.18 mm I.D. Channel

For the majority of the data, the theoretical values show an over prediction with ratios as low as 0.8 in Figure 6.25. The greatest under prediction is just under 1.4 while several points contain a ratio of nearly one.

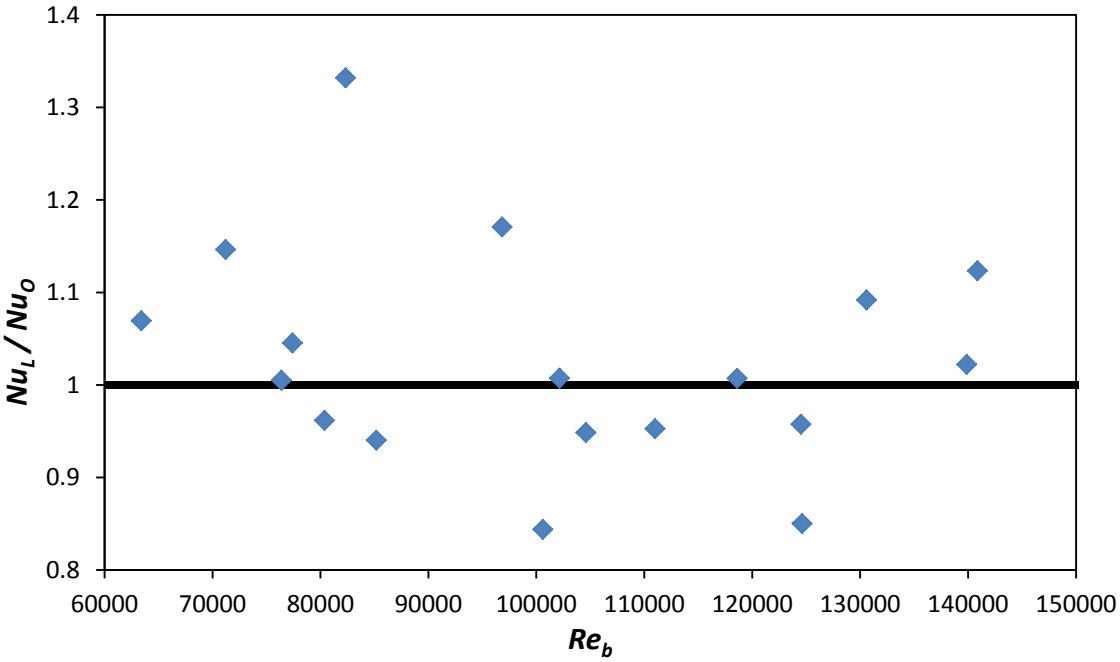

Figure 6.25: Nu_L/Nu_O vs. Re_b Plot for a 1.8 x 4.1 mm Channel

6.4.3 6.35 mm Inside Diameter Circular Cooling Channel

The behavior when increasing D_h is observed in Figure 6.26. Similar to previous increases of D_h, the range of Re_b is less with a range between 26,000 and 70,000. Nu_L is also lower with the exception to two outliers reaching up to 240 and the other around 136. Opposite to the HARCC, the Reynolds number range is larger while the Nu_L stays relatively constant in comparison.

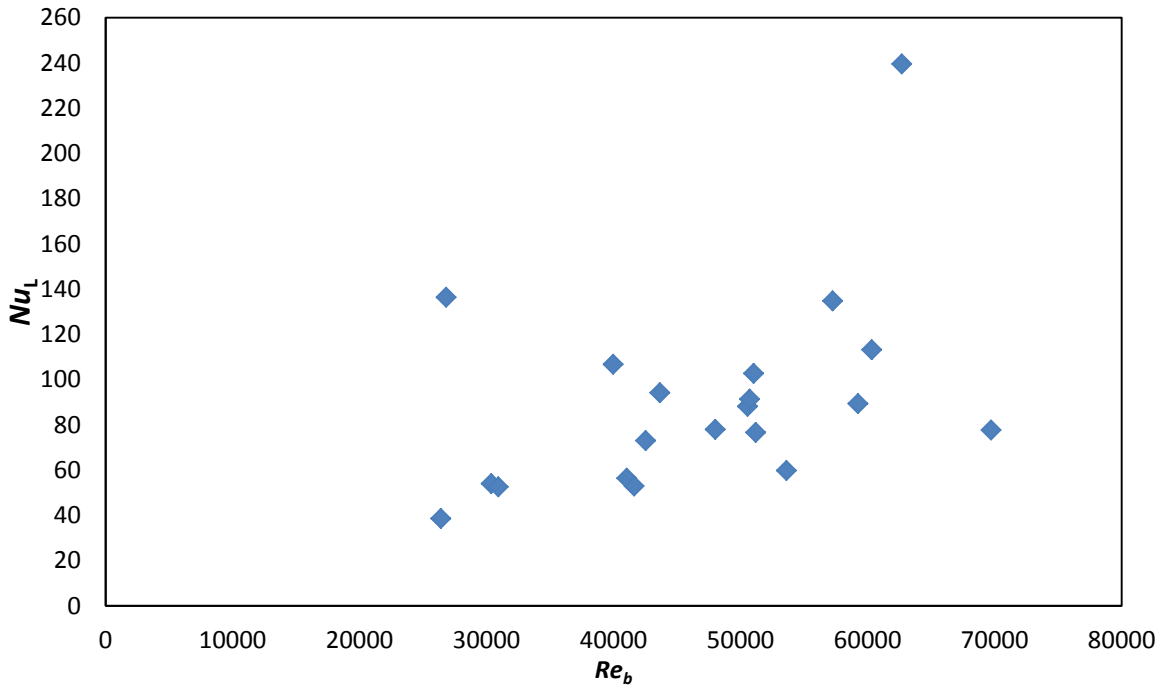

Figure 6.26: Nu_L vs. Re_b Plot for a 6.35 mm I.D. Tube

Due to the lack of increase in heat flux, Figure 6.27 does not support evidence of boiling in the channel. The lower heat fluxes in comparison to the prior channels also indicate that only sub-cooling is experienced through the line.

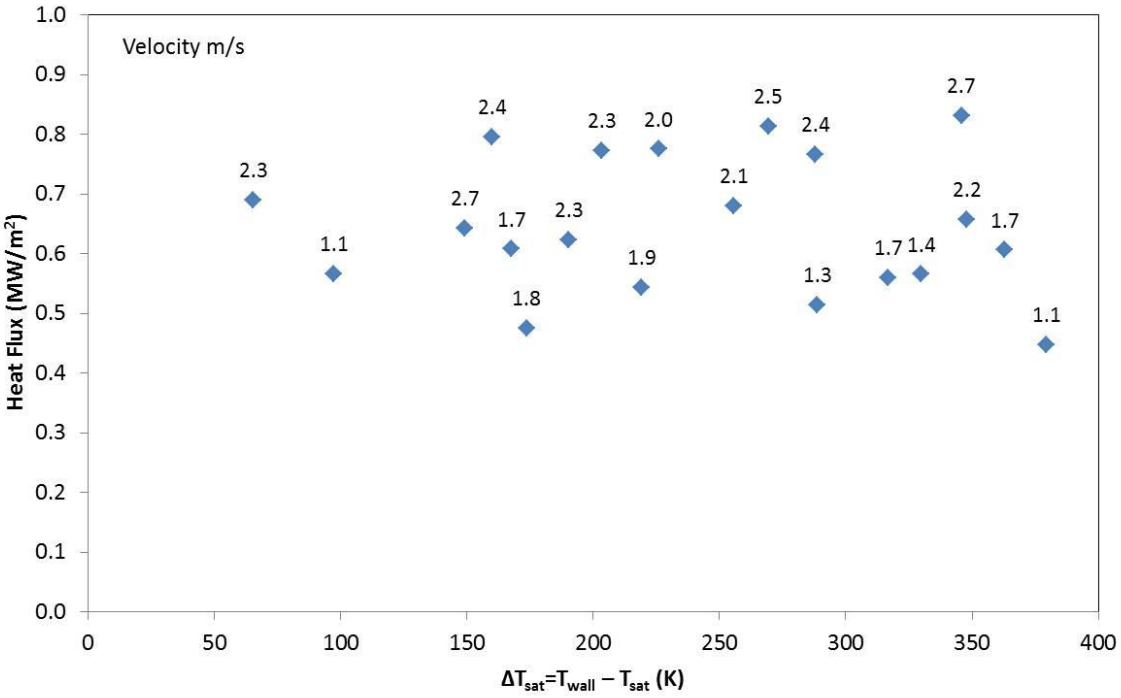

Figure 6.27: Heat Flux Curve Showing the Lack of Boiling Existing in the Channel

The correlation most suited to represent the dataset for a 6.35 mm I.D. was found to be a variation of the Jackson correlation (Eqn. 6.5). This correlation fits the data with an R^2 of 0.80 and a slope of .0795. This gives a clear indication that the correlation agrees with the experimental data for the given range of Re_b and Nu_L.

$$Nu_O = 0.026\, Re^{0.7} Pr^{0.5} \left(\frac{\rho_b}{\rho_w}\right)^{0.3} \left(\frac{C_{p,w}}{C_{p,b}}\right)^{0.9} \tag{6.5}$$

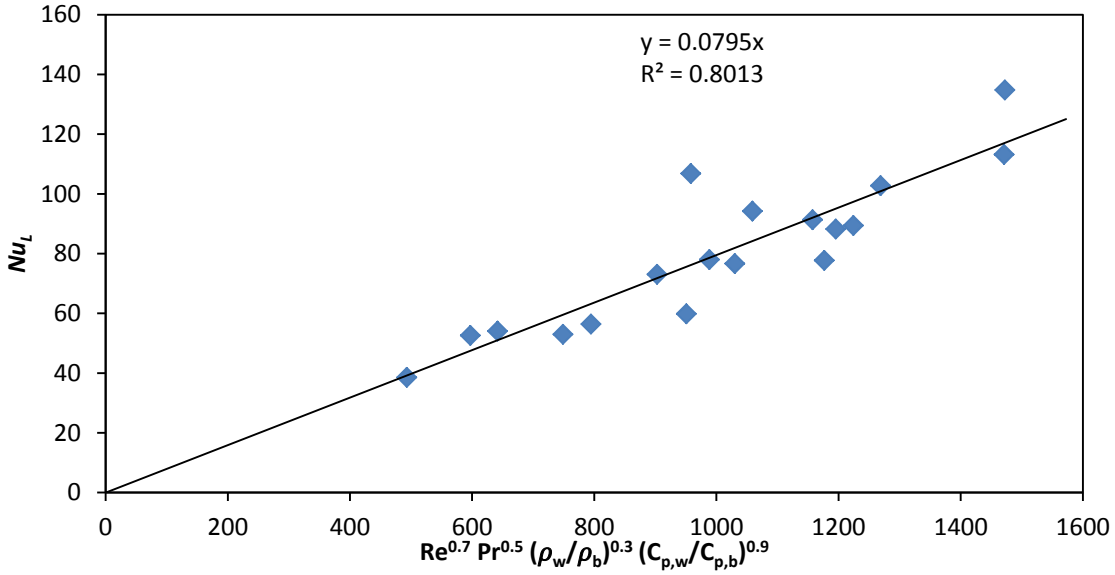

Figure: 6.28: Nu_L vs. Nu_O Number Plot for a 6.35 mm I.D. Tube

Figure 6.29 shows Nu_L in comparison to Nu_O. In terms of over prediction, few of the theoretical values fall below 0.8 meanwhile under predictions are generally below 1.2 with an outlier reaching up to 1.4. Overall, the theoretical correlation over predicts the data slightly but shows agreement with percent errors within 11% of the experimental value.

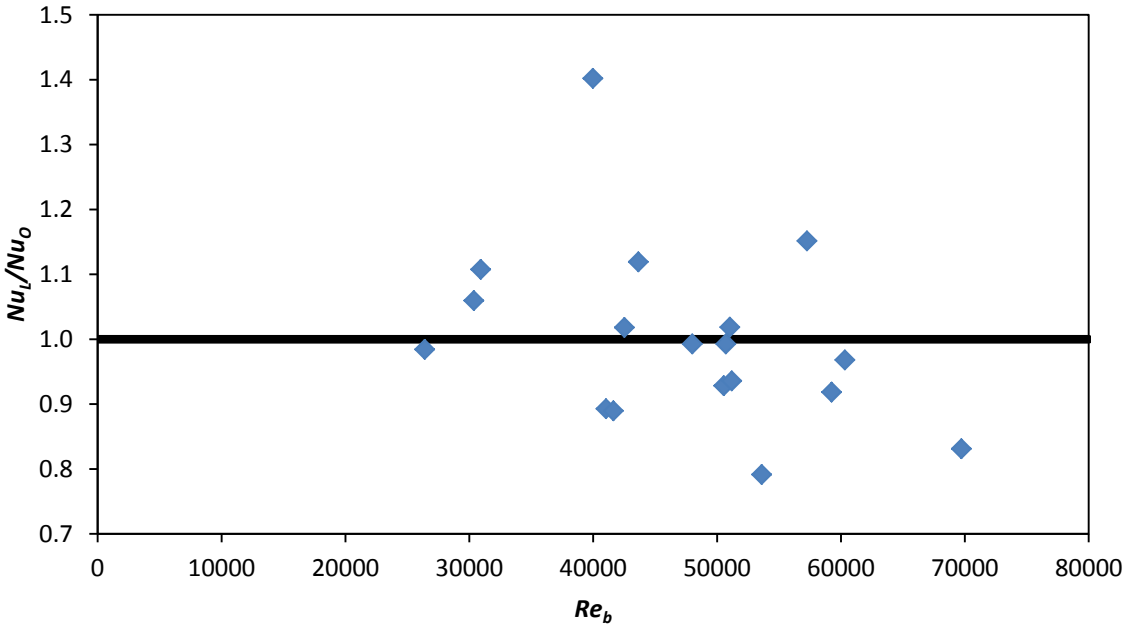

Figure 6.29: Nu_L/Nu_O vs. Re_b Plot for a 6.35 mm I.D. Tube

6.5 Discussion

The present study focuses on basic heat transfer equations to finally determine a *Nu* number correlation. The fluid temperatures evaluated at the bulk temperature (T_b) with the average inlet and outlet temperature serve to find the viscosity, densities, and specific heat to determine the following calculations.

Re_b is defined in Eqn. 6.5 using the density (ρ) and bulk viscosity (μ_b) from REFPROP. While the velocity (v) is determined from the mass flow meter measurements and D_h.

$$Re_b = \frac{\rho v D_h}{\mu_b} \tag{6.6}$$

To calculate the heat flux ($\dot{Q}$) subjected to the fluid inside the channel, the steady flow energy equation shown in Eqn 6.4 was implemented knowing the inlet temperature (T_{in}), the outlet temperature (T_{out}) specific heat (C_p) and mass flow rate ($\dot{m}$).

$$\dot{Q} = \dot{m} C_p (T_{out} - T_{in}) \tag{6.7}$$

The resultant heat flux is then used to calculate the local heat transfer coefficient h_x in Eqn 6.5.

$$h_x = \dot{Q}/A(T_s - T_m) \tag{6.8}$$

Where T_m is the mean temperature calculated using Eqn 6.6.

$$T_m = T_{in} + \frac{\dot{Q} p}{\dot{m} C_p} x \tag{6.9}$$

Where p is the perimeter of the cross sectional geometry and x is the axial location along the heated segment of the cooling channel. With h_x, an average heat transfer coefficient h_L was calculated by integrating for each time sequence.

$$h_L = \frac{1}{L} \int h_x dx \tag{6.10}$$

The measured Nu_L is then calculated using Eqn. 6.8.

$$Nu_L = \frac{h_L D_h}{k} \tag{6.11}$$

The measured Nu number Nu_L is used to determine the predictions along with the Re_b.

6.5.1 Measurement Uncertainty

The determination of the maximum uncertainty for the data points collected pertains mainly to accuracies of the components reported by the vendor. Using Table 6.6, which shows the error associated with each parameter, the propagation of uncertainty in Eqn 6.12 is used to find the combined error for each parameter considered to find the Nu number. This error is the resultant effect for the measured quantities from the flow meter, temperature, and pressures. The error in mass flow rate measurement is directly influenced by the flow meter during the calibration tests and the resultant pressure differential relationship attained during the actual LCH_4 test runs. Similarly, the heat transfer coefficient error stems from the temperature measurements associated with the channel wall and wetted thermocouples. The fluid state properties are evaluated using NIST REFPROP 8.0 which includes an accuracy of ±0.2 also affecting mass flow rate. Taking into account these values, the combined uncertainty is for Nu_L is estimated to be +/- 6.2%. Eqn 6.7 shows the method in calculating the propagation of uncertainty [20].

$$(U_{cal.})^2 = \sqrt{\sum \left(\frac{\partial f(Calculated)}{\partial Variable} Error_{variable} \right)} \tag{6.12}$$

Table 6.6: Measurement Accuracy Associated for Each Component

Parameter	**Error %**
Turbine Flow Meter	± 0.1
Mass Flow Rate	± 1.23
Pressure Transducers	± 0.25
Pressure Differential	± 0.35
E-Type Thermocouples	± 1
Temperature Differential	± 1.4
REFPROP (Fluid Properties)	± 0.2
Local Heat Transfer Coefficient	± 2.42
Measured Nusselt Number	± 6.2

6.5.2 Nusselt number Correlation Determination

The *Nu* number correlations studied are initially in the form shown in the following equations:

$$Nu = CRe^{m}Pr^{n} \tag{6.13}$$

$$Nu = C_1 Re^{m} Pr^{n} \left(\frac{\mu_b}{\mu_s}\right)^{C_2} \tag{6.14}$$

$$Nu = C_1 Re^{m} Pr^{n} \left(\frac{T_b}{T_s}\right)^{C_2} \tag{6.15}$$

The coefficients C, C_1, m, n, and C_2 are found either by trial and error or through the use of an iteration code fitting the data an attaining an optimum correlation. In this study, the factors that are most easily determined are C and C1 using the slope method as seen in Figure 6.15, 6.19, 6.23, and 6.27 where the slope "y" is indicated above the R^2 coefficient. Finding m has also been found by curve fitting a polynomial to the Nu_L vs. Re_b plot and the resultant power can be a starting point in finding the most adequate m coefficient. Future studies will incorporate the use of varying the remainder of the coefficients accordingly.

Chapter 7: Conclusion

7.1 Conclusion

The cooling channels tested serve as a valid representation of cooling channels in a regen engine. Through the use of the HHFTF, a total of 80 tests were successfully completed to characterize the heat transfer characteristics of LCH_4 at the defined cross sectional geometries. Results stemming from presented experiments are as follows:

- A cooling channel configuration 1.8 mm x 4.1 mm showed a strong correlation to the modified Jackson Nu number while showing signs of transition boiling for lower velocities.
- The same cooling channel geometry showed the most cooling in terms of the lowest attainable wall temperatures.
- The HARCC correlated the best to the Nu number presented by NASA/Rocketdyne, however, this included the lowest R^2 due to instabilities as Nu_L increased.
- Nu_O falls within 38% of Nu_L.
- A 3.4 mm diameter channel showed transition boiling throughout the tests and showed a strong correlation to two-phase conditions (Klimenko) supporting this theory.
- Increasing the I.D. to 6.4 mm showed an agreement to a mmodified version of the Jackson Nu number.
- Nu_O numbers were mostly in agreement within 12% of the Nu_L with outliers including 40%, 21% and 17% of Nu_L

Future work includes running additional tests for the purpose of definitively stating that boiling exists where sufficiently high heat fluxes are capable. The data presented aims on developing Nusselt number relationships and also focuses on finding a range of associated Re numbers. Developing a boiling curve will focus on fixing the fluid velocities to generate a curve similar to that in Figure 2.10.

Additional future work also includes developing test sections with artificial roughness, radii of curvature, longitudinal fins, and increased channel lengths.

References

[1] Neill, T. Judd, D. Veith, E. and Rousar, D. 2009. "Practical Uses of Liquid Methane in Rocket Engine Applications", *Acta Astronautica*, Vol. 65, pp. 696-705.

[2] Bates, R. W., Maas, E. D., Irvine, S. A., Auyeung, T. P. 2004. "Design of a High Heat Flux Facility for Thermal Stability Testing of Advanced Hydrocarbon Fuels", Air Force Research Laboratory, Accession no. ADA422733, Edwards AFB, CA.

[3] Cook, R.T. 1984. "Methane Heat Transfer Investigation Technical Progress Narrative" NASA Marshall Space Flight Center, NASA-CR-171199, Huntsville, AL.

[4] Green J. M., Pease G.M., and Meyer M. L. 1995. "A Heated Tube Facility for Rocket Coolant Research" 31st Joint Propulsion Conference and Exhibit, AIAA-95-2936, San Diego, CA.

[5] Noord, J.V. 2010. "A Heat Transfer Investigation of Liquid and Two-Phase Methane" NASA Glenn Research Center, NASA/TM-2010-216918, Cleveland, Ohio.

[6] Irvine S.A., and Burns R.M. 2005. "Preliminary Heat Transfer Characteristics of RP-2 Fuel as Tested in the High Heat Flux Facility" Air Force Research Laboratory, AFRL-PR-ED-TP-2005-545, Edwards AFB, CA.

[7] Bates, R.W., Billingsley, M.C., and Lyu, H.Y. 2007. "Experimental and Numerical Investigation of RP-2 Under High heat Fluxes", Air Force Research Laboratory, AFRL-PR-ED-TP-2007-150, AFB, CA.

[8] Billingsley, M.C. 2008. "Thermal Stability and Heat transfer Characteristics of RP-2", 44th AIAA *Joint Propulsion Conference*, AIAA 2008-5126, Hartford, CT.

[9] Huzel, K. D., and Huang, D. H. 1992. *Modern Engineering for Design of Liquid-Propellant Rocket Engines,* Progress in Astronautics and Aeronautics Volume 47, AIAA.

[10] Incropera, F. P. De Witt, D. P. Theodore B. L. Lavine, A. S. 2006. *Fundamentals of Heat and Mass Transfer.* 5th ed. NJ: John Wiley & Sons, Inc.

[11] Wadel, M. F. 1998. "Comparison of High Aspect Ratio Cooling Channel Designs for a Rocket Combustion Chamber with Development of an Optimized Design" NASA Lewis Research Center, NASA/TM-1998-206313, Cleveland, Ohio.

[12] Younglove, B.A., and Ely, J.F. 1987. "Thermophysical Properties of Fluids. II. Methane, Ethane, Propane, Isobutane, and Normal Butane", *J. of Physical Chemistry*, Vol. 16, No. 4.

[13] Garcia, C. P. 2013. *Pressure and Heat Flux Effects on the Heat Transfer Characteristics of Liquid Methane"* PhD Dissertation, University of Texas at El Paso, ProQuest/UMI. (Publication No. AAI365907.)

[14] Kreith, F., 2000. The CRC Handbook of Thermal Engineering, Boca Raton: CRC Press LLC.

[15] J.H. Lienhard, A Heat Transfer Textbook, 3rd ed. Phlogiston Press, Massahusetts.

[16] Sieder, E. N., and Tate, E. 1936. "Heat Transfer and Pressure Drop of Liquids in Tubes", Industrial Engineering and Engineering Chemistry, Vol. 28, No. 12.

[17] Çengel, Y. A. and Cimbala, J. M. 2006. *Fluid Mechanics: Fundamentals and Applications*. New York, New York: Mc Graw Hill Higher Education.

[18] Klimenko, V. V. 1990. "A Generalized Correlation for Two-Phase Forced Flow Heat Transfer-Second Assessment" *Int. J. of Heat and Mass Transfer,* Vol. 33, No. 10, pp. 2073-2088.

[19] Gu, H., Li, H., Wang, H., and Luo, Y. 2013. "Experimental Investigation on the Convective Heat Transfer from a Horizontal Miniature Tube to Methane at Supercritical Pressures" *Applied Thermal Engineering,* Vol. 58, pp. 490-498.

[20] Berendsen, H. J. C., 2011. *A Student's Guide to Data and Error Analysis,* Cambridge University Press, United Kingdom.

Appendix

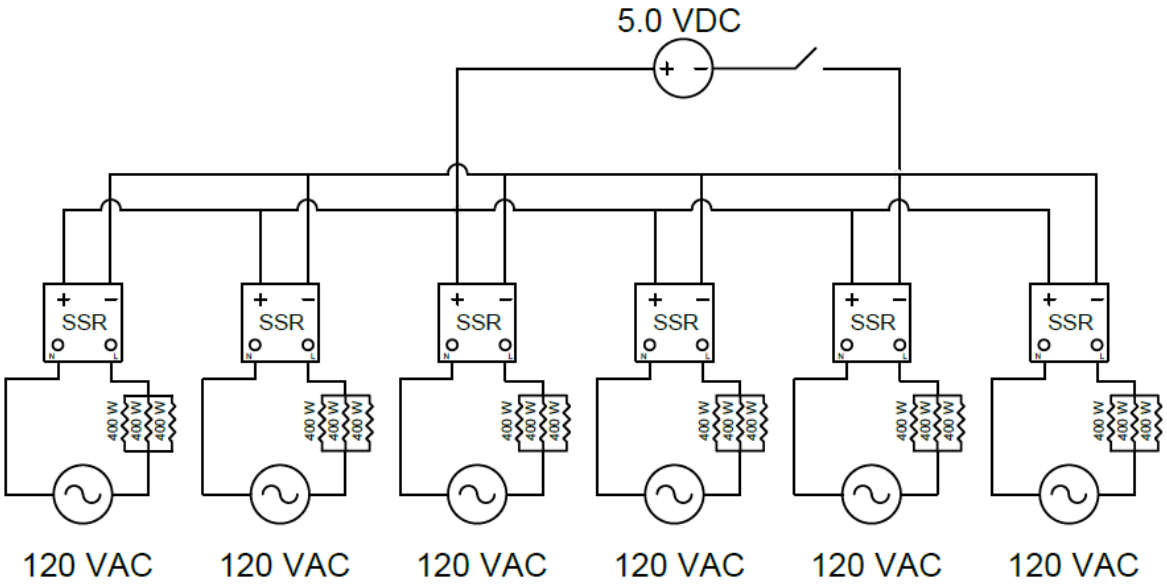

Wiring Schematic for the Cartridge Heater to Solid State Relay Connection.

Mass Equipment and Measurement List for all Components Associated with the HHFTF.

Item	Make	Model	Range	Accuracy	Use	Quantity
Exposed tip type E thermocouple	Omega Engineering	EMQSS-125E-6	-200 to 900°C (-328 to 1652°F)	1.7°C or 0.5% above 0°C, 1.7°C or 1.0% below 0°C	Test section wall temperature measurement	6
Sheathed ungrounded type E thermocouple	Omega Engineering	EMQSS-125U-6	-200 to 900°C (-328 to 1652°F)	1.7°C or 0.5% above 0°C, 1.7°C or 1.0% below 0°C	Test section inlet/outlet and condenser temperature measurement	8
Nextel ceramic insulated type K thermocouple	Omega Engineering	XC-14-K-12	-200 to 1250°C (-328 to 2282°F)	2.2°C or 0.75% above 0°C, 2.2°C or 2.0% below 0°C	Block temperature measurement	4
Thin Film Cryogenic Pressure	Omega Engineering	PX1005L-500AV	0 to 3.45 MPa (0 to 500 psia)	±0.25%	Condensing/run tank and test section	3

Transducer			-196 to 149°C (-320 to 300°F)		inlet/outlet pressure measurement	
Thermocouple Input Module DAQ device	National Instruments	NI 9213	Refer manual	Refer manual	Thermocouple data acquisition	2
Terminal Block with SCC Expansion Slots DAQ device	National Instruments	NI SCC-68	Refer manual	Refer manual	Pressure transducer and flow meter data acquisition	1
Turbine flow meter DC transmitter	Hoffer Flow Controls, Inc.	CAT315 5DCX1X	-40 to 85°C	±0.02% of full scale @ 20°C (68°F)	Turbine flow meter data transmission	1
Pressure transducer process meter and controller	Omega Engineering	DP25B-E-A	0 to 100 mV	±0.02% of reading	Pressure transducer signal conditioning	3
Convection-enhanced Pirani Sensor	Kurt J Lesker	K31714S	1×10^{-3} to 1.0×10^{3} Torr (1.9×10^{-5} to 19 psi)	±<1%	Vacuum chamber pressure measurement	1
Digital Convection Pirani Vacuum Gauge Controller	MKS	HPS 947	1.0×10^{-3} to 1.0×10^{3} Torr (1.9×10^{-5} to 19 psi)	±<1%	Vacuum chamber pressure digital reading	1

Detailed Experimental Procedure and Safety Hazard/Risk Mitigation Assessment
Pre-testing procedure:

1. Inspect instrumentation and equipment.
    a. Turn on power supplies and adjust required voltage.
        i. Actuated valves: 12 VDC.
        ii. Flow meter transmitter: 13-30 VDC.
        iii. SSRs: 5 VDC.
    b. Run the LabVIEW program titled "High Heat Flux Test Facility" located in the "LabVIEW programs" folder in the computer's desktop.
        i. Ensure that LabVIEW program outputs the data file into a folder titled "Methane Test Data" in the computer's desktop.
    c. Ensure that all pressure transducers and thermocouples are reading ambient conditions (13 ± 1 psia and 23 ± 3°C).
    d. Check that all solenoid valves indicated in the schematic function properly by performing an audible and current draw inspection.
        i. Current draw: 1.2 ± 0.1 A.
    e. Connect solid state relays to 120 VAC extension cords.
    f. Using a multi-meter, check that all cartridge heaters work properly by measuring the resistance across them.
        i. Resistance per group of three cartridge heaters is 12 ± 1 ohms.

2. Inspect testing area.
    a. Activate the ventilation system by turning on the ventilation fans.
    b. Check for leaks in the system using snoop liquid leak detector by pressurizing the lines with He to 50 ± 5 psia.
        i. After leak check is performed close He tank valve and vent system
    c. Close needle valve.
    d. Open MV2 valve and pull vacuum in the system with the line vacuum pump.
        i. Line vacuum levels: 2 ± 1 psia.
    e. Activate and configure oxygen monitor and flammable gas detector devices.
        i. Refer to Appendix A for configuration procedures.
    f. Close line vacuum chamber.
    g. Activate the pirani vacuum gauge controller.
    h. Pull vacuum inside the chamber with the chamber vacuum pump.
        i. Chamber vacuum levels: 0.05 ± 0.01 Torr.

3. Prepare for data collection.
    a. Create a folder in the "Methane Test Data" folder that entails the conditions to be tested i.e. heat flux and pressure.

4. Begin methane condensation.
    a. Turn off the line vacuum pump and close MV2 valve.
    b. Open CH_4 tank valve.
    c. Open MM1 valve.
    d. Put on cryogenic personal protective equipment (PPE), e.g., gloves, apron, face shield.
    e. Pressurize condensing/run tank to 70 psia.

f. Open MN1 valve and regulate dewar pressure to 150 psig.
g. Open LN_2 coil solenoid valve.
h. Open MN2 and MN3 valves.
i. Monitor LCH_4 levels using the tank thermocouples.
    i. At 70 psia, methane is liquid at -139°C.
    ii. Tank is filled with LCH_4 in 60 ± 15 min.
    iii. Please note that the condensing process and the block heating process should occur concurrently.
j. Close CH_4 tank valve.

5. Begin heating the copper block.
    a. Manually activate cartridge heaters by following a 3 sec on/off cycle.
        i. Use manual switch located on the switch panel.
    b. Heat the block until desired conditions are reached.
        i. Stop cycling manual switch.
        ii. Refer to test matrix for testing conditions.

Testing procedure:

1. Chill cooling channel and run lines with LN_2.
    c. Open LN_2 chill and Bypass solenoid valves.
    d. Open needle valve.
    e. Chill until inlet conditions are reached (-160 ± 5°C).
        i. Please note that chilling and pressurizing run tank occur concurrently.
    f. Close needle valve.

2. Pressurize run tank with helium.
    a. Open He tank valve.
    b. Open MH1 valve.
    c. Open Helium solenoid valve.
    d. Pressurize run tank to desired conditions.
        i. Refer to test matrix for testing conditions.

3. Stop LN_2 flow and adjust needle valve.
    a. Close MN1 valve.
    b. Close LN_2 coil and LN_2 chill solenoid valves.
    c. Open and adjust needle valve.

4. Begin data recording process.
    a. Flip “Record On” switch to on position on the GUI.

5. Run LCH_4 through run lines and cooling channel.
    a. Open Run solenoid valve.
    b. Monitor channel wall and tank temperatures.
        i. Tank temperatures warmer than -150°C indicate depletion of LCH_4.
        ii. Observe wall temperature profile in GUI to determine if steady state behavior is reached.
        iii. Channel wall temperature steady state behavior indicates successful test.

c. Close MH1 valve when LCH_4 is depleted.
d. Close Run solenoid valve and needle valve.

6. Stop data recording process.
    a. Flip "Record On" switch to off position on the GUI.

Post-testing procedure:

1. Close He tank valve.

2. Relieve residual system pressure.
    a. Open run solenoid valve.
    b. Gradually open needle valve.
    c. Check that all manual and solenoid valves are open to prevent pressure build up from residual fluids.
    d. Monitor system until ambient conditions are reached.

3. Deactivate all electronic devices.
    a. Turn off chamber vacuum pump.
    b. Check cartridge heaters' resistance to test functionality.
    c. Disconnect solid state relays from 120 VAC extension cords.
    d. Turn off power supplies.
    e. Turn off oxygen meter and flammable gas detector devices.

4. Check that data was collected and transfer it for processing.
    a. Data is used to find the heat transfer coefficient of methane and derive Nusselt number correlations.

Emergency Procedure

All safety considerations were taken and an emergency procedure was developed in case of an unwanted occurrence. Red lines are shown below to avoid a catastrophic failure of the hardware or facilities.

Red Lines:

- Line pressure must remain less than 350 psia.
- Methane tank pressure must remain less than 500 psia.
- Block temperature must remain less than 500°C.

Risks and Hazards:

Hazard	Risk	Mitigation
Cryogenics	Cold contact burns, explosion (pressure), asphyxiation	Cryogenic PPE, pressure relief valves, oxygen monitor device
Flammability	Burns, explosion (ignition)	Fire extinguisher, dilution of LCH_4

Table Describing Relevant Nusselt Number Correlations in the Presented Work.

Nusselt Number	Equation	Notes
Dittus Boelter (1930)	$Nu = 0.23{Re_D}^{0.8}Pr^{0.4}$	Developed for gas and liquids for Pr numbers greater than 0.7 and Re numbers between 20,000 to 300,000
Seider Tate (1936)	$Nu = C_1{Re_D}^{0.8}Pr^{1/3}\left(\frac{\mu_b}{\mu_w}\right)^{0.14}$	Developed for single phase fluids based off of experimentally testing three oils.
NASA Rocketdyne	$Nu = C_1{Re_D}^{0.8}Pr^{0.4}\left(\frac{T_b}{T_w}\right)^{0.14}$	Variation of the Taylor Nusselt number and reported for use with supercritical CH_4 with Re numbers on the order of millions.
Jackson Nusselt Number	$Nu = 0.026\,Re^{0.8}Pr^{0.4}\left(\frac{\rho_b}{\rho_w}\right)^{0.3}\left(\frac{C_{p,w}}{C_{p,b}}\right)^{0.4}$	Jackson Nusselt number was developed by testing several supercritical fluids while enduring large variations in thermal properties.
Klimenko	$Nu = 0.026\,Re^{0.8}Pr^{0.5}\left(\frac{\rho_b}{\rho_w}\right)^{0.5}\left(\frac{k_b}{k_w}\right)^{0.6}$	Experimentally tested water, Freon, cryogens etc. to develop a generalized correlation for nucleate boiling and vaporization.

Vita

Adrian Trejo received his Bachelors and Master's Degree from the University of Texas at El Paso in 2007 and 2009 respectively. He continued his education in 2010 when he was admitted into the Doctoral program in Environmental Science and Engineering.

Dr. Trejo received honors in volunteering and served as a NASA student Ambassador in 2013. He was also a recipient of a NASA student scholarship in 2012.

While pursuing his PhD, Dr. Trejo worked as a research assistant at the Center for Space Exploration Technology and Research and completed two internships at NASA Johnson Space Center. This summer, Dr. Trejo will continue his engineering career by working for the Missile Defense Agency.

Dr. Trejo presented his research in liquid methane heat transfer characteristics in conferences and meetings including the Joint Propulsion Conference and Southwest Energy Science and Engineering Symposium. He has also published his work in the Journal of Experimental Heat Transfer.

Dr. Trejo's dissertation, *An Experimental Investigation of the Cooling Channel Effects on the Internal Forced Convection of Liquid Methane,* was supervised by Ahsan Choudhuri.

Adrian Trejo

atrejo46@gmail.com